MEASUREMENT OF SHIELDING IN ELECTRICALLY LARGE METALLIC ENCLOSURES

Robert Armstrong

Thesis submitted for the degree of DOCTOR OF PHILOSOPHY

Department of Electronics,

University of York
February 2013

For ‘Granty S’

You always said I could do it

Abstract

The measurement techniques employed to obtain the shielding effectiveness (SE) of enclosures using the current version of IEEE 299.1 only apply to enclosures of side dimension greater than 0.1m, and are also lacking in a full analysis of the field distributions within the enclosure. The work presented here uses the IEEE 299.1 draft standard as a base and investigates different methods of obtaining the SE, as well as looking at making the measurement more applicable to physically small and electrically large enclosures, and hoping to inform future versions of shielding effectiveness standards for small enclosures.

The first part of this thesis investigates the use of a comb generator as a source in an enclosure under test (EUT), which provides a statistically uniform electric field inside the EUT when combined with a small mechanical stirrer. The EUT used here is an equivalent size to a 19 inch rack unit used in many equipment rigs; therefore investigations using it are of relevance to the real world.

It becomes apparent that it is important to be sure that statistical field uniformity is achieved within the EUT as well as in the test chamber. The chamber at the University of York is compared with the chamber used in Ancona, Italy. Meanwhile, it is found that the presence of a direct path or unstirred component distribution in an enclosure or chamber can change the measured SE.

A study of aperture dominated EUTs reveals that it is possible to obtain an indication of the SE of an enclosure using the $Q-$factor. This test method has the advantage that it can be applied to enclosures that have a low SE or have many apertures, as is the case in some real enclosures. Continuing the development into testing physically small enclosures that are outside the scope of IEEE 299:1997, it is shown that a physically small enclosure can be represented by an electrically equivalent larger enclosure. This is also of use when considering IEEE 299.1.

Contents

Declaration **17**

1 Introduction **18**

1.1 Research Aims 18

1.2 Research Scope 19

1.3 Outline of the Thesis 19

2 The Theory of Enclosures, Fields and associated Statistics **22**

2.1 Introduction 22

2.2 A Brief History of EMC 22

2.3 Shielding 23

2.3.1 Wave Impedance, the Near Field and the Far Field 25

2.4 Anechoic and Semi-Anechoic Chambers 27

2.5 Reverberation Chambers 28

2.5.1 Nested Chamber Method of Measuring Shielding Effectiveness of Enclosures 30

2.5.2 Modes and Mode Stirring 31

2.5.3 Mechanical Mode Stirring 33

2.5.4 Electronic Mode Stirring 35

2.5.5 Mechanical Stirring vs. Electronic Stirring, and choosing the step size 36

2.5.6 The $Q-$factor 40

2.6 Field statistics 43

2.6.1 Reverberation Chamber Field Distributions 43

2.7 The Kolmogorov-Smirnov test 46

2.8 Shielded enclosures 48

2.8.1 Measurements in Reverberant Environments 48

3 Separate Source Measurements - Uniformity, Shielding Effectiveness and Frequency Modulation 52

3.1 Chapter Introduction 52

3.2 CGE-02 and Experiment Setup 53

3.3 Mechanical Stirring and the CGE-02 59

3.4 Shielding Effectiveness Measurements using the CGE-02 61

3.4.1 Method 1 62

3.4.2 Method 2 64

3.4.3 Method 3 65

3.5 Frequency Modulation of a Separate Source 66

3.5.1 Frequency Stirring using Frequency Modulation 70

3.6 Frequency Modulation and the CGE-02 73

3.7 Chapter Summary 73

4 Comparing Reverberation Chambers Using a Shielded Enclosure 74

4.1 Enclosure Design 74

4.2 Repeatability of Results 76

4.3 Changing the SE 79

4.4 Chapter Summary 88

5 Rician Statistics and the $K-$factor 89

5.1 Introduction 89

5.2 Reverberation Chambers - Required Field Uniformity 89

5.3 Direct Paths in Enclosures 93

5.4 The Rician $K-$factor 96

5.5 Simulation of the Test Enclosure 97

5.5.1 Simulation of Paths 98

5.6 Experimental Setup - Creating a Direct Path 102

5.6.1 Experimental Results - Nested Chamber Measurements 107

5.7 Effect of Rician Statistics on the Measured SE 109

5.8 Chapter Summary 111

6 Estimating Shielding Effectiveness using Absorber Cross Sections 112

6.1 Experiment Setup 112

6.2 Centralisation of Measured Distributions 113

6.3 Comparing the measured results 115

6.4 Results 115

6.5 Chapter Summary 117

7 Using $Q-$factor to estimate shielding effectiveness 119

7.1 Introduction 119

7.2 SE and Effective Stirring 119

7.3 $Q-$factor review and application to this chapter 121

7.4 Enclosure Setup 123

7.5 Autocorrelation and Width of Autocorrelation 125

7.6 Obtaining the $Q-$factor from the Width of Autocorrelation 129

7.7 Experimental Results 129

7.8 Desktop Setup and Results 133

7.9 Chapter Summary 135

8 Electrical Scalability of Resonant Enclosures 136

8.1 Introduction 136

8.2 Enclosure Setup 137

8.3 Mode density considerations 140

8.4 Simulation of the $Q-$factor 142

8.5 Experimental Results 146

8.6 Chapter Summary 148

9 Conclusions and Further Work 150

9.1 Separate Source Measurements - Uniformity, Shielding Effectiveness and Frequency Modulation 151

9.2 Comparing Reverberation Chambers Using a Shielded Enclosure 151

9.3 Rician Statistics and the $K-$factor 152

9.4 Estimating Shielding Effectiveness using Absorber Cross Sections 153

9.5 Using $Q-$factor to Estimate Shielding Effectiveness 153

9.6 Electrical Scalability of Resonant Enclosures 154

9.7 Overall Conclusions 154

9.8 Further Work 156

10 Appendix 1: MatLab Code 157

10.1 Mechanical Stirring Code 158

10.2 Frequency Stirring Code 161

10.3 Peak finding Code 163

10.4 Distribution Combination code 165

List of Acronyms 182

List of Symbols 184

List of Figures

2.1 Diagrammatical representation of Shelkunoff Shielding Model 24

2.2 Field regions close to radiation sources 26

2.3 Change in Impedance as a function of distance from a dipole source. . . . 27

2.4 Schematic diagram of screened rooms, with the reverberation chamber on the left and the anechoic chamber on the right 29

2.5 The reverberation chamber as used in the majority of work in this thesis. This is set up as per the nested chamber method - see section 2.5.1 and figure 2.6 30

2.6 Schematic of nested reverberation chamber used for enclosure SE measurements 31

2.7 The stirrer paddle used in the reverberation chamber. 34

2.8 Evidence of tracking on points that are not statistically independent. The test frequency is 8GHz. 37

2.9 No tracking evident using the same stirrer step size as in figure 2.8 but using a 3GHz test frequency 38

2.10 Distribution Overview 44

2.11 Graphical representation of the KS test. 47

2.12 Nomenclature of ports for reference when considering corrected S parameters for the calculation of SE. Power is transmitted into the chamber on port 2, the unshielded measurement on port 1, and the shielded horn on port 1_h and monopole on 1_m 50

3.1 Direct Output Power for the CGE-02 comb generator in both modes from 250MHz to 26GHz. 54

3.2 Comb Generator Emitter CGE-02 and battery pack BP-01. The monocone antenna is inside the plastic cover. 55

3.3 Right angle drive constructed to allow the tall DC motor and gearbox (inside the black tube) to drive the small stirrer. 57

3.4 The CGE-02 and DC stirrer present in the test enclosure. The inset shows the cable layout providing 5V DC to both the motor and the CGE via a BNC bulkhead connector 57

3.5 CGE-02 output suffering from interference on the 5V supply caused by the continuous running of the DC motor. 58

3.6 The CGE-02 present in the test enclosure. The 5V PCB supply plate can also be seen, separated from the enclosure by an insulating layer. 59

3.7 KS test results for both modes of the CGE-02 comb generator. Where no bar is shown the distribution is wholly rejected. 60

3.8 Schematic of the three different methods used to compare measurement techniques for shielding effectiveness measurements using a separate source. 61

3.9 Results of the three different methods used compared with a data set measured with a network analyser. 62

3.10 Lexmark Kiss waveform 67

3.11 A 3GHz carrier modulated by a sine waveform 68

3.12 A 3GHz carrier modulated by a triangle waveform 68

3.13 Schematic of FM trace and discrete peaks 69

3.14 KS test results for frequency stirring using frequency modulation in the large chamber. Both distributions are tested; the double Rayleigh case does not show as it is fully rejected (0% acceptance) at all frequencies. . . 72

3.15 KS test results for frequency stirring using frequency modulation in the inner enclosure. Note that no Rayleigh distributions are established throughout. 72

4.1 Verification enclosure showing the position of the three SMA monopole antennas 75

4.2 System of washers and finger strip used to ensure good contact; (a) is just before good contact, (b) is tightened to standard SMA spanner torque of 8 lbin. Spacing washers are included to avoid crushing the finger strip. . . . 76

4.3 Port repeatability over 4 runs 77

4.4 Port repeatability over 4 runs, results taken by Franco Moglie and Valter Mariani 78

4.5 Measured SE using comparable methodology in two different labs. 78

4.6 Short slot configuration, with lid removed for clarity. Note spacing washers still in place to prevent distortion of the lid. Two of the measurement monopoles can be seen, the third is in the lid. 79

4.7 Medium slot configuration with lid removed for clarity. Note spacing washers still in place to prevent any distortion of the lid which may reduce finger strip effectiveness, and also to prevent crushing of the finger strip. 79

4.8 Long slot configuration with lid removed for clarity. Note spacing washers still in place to prevent distortion of the lid, which was more pronounced when using the long slot without the spacing washers. 80

4.9 SE of enclosure using short slot apeture. All ports are shown. 81

4.10 SE with medium slot. Note the SE is generally lower than that of the short slot. 82

4.11 SE with the long slot. Note that this is generally less than both the medium slot and short slot SE value. 82

4.12 Comparison of the measured SE averaged over the three ports. The difference in SE is less at higher frequencies as the efficiency of the finger strip decreases. 83

4.13 Internals of the EUT showing the added absorber block 83

4.14 Short slot SE with absorber present. 84

4.15 Medium slot SE with absorber. 84

4.16 Long slot SE with absorber. 85

4.17 Comparison of the measured SE using port 3 with and without the absorber block present. The short slot configuration is shown. 86

4.18 DC stirrer present in the enclosure. A similar stirrer paddle is used in chapter 3 86

4.19 DC stirring compared to post process frequency stirring. 87

5.1 Illustration of a direct path in a reverberation chamber. It can be seen that the power received on (2) will change as the stirrer rotates, and also that the power received on (4) will not. In addition, the power received at (5) will be different from the power received at (4) 90

5.2 Schematic Diagram illustrating the various path options set up on the test enclosure 94

5.3 Diagram of the monopole arrangement used as apertures 94

5.4 Close up of a single 19mm monopole with SMA connector. This one is on a ground plane, two are used with a female to female connector to create an aperture in an enclosure 95

5.5 Plot of the Rician $K-$factor against the offset from zero of the mean of a Gaussian Distribution. 97

5.6 Histogram of the simulated distribution with ϕ = ϕ_{min} = 1.4 99

5.7 Histogram of the simulated distribution with ϕ = 5 100

5.8 Histogram of the simulated distribution with ϕ = ϕ_{min} = 1.4 100

5.9 Histogram of the simulated distribution with ϕ = 5 101

5.10 Histogram of the simulated distribution with ϕ = 10 101

5.11 Experimental setup to obtain a large Rician component in the reverberation chamber 103

5.12 Experimental setup to obtain direct paths of varying $K-$factor within the EUT 104

5.13 Histogram of the measured distribution along Path A compared with the assumed double Rayleigh distribution. 105

5.14 Histogram of the measured distribution along Path B compared with the assumed double Rayleigh distribution. 106

5.15 Histogram of the measured distribution along Path C compared with the assumed double Rayleigh distribution. 106

5.16 Rician distributed reference measurement (ϕ = 7.5 on both component Gaussian distributions) compared to a Rayleigh distributed reference measurement This Rician distribution is termed the ‘small’ Rician. 107

5.17 Rician distributed reference measurement (ϕ = 15.6 on both component Gaussian distributions) compared to Rayleigh distributed reference measurement. This Rician distribution is termed the ‘large’ Rician. 108

5.18 Zero offset Rician reference measurement compared to Rayleigh reference measurement. They are shown to be the same. 108

5.19 SE measurement with small Rician inside the EUT and Rayleigh outside . 110

5.20 SE measurement with small Ricians inside and outside the EUT 110

5.21 SE measurement with large Ricians inside and outside the EUT 111

6.1 Experimental setup showing shielded and unshielded measurment arrangements. 113

6.2 Schematic Diagram illustrating offset measurement centering 114

6.3 Exaggerated illustrative direct path with non-zero means 115

6.4 Transmission across the reverberation chamber with and without a 0.4m × 0.4m sample of pyramid absorber. Note how the absorber dampens the resonances evidenced by the smoother loaded trace 116

6.5 Loss ratio with using a loaded enclosure with different aperture sizes . . . 117

7.1 Aperture Configuration on front panel of test enclosure. 122

7.2 EUT in place in the Anechoic chamber. The front panel is facing the camera and the ridged waveguide antenna - current aperture configuration is ”Large Hole”. 124

7.3 Autocorrelation plot for the ‘large hole’ configuration at 4GHz. 50MHz and 100MHz span widths are shown 127

7.4 Extreme shouldering effect observed on autocorrelation peak with 6GHz frequency response. The different colours correspond to different aperture configurations. 128

7.5 Simulated $Q-$factor Vs Autocorrelation width for measurement span of 50MHz 130

7.6 Simulated $Q-$factor Vs Autocorrelation width for measurement span of 100MHz 130

7.7 Autocorrelation width plotted against $Q-$factor for the 1.2dB cutoff level 131

7.8 Log of the autocorrelation width plotted against log of the $Q-$factor for the 1.2dB cutoff level 131

7.9 Measured $Q-$factor plotted against measured SE 132

7.10 Measured $Q-$factor plotted against measured SE for 50MHz bandwidth . 133

7.11 Measured $Q-$factor plotted against measured SE for 100MHz bandwidth 134

7.12 Q factor against realitve SE for different experiment environments 134

8.1 The three enclosures used in this chapter - designated ’large’, ’medium’ and ’small’ 138

8.2 Aperture configuration applicable to all three enclosures. The black outer square is the dimesion of the inside of the test enclosure 139

8.3 Number of modes below the minimum frequency for cubic enclosures with varying side dimension 141

8.4 Calculated Q factor components for different aperture configurations using the large 300mm enclosure. The apertures vary in size (see figure 8.2) from the smallest (1) to the largest (4) 143

8.5 Aperture Q factor for the three enclosures under test. 145

8.6 comparison for the three different enclosures. 146

8.7 Aperture configuration against measured $Q-$factor. The pink squares are the simulated aperture $Q-$factor 147

8.8 Measured Q factor vs. SE. Higher $Q-$factor groupings are within circles and squares for clarity. 148

List of Tables

2.1 Distribution Forms 45

Acknowledgments

The people who have helped me on this PhD journey are too numerous to list. Support has been gratefully received from all sides, but the following require a special mention.

Firstly to my supervisor Professor Andy Marvin, whose invaluable support, guidance and encouragement have meant and helped more than he knows. Dr John Dawson also deserves special thanks for his in depth and helpful review of this thesis.

I also wish to thank my mum Margaret, my dad Phil, my sister Helen and both sets of Grandparents, for your unending patience and support. For being there, encouraging and keeping me sane, thanks also go to my girlfriend Jenni.

Thanks also go to York EMC Services, whose important funding contribution meant I could get started on this journey, and for their continued support throughout this work.

Last but not least, I also need to say thank-you to the whole EMC research group for making these years a fun and interesting time, particularly Dr Ian Flintoft and Dr Linda Dawson, and also to the lifelong friends I have met along the way, both inside and outside the academic world.

Declaration

The work presented in this thesis is based purely on my own research; where it is not, this is explicitly stated in the text. No part of this work has previously been submitted for any other qualification. For aspects of this work that have been published, see below.

Robert Armstrong, February 2013

Parts of this work have been previously published in the following:

Armstrong, R and Marvin, A.C: The Effect of Rician Statistics on the Measurement of Shielding Effectiveness of Enclosures in Reverberation Chambers, EMC Europe Wroclaw, Poland, 2010.

Armstrong, R, Marvin, A.C and Dawson, J.F: An Experimental Investigation of the use of Q-Factor to Determine the Shielding Effectiveness of Electrically Large Equipment Enclosures with Apertures, EMC Europe York, United Kingdom, 2011.

Armstrong, R, Marvin, A.C and Dawson, J.F: Shielding Effectiveness Estimation of Physically Small Electrically Large Enclosures through Dimensional Scaling, IEEE International Symposium on Electromagnetic Compatibility, Pittsburgh PA, United States of America, July 2012.

Chapter 1

Introduction

1.1 Research Aims

Electromagnetic Compatibility (EMC) is one of the most important aspects of electronic design. In essence, EMC encompasses the electromagnetic emission and immunity properties of any specific electronic devices. As all electronic components have the potential to emit radio-frequency and also low frequency electromagnetic radiation when in operation, some mechanism or aspect of design is required to make sure that the emission from one component, or even from the electronic device as a whole, does not interfere unduly with the operation of other components or other device. This can be done by reducing the amount of radiated energy from the device (reducing emissions), reducing the ability to be influenced by incoming radiation (increasing immunity), or by a combination of the two. A measure of the Shielding Effectiveness (SE) of any given electronic equipment enclosure can be used to help quantify the immunity and emission characteristics of the equipment in question.

Although separate immunity and emission experiments can be carried out, what is of interest here is the ability of an equipment enclosure to reduce emissions and boost immunity. The basics of testing and measurement, even in very large chambers [1] and the electromagnetic physics behind an SE measurement are well understood [2][3][4]. What is looked at in this thesis involves the statistics of the electromagnetic fields both inside and outside any given enclosure. The underlying reason for this work is to further the understanding of the mechanisms in operation involved with an SE measurement in a reverberation chamber, as well as to develop ways of measuring the SE that differ from and help inform the standard measurement procedure outlined in the IEEE (Institute of Electrical and Electronics Engineers) 299.1 [5], used for measuring the SE of physically small enclosures .

1.2 Research Scope

The measurement of physically small and electrically large equipment enclosures has been under research internationally for some years now, with many aspects covered. The IEEE Standard 299.1 [5] concerns the measurement and classification of electrically large enclosures with a side dimension between 0.1m and 2m and utilises a nested reverberation chamber set-up [6][7]. The theory of this measurement is covered in the background section. The scope of this thesis is to expand and inform on the methodology and understanding involved in the IEEE 299.1 standard. Furthering the knowledge behind the current measurement procedure results in some new ways of obtaining the SE of equipment enclosures, and an in depth study of the underlying statistics involved in taking a measurement in a reverberation chamber is carried out. Varying methods of measuring the SE are tried with the intent of making the measurement quicker and easier to obtain, while bearing in mind the lessons learned from analysing the statistics present in the nested chamber arrangement. Later on the electrical scalability of enclosures is investigated and compared to how the theoretical $Q-$factor in an enclosure can be used to help inform and measure the shielding effectiveness.

1.3 Outline of the Thesis

After this introduction, the background theory of the physics and statistics behind reverberation chambers is examined in Chapter 2, including the $Q-$factor and set-up of the nested chamber method. An introduction to shielding effectiveness and field statistics is also covered.

Chapter 3 involves the discussion of stirring methods in small enclosures using the York EMC Services (YES) provided Comb Generator Emitter (CGE) as an emitting source inside the enclosure under test (EUT). A small mechanical stirrer is designed and the two measurement ideas combined into a single instrument. The use of frequency modulation for frequency stirring is also investigated.

Chapter 4 describes the work done on an enclosure designed to be used as a round robin EUT in order to test the methods and chambers of different institutions around the world. Results from the University of York (UoY) and the University of Ancona (UoA) in Italy are presented, and a comparison between DC stirring (using a direct current motor to mechanically stir) and post-processing stirring is examined.

Chapter 5 involves investigations into direct paths in enclosures and how the presence of such direct paths, which are identifiable by the presence of a Rician distribution of electric field, changes the measured shielding effectiveness.

Chapter 6 looks at estimating the shielding effectiveness of an aperture dominated enclosure by measuring the difference in power transmitted across the chamber when an EUT loaded with radio absorbing material (RAM) is present and its apertures changed.

Chapter 7 concerns using the $Q-$factor to obtain an estimation of the SE in the case of an aperture dominated EUT.

Chapter 8 details the concept of equal electrical size to test an enclosure of different physical size. Theoretical considerations of the effect of the $Q-$factor as the physical size of the enclosure becomes smaller are investigated. The potential uses of this method is to test previously untestable physically small enclosures that have an impractically high minimum frequency restriction.

Chapter 9 summarises, discusses and draws conclusions from the previous chapters and brings the whole research together, and also suggests further work.

The Chapters are followed by an Appendix, Chapter 10, which reproduces some of the MatLab code used to process the results.

The thesis as a whole involves using a number of methods and techniques in order to investigate the measurement of shielding in electrically large metallic enclosures. Development of an instrument for use in enclosures highlighed some issues with the existing draft IEEE 299.1 standard, used for testing the shielding of enclosures. The main issue identified that is concentrated on is the lack of rigour in testing the statistical distribution of the field present in both the testing chamber and the enclosure when using a nested reverberation chamber setup, and the effect that this can have on the measured value of the SE. It is hoped that the work presented in this thesis will add to the knowedge base that will be used in the creation of new standards for enclosure testing, or help with updates to the existing IEEE 299.1.

Chapter 2

The Theory of Enclosures, Fields and associated Statistics

2.1 Introduction

This Chapter provides an overview of previous research in the field of electromagnetic compatibility (EMC) with regards to shielded enclosures and the statistics of the internal electric fields. First, shielded enclosures are examined with emphasis on the reverberation chamber. This involves an overview of modes and mode stirring, then a look at the $Q-$factor of a reverberation chamber and how shielding works. This Chapter explains the theory and lays out the underlying physics needed to inform the work carried out later in the thesis. Throughout this thesis the external screened room will be referred to as the 'chamber' and the internal enclosure will be referred to as the 'enclosure' or 'enclosure under test (EUT)'. The EUTs used are metallic, electrically large, and representative of real world enclosures, for example a 19 inch rack unit.

2.2 A Brief History of EMC

Electromagnetic interference (EMI) first became apparent during the telecommunication boom in the 1920s, once the transmission of radio waves started to become more widespread. In 1934, in Paris, the first meeting of CISPR (Comité International Spécial des Perturbations Radiolectriques) was held [8], incorporating members of the IEC (International Electro-technical Commission); eventually producing documentation that began to address the EMI problems that were starting to occur. In 1996, these documents were accepted as part of the European Directive on EMC, a version of which is still in use throughout the European Union (EU). Technological advances in the field of semiconductors meant that improving EMC rapidly increased in importance: from concerns over radio system protection, to the need to include emission and immunity aspects in the design of electronic systems. This lead to the extensive development of test methods designed to encourage reliable and repeatable EMC testing throughout the electronic world [9][10] [11] [12]. An important part of these test methods, described by standards such as the Institute of Electrical and Electronics Engineers Standard 299 (IEEE 299) [5], is the ongoing development of equipment enclosures, and a continuing increase in the level of understanding behind the measurements being taken.

2.3 Shielding

The mechanism by which a material shields against EM radiation is described by the Schelkunoff model [13]. Developed in 1938 from the concept of an electromagnetic wave having an impedance, a schematic representation of the model, in which an electromagnetic wave in free space impinges on a infinite flat sheet of shielding medium, is shown in figure 2.1

The fraction of the incident wave E_i that becomes the reflected wave E_r is dependent on the reflection coefficient of the surface of Medium 2. The remaining portion carries on into the material, being attenuated by the factor $e^{\frac{-d}{\delta}}$, where δ is the skin depth of Medium 2 and d is the thickness of Medium 2, until it reaches the other side. Upon exit from Medium 2, (the right hand side of Medium 2 in figure 2.1), another reflection/transmission occurs; in this case the reflected wave returns back through the material and the portion that is transmitted helps make up E_t. Multiple reflections occur inside the material, adding up to the total E_r and E_t, although due to the attenuation inside Medium 2 subsequent reflections and transmissions are much reduced. If the width of Medium 2 is larger than δ then the subsequent reflections can be ignored, as their contribution to the total E_r and E_t is small.

The well known property δ, the skin depth, is related to the material properties of the shielding material: σ the conductivity and μ the permeability, and is defined in equation 2.1. The skin depth is dependent on frequency f: as the frequency increases the skin depth decreases, and so the thickness of a material required to effectively shield is reduced.

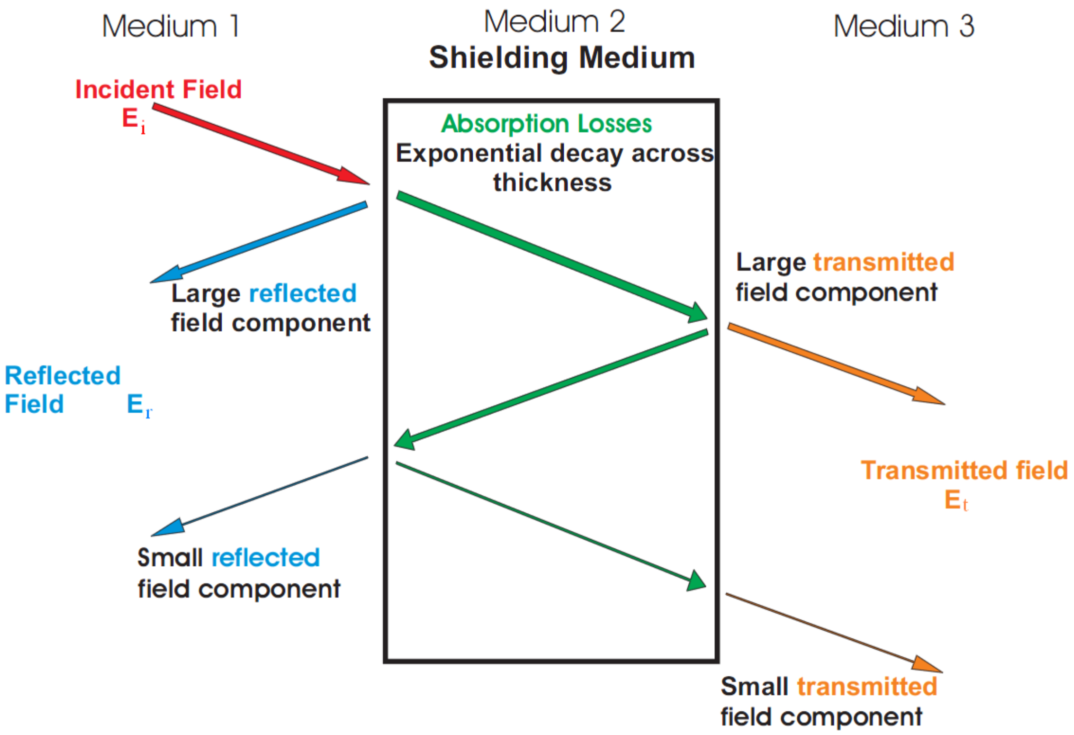

Figure 2.1: Diagrammatical representation of Shelkunoff Shielding Model

$$\delta = \sqrt{\frac{1}{\pi f \sigma \mu}} \tag{2.1}$$

The measure of shielding effectiveness (SE) is used to describe how well any given material attenuates an electromagnetic wave. The accepted method of measuring this effect is to simply measure the electric field strength on either side of the material in question.

Consider the case shown in figure 2.1. The field strength on the illuminated (left hand) side of Medium 2 will be higher than that on the shadowed side (i.e $E_i > E_t$); and a simple and accepted way of expressing this is to take a ratio between these two quantities. The SE can be given in the form of the electric field strength E, the magnetic field strength H or the power density S. Usually, the SE is expressed in decibels, obtaining the following forms [5]:

$$SE_{dB} = 20 \log_{10} \left(\frac{E_i}{E_t} \right) \tag{2.2}$$

$$SE_{dB} = 20 \log_{10} \left(\frac{H_i}{H_t} \right) \tag{2.3}$$

$$SE_{dB} = 10\log_{10}\left(\frac{S_i}{S_t}\right) = 10\log_{10}\left(\frac{P_{out}}{P_{in}}\right) \tag{2.4}$$

where the denominators E_i,H_i,S_i are the unshielded reference measurements, equivalent to the incident wave E_i in figure 2.1, and the numerator E_t,H_t,S_t are the shielded measurements, equivalent to the transmitted wave E_t in figure 2.1. The quantity P_{out} is the power measured outside an EUT and P_{in} is the power measured inside an EUT. The process of obtaining the two quantities used to obtain the SE is widely used in both material shielding and enclosure shielding (see section 2.8) experiments and tests [5], [7], [14], [15].

2.3.1 Wave Impedance, the Near Field and the Far Field

Referring to the previous section, the overall SE of any barrier is dependent on the magnitude of the transmitted wave, which in itself is a function of the reflection and attenuation coefficients of the material in question. As stated, the attenuation of the material is defined by $e^{\frac{-d}{\delta}}$, and depends on the skin depth and the thickness. In the far field regime, the reflection coefficient is dependent purely on the material properties, as a ratio of the impedance in the material and the wave impedance [13].

The impedance of an electromagnetic wave (Z) was developed in [13] and is given in equation 2.5, and arises from the plane wave solution to Maxwell's equations:

$$Z = \frac{E_i}{H_i} \tag{2.5}$$

where E_i and H_i are the magnitudes of the electric and magnetic field components. These are orthogonal to each other and normal to the direction of propagation of the wave. The amplitudes of the two waves (electrical and magnetic) are related to each other through the intrinsic impedance of free space, which has a value of 377Ω or $120\pi\Omega$. Therefore it follows that in free space, $\frac{E_i}{H_i} = 120\pi\Omega$.

This relationship is only true in the region known as the far field region, where the EM wave is fully established . The definition of the far field (also known as the Fraunhofer region) is normally taken as $\frac{2D^2}{\lambda}$. This distance, also known as the Rayleigh Range, arises from the dominance of the $\frac{1}{R}$ at values of R (the distance from the antenna) where the $\frac{1}{R^2}$

and higher terms in the solutions to Maxwell's equations can be regarded as vanishingly small [16]. The various parts of a radiation pattern are shown in figure 2.2, where D is the size of the antenna in question. The boundary between near and far field regions is also given independently of the antenna size as $\frac{\lambda}{2\pi}$ [17]; this arises when the inductive term from a magnetic source and the radiative term from an electric source are balanced, and the antenna is considered to be small compared to the measurement distance. There is a transition region before full establishment of the far field situation, shown in figure 2.3.

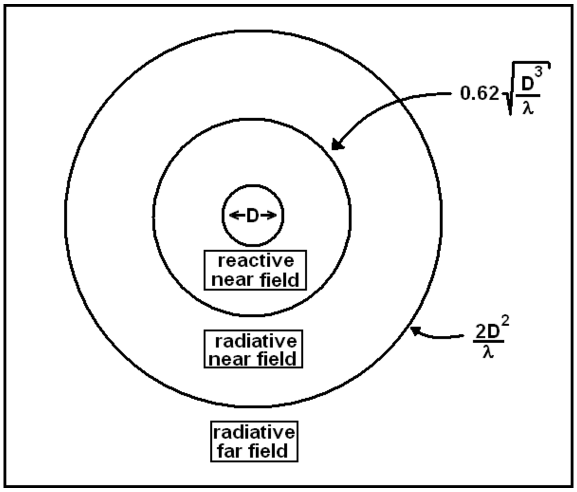

Figure 2.2: Field regions close to radiation sources

Inside the far field definition lies the near field, where the distance from the source (in this case a dipole antenna) is not large enough to discount the $\frac{1}{R^2}$ term for magnetic fields and the $\frac{1}{R^3}$ term for electric. For a loop antenna then the electric field has a $\frac{1}{R^2}$ dependency and the magnetic field a $\frac{1}{R^3}$. It is worth noting that the near field is split up into the reactive near field (nearest the antenna) and the radiating near field (or Fresnel) region (between the reactive and transition regions)[16], with the boundary between them being stated as $0.62\sqrt{\frac{D^3}{\lambda}}$ when $D > \lambda$.

In the case of an electric dipole, therefore, the wave impedance is proportional to $\frac{1}{R}$ and normally larger than 377Ω. In the case of a magnetic loop, the impedance is proportional to R, usually less than 377Ω. This is expressed in figure 2.3, based on similar diagrams found in [18] and [17] derived from equations in [16].

This necessitates that all measurements are done in the far field, so that the $\frac{1}{R}$ dependence can be preserved. This is particularly relevant for the working volume considerations when using a reverberation chamber. In the near field, the SE of the material needs to be considered separately for magnetic shielding and electric shielding, i.e. it depends on

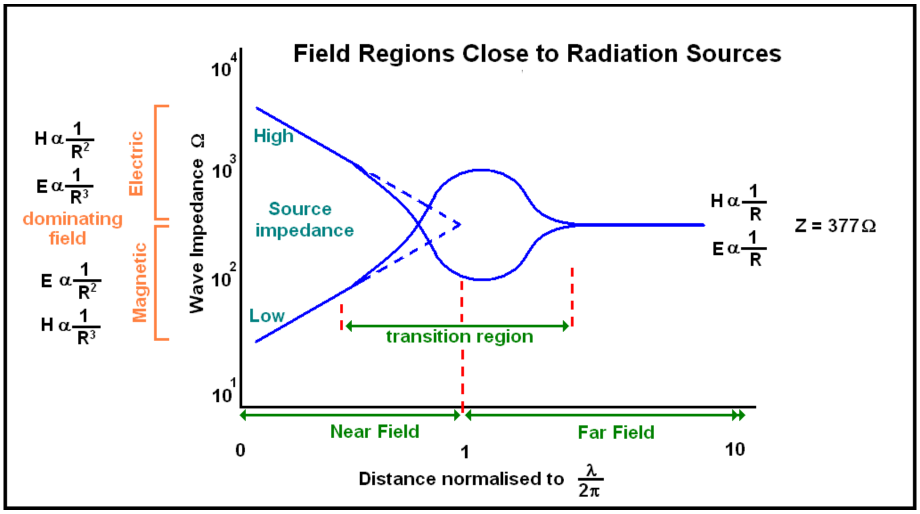

Figure 2.3: Change in Impedance as a function of distance from a dipole source.

whether the source is magnetic (low wave impedance) or electric (high wave impedance). In this work, the frequencies used are high enough to ensure far field criteria are easily met. At 1GHz (the wavelength is 300mm) for example the far field distance approximation of $\frac{\lambda}{2\pi}$ is 48mm when the antenna is assumed to be small, and 2.4mm using a 19mm monopole antenna and the $\frac{2D^2}{\lambda}$ approximation. However, due to the nature of the fields inside a reverberant volume, this far field approximation is not applicable to enclosures and chambers.

The concept of an 'electrically large' object is viewed as one that is more than $\frac{\lambda}{10}$ (for antennas) [19]. In enclosure terms this is expanded to mean a multi-moded enclosure [20], i.e. there are sufficient modes for the statistical approach to be valid. It is worth noting at this point that the above discussion of near and far field situations applies for antennas in free space, and that the behaviour in an enclosure is different, and it is considered sufficient to be at a reasonable distance from the walls, normally stated as $\frac{\lambda}{4}$ [21][22].

2.4 Anechoic and Semi-Anechoic Chambers

An anechoic (literally meaning echo-free) chamber is an enclosed volume in which any internal reflections of internal electromagnetic waves are minimised by the application of radio absorbing material (RAM) to the inside of the walls. Anechoic chambers are usually built as a screened room, meaning that the internal environment is separated from the external electromagnetic environment, providing a repeatable test and measurement environment. Anechoic chambers can be used for measuring electromagnetic emissions of electronic equipment; they also allow immunity testing by means of plane wave illumination of the EUT. This is achieved by transmitting power into the chamber, with either a wall-mounted or free standing antenna; the RAM on the insides of the walls helping to minimise any reflections. An example of an anechoic chamber can be seen on the right of figure 2.4. In an anechoic chamber, the RAM can be either in the form of ferrite tiles for use up to around 1GHz, or triangular section carbon loaded foam for frequencies higher than that; the absorption properties being dependent on the construction of the absorber, the density of the carbon foam and the size of the absorption cones. It is this absorber that limits the useful size of the anechoic chamber, because the pyramids have to be increased in size as the required frequency is reduced. This is due to the fact that the pyramidal absorber is at its most efficient when the 'cone' of the pyramid is $\frac{\lambda}{4}$ [23]. A full anechoic chamber has RAM applied to all the internal walls, whereas a semi-anechoic chamber has a reflective floor with no applied RAM, analogous to an OATS (Open Area Test Site), A semi or fully anechoic chamber has the added advantage over an OATS of the ability to use high field strengths for immunity testing without the public interference problems that would arise from such a measurement on the OATS.

Due to the nature of the anechoic chamber, and the possibility of high directivity of the EUT, the EUT is rotated 360^o around a vertical axis relative to the external measurement antenna in order to fully illuminate all sides. This rotation has to be performed during both emission and immunity measurements. For a full characterisation of an enclosure then it would be beneficial to also perform a 360^o scan around a horizontal axis, however this is somewhat impractical and so is not usually done. The anechoic chamber used in Chapter 7 is a fully anechoic shielded room of dimensions 4.70m $\times$ 3.00m $\times$ 2.37m. The way round the need for moving the EUT in an intermediately sized chamber, i.e. a chamber that only has space for a single antenna and/or no space for antenna scanning, is to use a reverberation rather than an anechoic chamber.

2.5 Reverberation Chambers

A reverberation chamber is a particular variety of screened room that has highly reflective internal walls. The chamber has a high quality factor, termed $Q-$factor, and is intended to create a statistically uniform, isotropic and randomly polarised internal electric field.

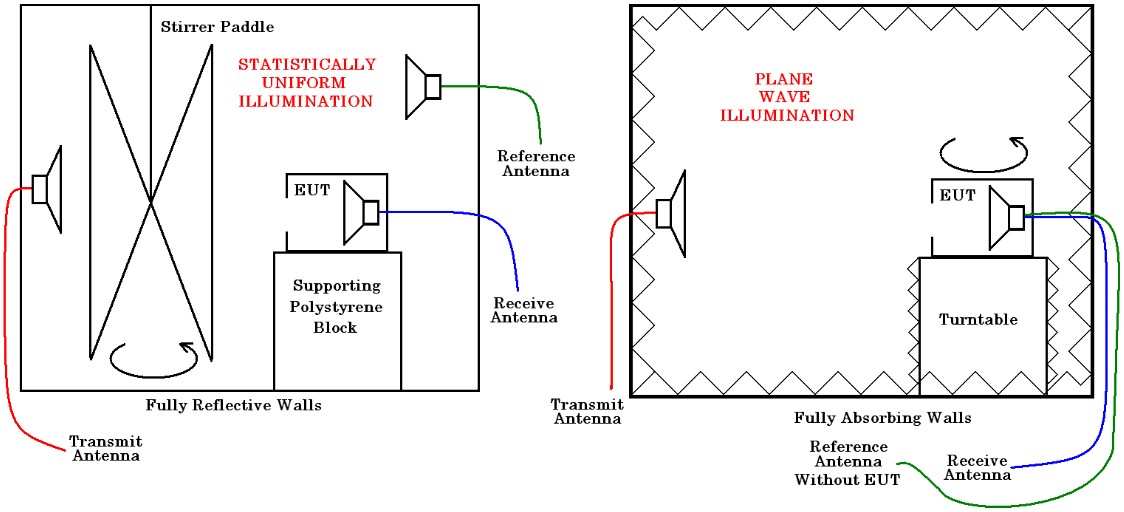

Figure 2.4: Schematic diagram of screened rooms, with the reverberation chamber on the left and the anechoic chamber on the right

This is achieved by multiple reflections within the chamber, combined with stirring, hence the term reverberation. The construction of the chamber enables the high $Q-$factor and multiple reflections, as the internal walls are covered in highly conductive (and therefore electromagnetically reflective) material, such as zinc galvanised steel. It is possible to mode stir (continuously varying the boundary conditions) or mode tune (discretely vary the boundary conditions) in order to achieve statistically average uniform fields, as minimal variation of boundary conditions within the chamber results in large field variations at fixed points inside the chamber. This allows the EUT to be placed anywhere within the working volume of the chamber. The reverberation chamber used in this work is installed in the Physical Layer research group at the UoY, and is a double-skinned sealed zinc galvanised metal box of dimensions 4.70m $\times$ 3.00m $\times$ 2.37m. It can be seen in figure 2.5. There is a door in one of the sides that is fully shielded; this chamber can be used as a reverberation chamber down to around 300MHz. The EUTs used here are substantially smaller than this chamber, with long side dimensions ranging from 0.1m to 0.5m. A schematic of a reverberation chamber can be seen in the left of figure 2.4. The following sections examine the workings of a reverberation chamber in more detail. Although not prevalent in EMC testing standards, reverberation chambers have been shown to be an excellent way of obtaining maximum emitted power and of providing a high field level with relatively small initial expense [24][25][26].

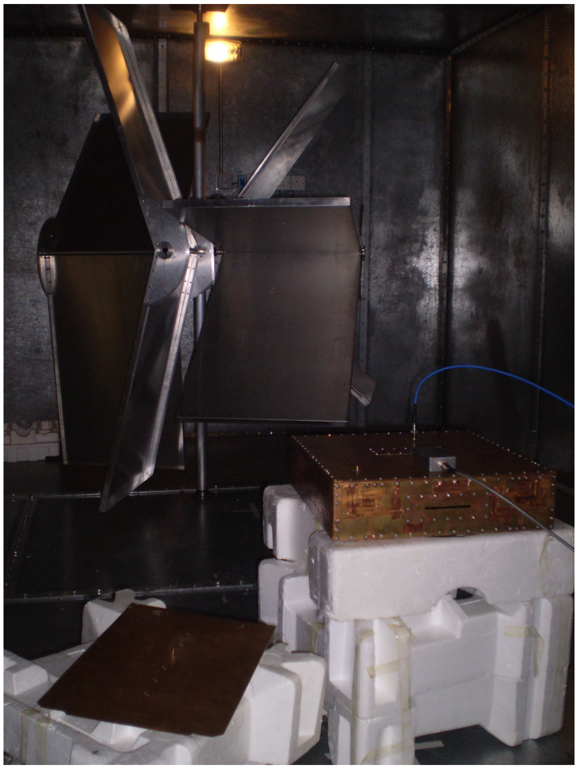

Figure 2.5: The reverberation chamber as used in the majority of work in this thesis. This is set up as per the nested chamber method - see section 2.5.1 and figure 2.6

2.5.1 Nested Chamber Method of Measuring Shielding Effectiveness of Enclosures

The method for measuring the SE of enclosures outlined in IEC-61000-4-12 and in both IEEE 299 and 299.1 is the nested chamber method [4], [5], [27]. This involves situating the enclosure inside the chamber and using both as reverberant volumes. For material shielding, a single large aperture between the two chambers can be covered with the material under test. The received power within the chambers is measured with and without the material present, thus the SE of the material can be measured. This method can be adapted to measure the SE of enclosures by measuring the received power inside and outside the EUT. The equations shown previously (section 2.8, equations 2.4 and 2.20) are used for this, meaning both a reference measurement and a shielded measurement needs to be taken. A nested chamber measurement setup for measuring SE of enclosures as outlined in [5] and [27] is shown in figure 2.6. In a nested chamber with two empty reverberant volumes (although a chamber with empty EUT inside is still viewed as empty, this is not the case if the EUT is loaded [28]) the SE of the enclosure is dependent on the size and number of apertures in the enclosure [29].

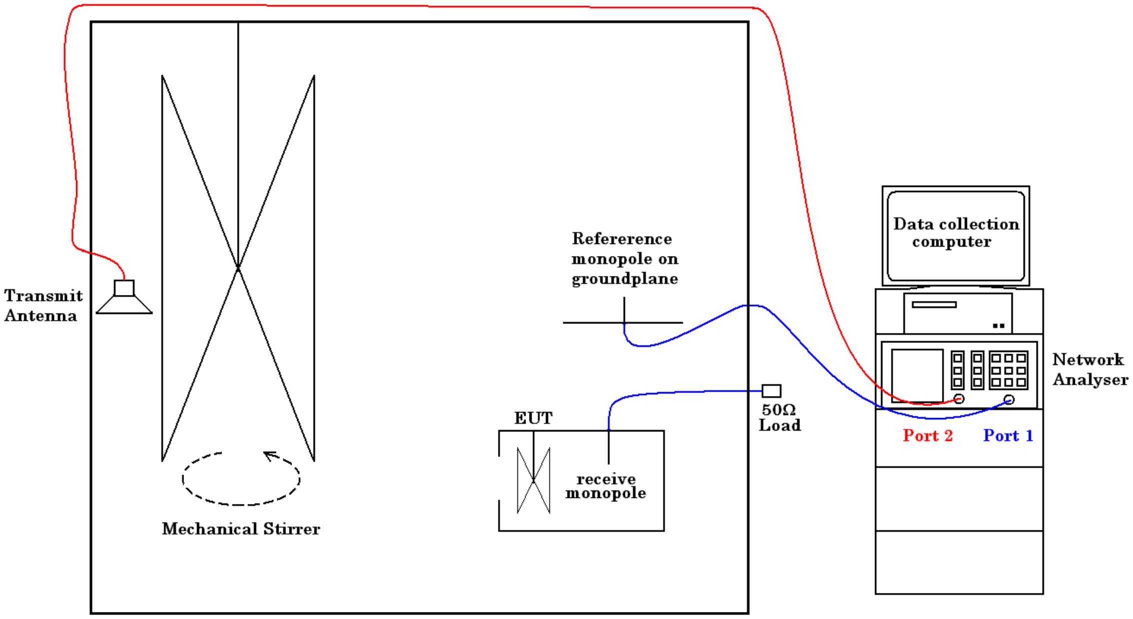

Figure 2.6: Schematic of nested reverberation chamber used for enclosure SE measurements

As can be seen from figure 2.6, Port 1 on the Vector Network Analyser is used to receive data from both inside and outside the EUT, Port 2 is used to transmit. These are then used in equations 2.4 and 2.20. Port 2 is used to transmit into the chamber and the transmit antenna is oriented so as to reduce the probability of a direct path. The measurement is controlled by software on the data collection computer. This has the capacity to move the stirrer to a single position and then trigger the network analyser, which performs a measurement whilst the the stirrer is stationary at this position. The S-parameter data for this stirrer position is saved to disk, then the process repeats for a user defined number of positions. Post-processing of data is done in MatLab. Some examples of the code used can be seen in the Appendix, Chapter 10.

2.5.2 Modes and Mode Stirring

If the walls of the cavity in question are highly reflective, as in the case in a reverberation chamber, then in a steady state environment (such as a chamber with a stationary paddle), a number of electromagnetic standing waves will be set up in the cavity [30]. These standing waves are known as modes, and are dependent on the size of the enclosure and also the frequency of the EM wave. For an electrically large reverberant cavity with dimensions $a \times b \times c$, resonant modes are established at distinct frequencies f_{mnp} (in MHz) , described by the following well known Helmholtz equation for a parallelipiped structure, where c_0 is the speed of light in a vacuum [31]:

$$f_{mnp} = \frac{c_0}{2}\sqrt{\left(\frac{m}{a}\right)^2 + \left(\frac{n}{b}\right)^2 + \left(\frac{p}{c}\right)^2} \tag{2.6}$$

From equation 2.6 the frequencies of the lowest resonant modes in Hertz, where one of the three orthogonal mode numbers m, n, and p, is zero, can be deduced: the lowest resonant frequency being controlled by the volume of the cavity. Therefore it is obviously beneficial for maximum measurement potential to have as large a cavity as possible, in order to lower the frequency of the first resonant mode. In most labs, the size of the reverberation chamber is limited by the space available and the cost of construction.

Reverberation chambers are rarely used near the first resonant mode, as with only a few modes present, the statistical uniformity of the electric field is very low [22][32], and the point of the reverberation chamber (namely to provide a statistically uniform electromagnetic environment) is missed. To allow the chamber to perform as intended, there is a limit on the lowest usable frequency (LUF). A rough approximation, assuming that $a > b > c$, for the LUF is three times the lowest resonant frequency f_{110} [31][33]. However, it is regarded as a general rule, that the lower frequency limit for statistical uniformity is the frequency below which 60 modes exist inside the reverberant cavity [14].

The number of possible resonant modes N_m below a particular frequency f in an enclosure of volume V is given by the analytical expression known as Weyl's law, shown in equation 2.7. This can be obtained numerically from equation 2.6 [31].

$$N_m = \frac{8\pi V f^3}{3{c_0}^3} \tag{2.7}$$

A more exact form of Weyl's law for rectangular cavities giving the number of modes N_m below a frequency f, for an enclosure of volume V and side dimensions a,b, and c is given in [34] and shown in equation 2.8:

$$N_m = \frac{8\pi V f^3}{3{c_0}^3} - \frac{(a+b+c)\,f}{c_0} \tag{2.8}$$

Two things are needed to obtain the statistically uniform aspect involved with reverberation chambers: sufficient modes and effective stirring. The modes are stirred, either mechanically via a motorised stirrer [31], or electronically by scanning the measuring frequency [35]. Although not used in this work, antenna stirring and load stirring are also options [36],[37],[38], as is stirring by moving the walls of the reverberant volume [39], and hybrid systems as in [40]. The effect that any stirring has is to change the boundary conditions in order to set up different mode patterns inside the cavity. If at least 60 modes are excited below the test frequency [14], [18], [41], and if the (in the case of mechanical stirring) paddle is large enough [42] and moves enough to perturb the eigenvalues, then effective stirring will occur.

A useful measure is D_m, the mode density (per Hertz), obtained by differentiating N_m with respect to f, and shown in equation 2.9.

$$D_m = \frac{8\pi V f^2}{{c_0}^3} - \frac{(a+b+c)}{c_0} \tag{2.9}$$

Mode density increases with the square of the frequency, so it can be seen that higher values of f are beneficial in obtaining high mode density, and therefore being able to imply higher field uniformity. This is one of the reasons why reverberation chambers are effective at high frequencies.

The actual number of modes in a reverberant cavity depends on the mode density and the bandwidth covered by each mode [32]. The overmoded condition, which is desirable for good field statistics, is not purely dependent on the number of modes but is also linked to the number of modes within a -3dB bandwidth of a dominant mode [32]. The Rayleigh distribution of the magnitude of individual field components (see section 2.6) is also dependent on the ratio of the mode bandwidth to the mode density being significantly larger than 1 [22].

2.5.3 Mechanical Mode Stirring

Mechanical mode stirring involves moving a large metallic paddle within the volume of the reverberation chamber. Two types can be used, mechanical mode stirring where the paddle is turned continuously, and mode tuning where the stirrer is stopped while the frequency response of the chamber or system is measured [36]. The chamber used here is always mode tuned. Mode tuning is a more satisfactory as the network analyser can be set to take slow and accurate measurements with a small IFBW, however this is a more time intensive system than the mode stirring method. The mode tuning method also differs in that the $Q-$factor and field levels cannot change while the data is being read, as the electromagnetic environment is in a steady state. The way round this limitation when mode stirring is to take the measurements very quickly. There is no set usage though, some individuals advocate continuous stirring while others advocate stepped [36]. Due to the statistical nature of the reverberation chamber, as long as the stirring is effective and predictable then the measurement should be satisfactory. The paddle has to occupy a significant volume of the chamber, practically limited by still needing a volume in which to place test equipment [42]. The paddle used in the University of York chamber can be seen in figure 2.7. If the paddle is too small, the boundary condition and therefore the mode pattern will not be modified to a large enough extent to allow independent samples. The paddle is moved in steps using a user controlled stepper motor and the frequency response taken at each step; these results are then averaged over a full stirrer rotation to give an average received power. It is this average received power that is used in the equations used to calculate SE. In the University of York chamber, the stepper motor is situated on the ceiling of the chamber. The motor control system is designed and integrated into the measurement system so that the paddle is perfectly stationary when the frequency response is taken to ensure maximum accuracy.

Figure 2.7: The stirrer paddle used in the reverberation chamber.

The paddle stirrer method changes the electrical shape of the chamber, and therefore changes the conditions for creating standing waves. This changes the mode pattern within the chamber. The effect of the mechanical mode stirring is to change the positions of the maxima and minima associated with the electric field inside the chamber. Over one rotation of the paddle, if enough stirrer positions are used (see 2.5.5) then the field inside the chamber can be viewed as statistically uniform. Any EUT that is placed within the working volume of the chamber will be uniformly illuminated in this case. The working volume of the chamber is generally said to be the volume more than $\frac{\lambda}{4}$ [22][24][43] from the walls. Within the working volume, above 400MHz, the standard deviation of the mean field power over one rotation (or other means of averaging) at any particular point should be within within 3dB of any other point for an effective chamber, this is part of the reverberation chamber guidelines in IEC 61000-4-21 [4]. In addition to that, MIL 285 [9] states that the difference in levels should be 20dB between the maximum and the minimum over one stirrer rotation ([9] advocates mechanical stirring). All the measurements are done well above 400MHz in this work; average statistical field uniformity tends to improve as the frequency increases [35].

2.5.4 Electronic Mode Stirring

Electronic mode stirring utilises the fact that different frequencies excite different mode patterns; this can be seen by examining equation 2.6. The frequency spacing is analogous to the paddle stirrer step size, with the similar proviso that enough points are needed to enable the statistics to function correctly. This works due to the fact that the mode patterns are highly frequency dependent [35][44][45]. There are some useful criteria set out for electronic mode stirring in [35], they are summarised here.

- The measured spectrum should be as flat as possible across the measurement bandwidth
- The signal should be ergodic or loosely time stationary over the averaging period
- The centre frequency and measurement bandwidth should be variable over a wide parameter to make the test flexible
- The average output power of the source should be variable in order to take into account varying cavity sizes and $Q-$factors

Electronic stirring (sometimes called frequency stirring) is implemented in this work after the data is obtained, as the measurement instrument is set up to give the correct frequency spacing between data points. This satisfies the second item stated in [35]; the third and fourth are less of a problem as there is only one size of external reverberation chamber being used in this work. The easiest way to implement frequency stirring is to average a frequency response over a suitable bandwidth (BW). There is a minimum bandwidth criterion shown in equation 2.10 [7] under which frequency stirring will not be effective.

$$BW >> \frac{{c_0}^3}{8\pi V_e f^2} \tag{2.10}$$

Equation 2.10 arises from the fact that there must be a significant number of modes within the bandwidth for the stirring to be effective; this links with the minimum number of modes and the LUF detailed earlier in section 2.5.2. There is a less well defined criterion for the maximum bandwidth, it is more that the user has to be careful not to go too far, as if the bandwidth is too large, the $Q-$factor of the enclosure may change significantly within the bandwidth [7].

2.5.5 Mechanical Stirring vs. Electronic Stirring, and choosing the step size

The main disadvantage of mechanical stirring as a method is that the time taken to obtain a result can be large, especially in a twin stirred environment, i.e. one stirrer in the chamber, another in the enclosure. This stems from the fact that there have to be enough data points in one rotation to be able to get enough for meaningful statistics. Standard error theory states that as more data points (N_s increases) are used to calculate the mean, the less error there is on the mean, and the closer the mean becomes to that of the ideal mean, where all the population is sampled, i.e. standard error $\propto \frac{1}{\sqrt{N_s}}$. Ideally there should be as many statistically independent points as possible. A statistically independent point is one that is not linked in any way to the points on either side of it. In this case, it means that the movement of the stirrer paddle has got to be large enough to ensure that there is a significant change in the boundary conditions. If the movement is too small, then a phenomenon known as tracking is observed on a phase-quadrature plot of the received data, as in figure 2.8.

It can clearly be seen in figure 2.8 how the points are linked in this example, where the stirrer step is too small for the wavelength of the radiation used; the points are not statistically independent, and tracking is seen. This is a direct consequence of too many stirrer positions, which can of course be reduced. Using the method of calculating statistical independence given in equation 2.11, then taking every sixth measurement point from figure 2.8 results in a statistically independent set, bearing in mind the limitations of this method mentioned in the last paragraph of this sub-section.

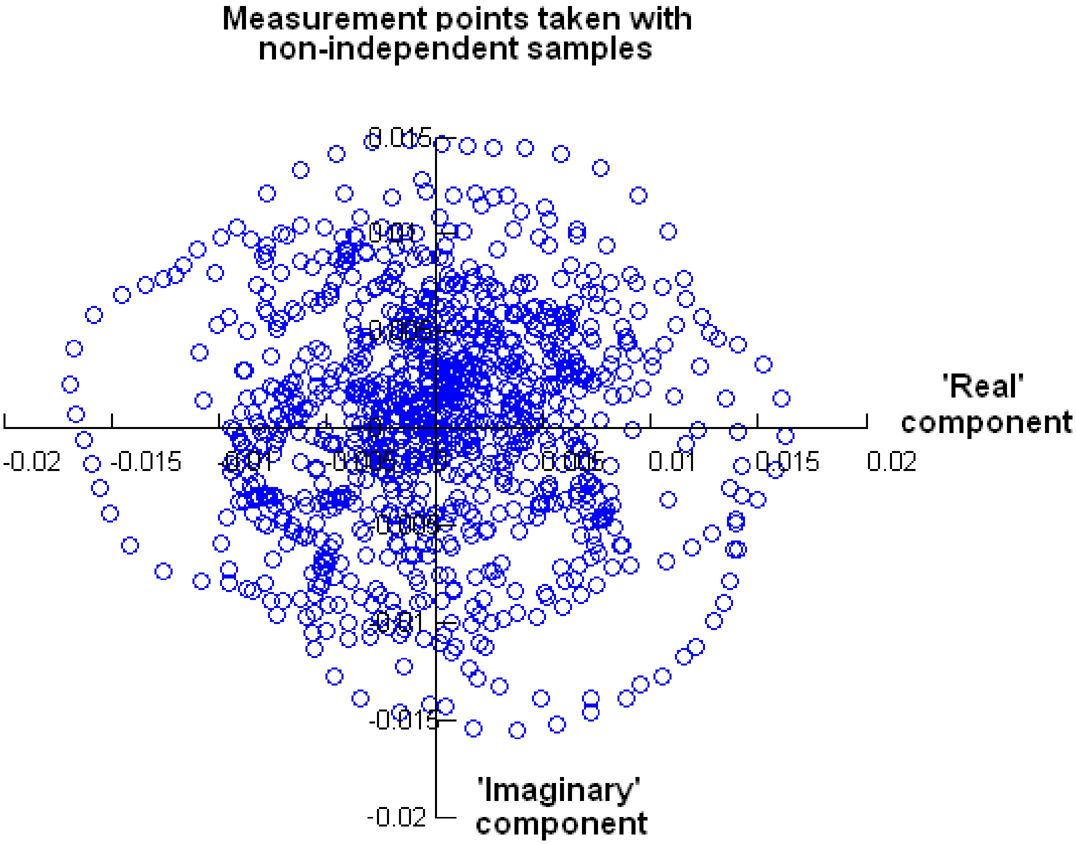

Figure 2.8: Evidence of tracking on points that are not statistically independent. The test frequency is 8GHz.

A point to note here is that using the same number of stirrer positions at a lower frequency results in no observable tracking. This can be seen in figure 2.9. This is because the movement at the outer edge of the paddle is larger relative to the wavelength of the test frequency at lower frequencies, meaning greater perturbation of the fields for each paddle movement and a higher level of statistical independence.

If insufficient stirrer positions are used, there are not enough points to make meaningful statistical distributions; therefore it can be seen that it is important that the number of stirrer positions is chosen carefully. Another issue with numerous stirrer steps is time. If, for example, the vector network analyser (VNA) used to obtain the results takes a minute

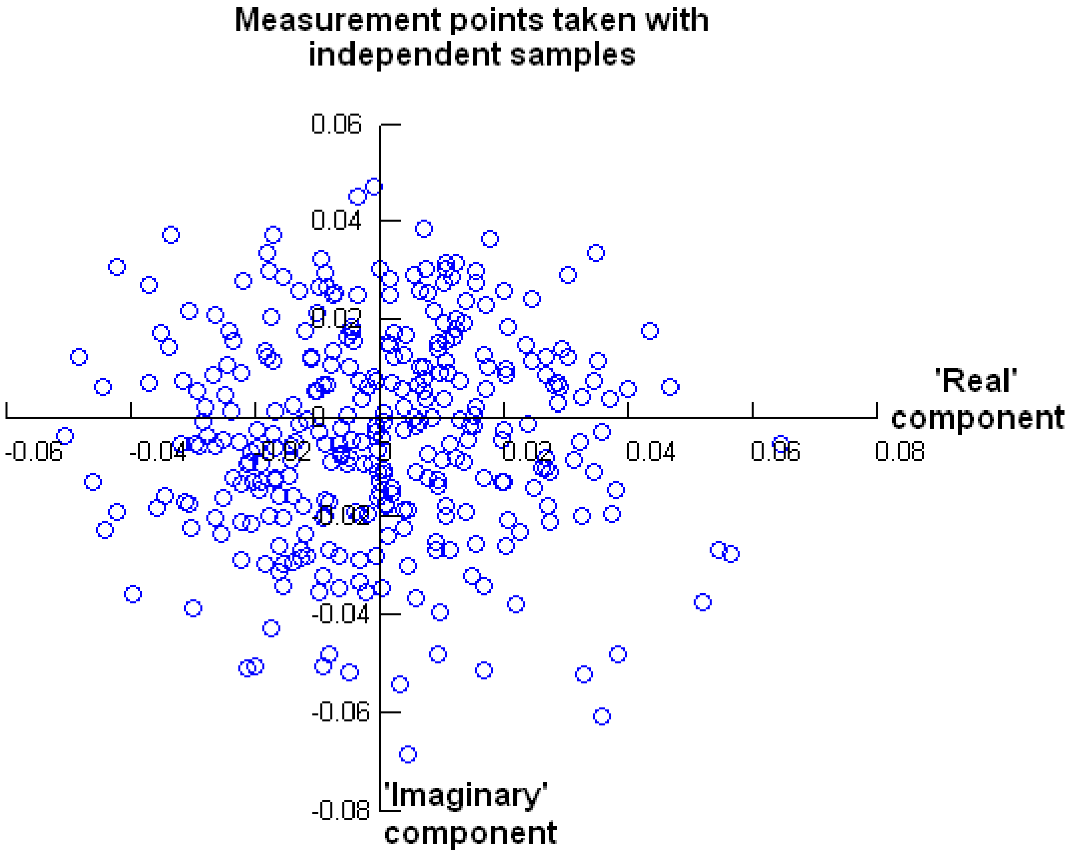

Figure 2.9: No tracking evident using the same stirrer step size as in figure 2.8 but using a 3GHz test frequency

to take data at each stirrer position from the chamber, then, if all the positions on the UoY stirrer are used, the measurement will take at least 6400 minutes. There also has to be time allowed for the stirrer to move and also for it to stop moving. The stirrer program used was written including a wait time in order to take account of the 'rebound' effect from the large inertial mass of the paddle stretching the belt that drives it after the stepper motor is stopped. This leads to an enormous amount of time needed to obtain one result: over 100 hours for this example. The only ways to reduce the time taken are to use fewer stirrer positions, or reduce the accuracy of the VNA by reducing the sweep time. The time problem is exacerbated when a multiple stirrer setup is used, and this limits the number of steps that can be used if the experiment is to be done quickly.

The advantages of mechanical stirring are that the statistics are well understood and the measurements are repeatable. The disadvantages of frequency stirring are in the fact that the stirring bandwidth is limited. The use of a frequency-modulated single frequency that give spaced frequency peaks can reduce this effect. This new way of frequency stirring is covered in Chapters 3 and 4. Frequency stirring has the advantage of being a much faster method, however the underlying statistics are not as well understood as those of the MS method; this makes it more difficult to troubleshoot anomalous effects in the results. Frequency stirring is also limited by the minimum frequency criterion. It appears to be more critical to establish enough modes when results are taken using frequency stirring, with possibly more than 60 modes being needed below the test frequency f to create a reliable statistical environment. This hypothesis is dealt with in Chapter 4.

The number of stirrer positions required is examined statistically in [46], which states that the number of independent stirrer positions is usually obtained using an autocorrelation method for the steps size of the stirrer. The EMC standard that involves reverberation chambers (IEC61000-4-21) [4] uses this method of calculating independent stirrer steps. IEC61000-4-21 states that the samples are independent if the first order autocorrelation function (ACF), seen in equation 2.11 [4][46], is less than $1/e \approx 0.37$.

$$r = \frac{covar(x,y)}{\sqrt{var(x)}\sqrt{var(y)}} \tag{2.11}$$

In equation 2.11, r is calculated using a single measured data set x, and a data set y, which is the same data set as x but shifted by one point. The autocorrelation operation results in a measure of independence due to the fact that the measured data set is compared with itself, so that the relationship between one point and its neighbour can be examined. $covar$ and var are the covariance and variance operators. The data set is normally taken over one 360^0 stirrer rotation.

It is suggested in [46] that this approach is only realistic for sample sizes less than 100. In the informative part of [4] the cutoff point between the result of this method being realistic and being unrealistic is identified as when the number of samples is equal to 450. In [46], a second order ACF is used to reduce the measurement uncertainty by increasing the knowledge of sample independence.

2.5.6 The $Q-$factor

The $Q-$ or quality factor of a reverberation chamber can be used as a measure of chamber performance, as the walls are made of real metallic materials that allow some EM penetration. For flat sheets of real wall material, the $Q-$factor can be related to the skin depth and the surface resistance [47][35][48], seen in equation 2.12. For reverberation chambers, this is a useful measure of the physical performance capability of the chamber, as a low $Q-$factor resulting from low reflectivity or highly absorbent walls will indicate that the reverberant nature of the chamber is reduced.

The $Q-$factor of an empty rectangular reverberation chamber is given in equation 2.12

$$Q_1 = \frac{3}{2}\frac{V}{S_a\delta} \tag{2.12}$$

where V is the volume of the chamber, S_a is the surface area and δ is the skin depth given in equation 2.1. The $Q-$factor in this equation is dependent on the size and the construction material of the chamber. For a more accurate representation of the $Q-$factor, useful in the case where the chamber is either loaded with RF absorber to some extent or has an antenna or aperture present, some aspects other than the walls need to be taken into account. It is shown by Hill et al [49] that for a given enclosure there is a composite $Q-$factor that takes into account the various loss mechanisms present in a real chamber. As the $Q-$factor is a measure of the ensemble average (over all stirrer positions) energy stored in the chamber [24][49][50], then the composite $Q-$factor can be viewed as essentially accounting for the various losses within the chamber. The composite $Q-$factor Q is shown in equation 2.13.

$$Q^{-1} = Q_1^{-1} + Q_2^{-1} + Q_3^{-1} + Q_4^{-1} \tag{2.13}$$

Due to the reciprocal nature of equation 2.13, the smallest of the values of Q_1, Q_2, Q_3 and Q_4 will dominate; i.e. the largest loss mechanism resulting in the lowest $Q-$factor will dominate. It is worth noting that these $Q-$factors are ensemble average over all stirrer positions. Details of the statistical nature of the $Q-$ factor are given in [51].

The various loss mechanisms shown in equation 2.13 are as follows. Q_1 represents the wall losses, shown in equation 2.12, and can be used as the sole measure of $Q-$factor when all the other reciprocal $Q-$factor components in equation 2.13 are small enough to be ignored, for example in a completely sealed, empty enclosure. Q_2 represents the losses resulting from any absorption within the chamber, for example any lossy material or RF absorber within the chamber. The absorber $Q-$factor component is described in equation 2.14 [49]:

$$Q_2 = \frac{2\pi V}{\lambda < \sigma_a >} \tag{2.14}$$

where λ is the free space wavelength, $< \sigma_a >$ is the absorption cross section, and again V is the volume. It is mentioned [49] that obtaining Q_2 is challenging due to the complicated frequency dependence of $< \sigma_a >$.

In many ways the most interesting component, Q_3 describes the aperture losses, simply the energy that is lost through having a hole in the reverberant cavity. This is more applicable to EUTs than full-size reverberation chambers, as the aperture losses in an effective test chamber should be very small, even though there will be apertures for purposes such as ventilation. Q_3 depends on the volume V of the chamber, the wavelength λ of the testing frequency and the transmission cross section $< \sigma_t >$ of the aperture, shown in equation 2.15

$$Q_3 = \frac{4\pi V}{\lambda < \sigma_t >} \tag{2.15}$$

For electrically large apertures, $< \sigma_t >$ is independent of frequency; meaning Q_3 is proportional to the frequency when electrically large apertures are present.

If the aperture under examination is of arbitrary shape and is assumed to be in a flat infinitely large conducting panel of zero thickness then aperture theory [52] provides a way of obtaining $< \sigma_t >$. Using the geometric optics approximation and restricting the integral over the incident elevation angles to $\pi/2$ (as the aperture is only exposed to the field on one side), a value for $< \sigma_t >$ can be obtained. This relationship turns out simply as equation 2.16 with A_a as the area of the aperture in m^2. This approximation is only valid provided the aperture is electrically large and non-resonant.

$$< \sigma_t >= \frac{A_a}{2} \tag{2.16}$$

The treatment of electrically small apertures is similarly derivable, however the cross section for a resonant aperture is not a simple relationship [49].

The value of Q_4 is related to the losses due to the energy absorbed by the measurement antenna(s), shown in equation 2.17. For the receive antenna, 16π is used; for the transmit antenna, 8π is used.

$$Q_4 = \frac{16\pi^2 V}{m_a \lambda^2} \tag{2.17}$$

The antenna mismatch factor m_a can be calculated from the reflection coefficient, obtained using the reflection parameters $S11$ or $S22$ for a two port network. The $S11$ parameter is a measure of how much power is reflected back towards the output of port 1 of the VNA: a well matched antenna such as a ridged horn will have a low mismatch and a low reflection coefficient.

In the majority of experiments carried out in this work, the EUT consists of an empty brass box. This means that the composite $Q-$factor can be reduced to Q_{EUT}, shown in equation 2.18. This is the $Q-$factor for an empty enclosure: the contributions from the losses across the EUT and the reciprocal contributions from the wall losses are small compared to the aperture Q_{AP} and antenna Q_{AN} losses.

$$Q_{EUT}^{-1} = Q_3^{-1} + Q_4^{-1} = Q_{AP}^{-1} + Q_{AN}^{-1} \tag{2.18}$$

2.6 Field statistics

Using the method of mechanical stirring, the raw data obtained from the receive antenna at each stirrer position is then averaged over all the positions used. As mentioned in section 2.5.2, there needs to be sufficient stirrer positions to allow the statistical treatment of the data to be valid. In a mode stirred chamber, it has been shown that the statistical probability density function (PDF) of the magnitude of the electric field averaged over all positions follows the Rayleigh distribution [7][31][53] [54], arising from the application of the root sum of the squares method to the normally distributed in phase and phase quadrature components of the field [21][55] [56][57] . The shapes of the PDFs obtained are shown in figure 2.10 and the mathematical forms are shown in table 2.1.

Hill demonstrates in [31] and [58] that in a reverberant environment the rectangular field components of a sinusoidal waveform E_x,E_y,E_z and H_x,H_y,H_z will have normally distributed in phase and phase quadrature components (which are measured by a network analyser as real and imaginary components). The waveform statement is true if the samples are taken over a statistically significant number of independent stirrer positions and makes the assumption that each point is uniformly illuminated with all phases and all polarisations. The rectangular components follow the form of equation 2.19, where the means of the distributions of the real and imaginary parts are zero, and their variances are equal.

$$E_x = E_{xr} + jE_{xj}, E_y = E_{yr} + jE_{yj}, E_z = E_{zr} + jE_{zj} \tag{2.19}$$

2.6.1 Reverberation Chamber Field Distributions

The magnitude of the rectangular field components in a well-stirred environment is assumed to be Rayleigh distributed and is obtained using the root sum of the squares method on the zero-mean normal distributions of the phase and phase quadrature components. As the reverberation chamber is not a perfect system, there is often a slight deviation from the true Rayleigh distributions predicted. The deviations manifest themselves as the appearance of a Rician distribution (seen in table 2.1) in the chamber or enclosure. This occurs due to the normally distributed phase and phase quadrature components having non-zero means, suggesting that the stirring is inefficient, and/or that there is a direct path present

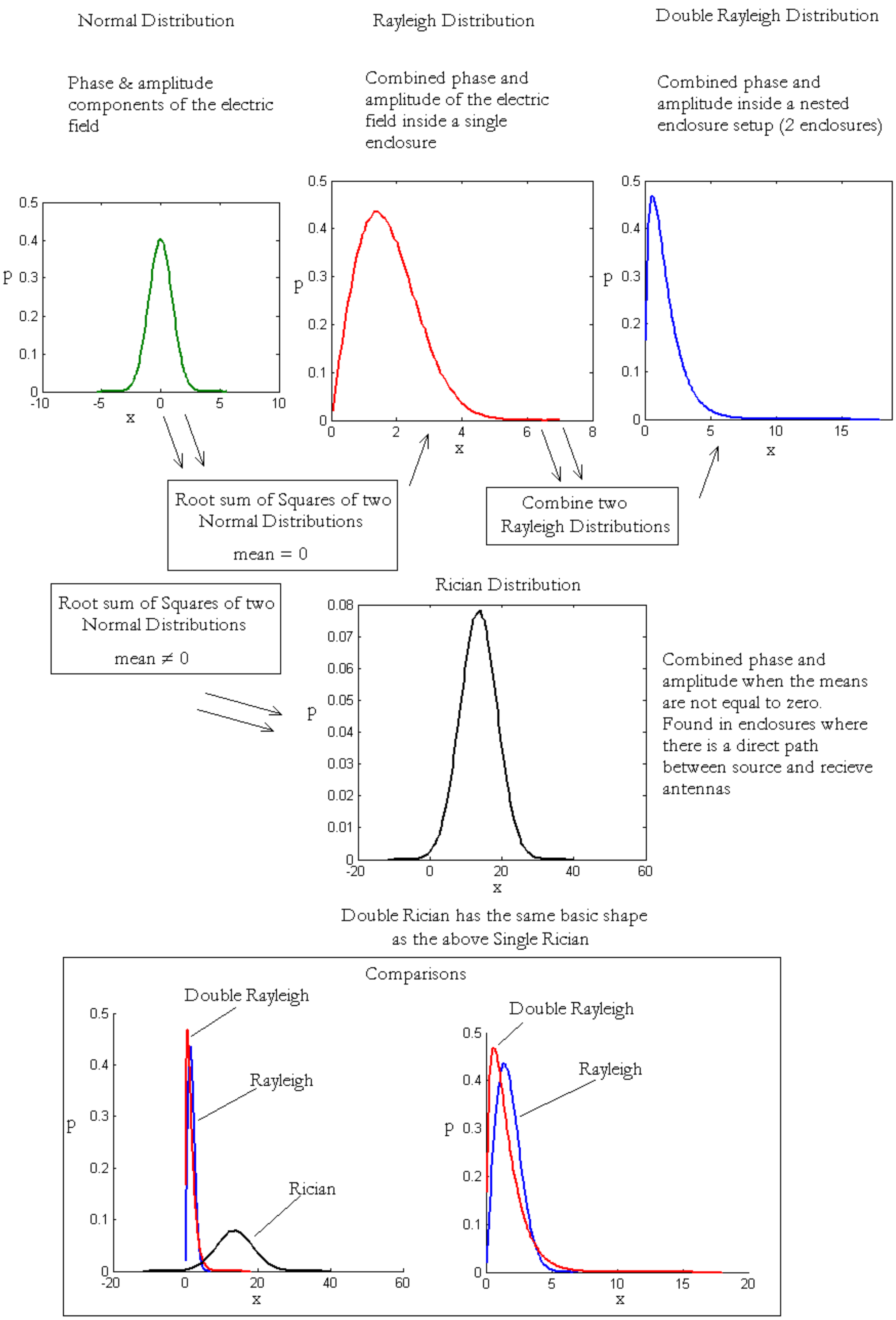

Figure 2.10: Distribution Overview

Table 2.1: Distribution Forms

Distribution	Form	Notes
Normal	$p(x) = \frac{1}{\sigma_v\sqrt{2\pi}}e^{\frac{-(x-\mu_m)^2}{2\sigma_v^2}}$	μ_m: mean σ_v: variance
Rayleigh	$p(x) = \frac{x}{{S_p}^2}e^{\frac{-x^2}{2S_p^2}}$	S_p: Scale Parameter
Double Rayleigh	$p(x) = \frac{x}{{S_p}^2}K_0\left(\frac{x}{S_p}\right)$	S_p: Scale parameter K_0: Zeroth order Bessel Function
Rician	$p(x) = \frac{x}{{S_p}^2}e^{\left(\frac{-(x^2+v^2)}{2{S_p}^2}\right)}K_0\left(\frac{xv}{{S_p}^2}\right)$	S_p: Scale parameter K_0: Zeroth order Bessel Function v: Peak offset from Reference

in the reverberation chamber. A direct path is a way that the radiation can couple directly to the receive antenna from the source, and can be considered as an unstirred component [59]. The size of the offset of the resultant Rician distribution and the relationship to the stirring effectiveness can be described using the Rician $K-$factor [60]. This effect is discussed in much more detail in Chapter 5.

When a reverberant enclosure is placed within a reverberant chamber, then the resulting distribution inside the enclosure is said to follow the double Rayleigh distribution form, seen in table 2.1[56][61], as any aperture connecting the enclosure and the chamber acts as a transmit antenna into the enclosure, setting up another set of Rayleigh statistics inside the enclosure. These two Rayleigh distributions combine to form the double Rayleigh. As with the Rayleigh distribution, this double Rayleigh can be used as a check for ensuring that the enclosure and chamber are being effectively stirred. This is covered in more detail in Chapter 5, where the development of the distributions present in an EUT is investigated further.

The distribution inside the inner enclosure in a nested reverberation chamber is not always Double Rayleigh, however, but is dependent on the size of any apertures that may be present in the enclosure. If the apertures are electrically large and/or there are enough of them, then the radiation will couple fully into the inner enclosure resulting in the two chambers behaving as one. This shows itself as a Rayleigh distribution in the inner chamber where a double Rayleigh would be expected under a situation where the reverberant environments are sufficiently electromagnetically separated. This field coupling results in differing shielding levels: high field coupling is equivalent to low SE and low field coupling is equal to a higher SE. The transition between Rayleigh and double Rayleigh in the inner enclosure seems to be a gradual one. It is also not fully understood how multiple apertures affect the outcome of the inner distribution; obviously the shielding is reduced if the size of the apertures is large enough but the way the distributions behave still merits investigation.

2.7 The Kolmogorov-Smirnov test

As the electric field distributions can be used to evaluate the effectiveness of the stirring, it makes sense to compare the obtained results against a simulation using a distribution test. The test used is the Kolmogorov-Smirnov (KS) goodness of fit test [62]. This allows the user to compare a simulated distribution with any given data set. It has the advantage over other goodness of fit tests as it can be tailored to any particular distribution. The KS test works by comparing the cumulative probability density function (CDF), of the data against the simulated CDF. A graphical representation of how the KS test works can be seen in figure 2.11.

Here, $F_0(x)$ is the simulated CDF, and the stepped function $F(x)$ is the CDF under test. The KS test looks at how far the CDF under test deviates from the simulated CDF. This deviation is d_a, and is specified when the test is set up, normally as 5%.

The differences between the curves are used as the measure of how well the distributions fit. A value for d_a is specified such that if the difference between the simulated CDF and the CDF under test is larger than d_a , the CDF fails the test and can be said not to be a fit to the simulated CDF. The KS test is used on the S_{12} data received on Port 2 of the VNA, as that should be Rayleigh distributed in a single enclosure. One of the advantages of the KS test is that it can be used to test any CDF, including Rayleigh, Double Rayleigh and Rician.

The main problem with the KS test is that it is unreliable in cases where the data has

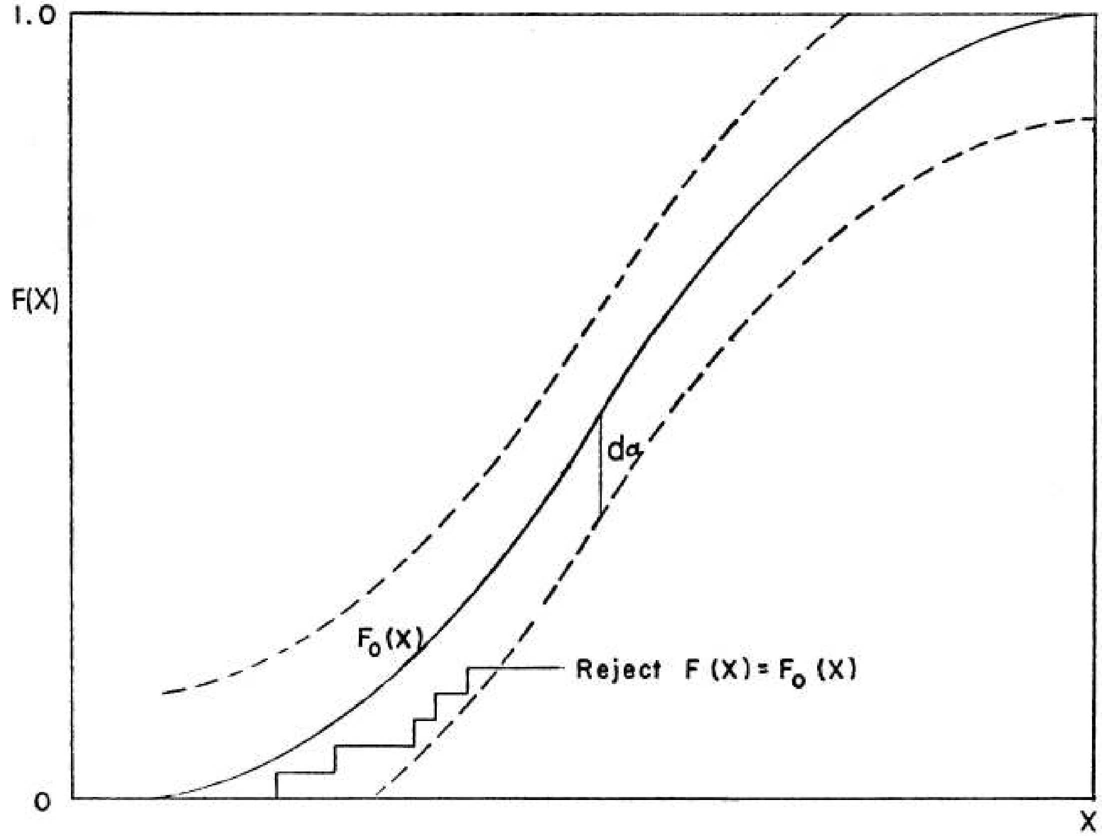

Figure 2.11: Graphical representation of the KS test.

been used to obtain the simulated CDF. The simulated CDF (in the case of a Rayleigh distribution) is calculated from the Rayleigh parameter, which is obtained from experimental data. Therefore the situation can arise where the KS test is testing the data against a CDF derived from the data; this can give unpredictable results. As a precaution against this, the KS test is applied multiple times on the occasions when it is utilised.

2.8 Shielded enclosures

A shielded enclosure, cavity, chamber or screened room can be of any physical size, and is designed to attenuate electromagnetic radiation to insulate the internal volume or contents against external electromagnetic effects. This also has the effect of containing any electromagnetic environment, for example, emissions from contents, or to establish a well-defined field needed for testing. Various apertures, vents and bulkhead connections are needed; these need to be designed so as to preserve the attenuation and therefore the level of shielding. The level of attenuation is referred to as the shielding effectiveness, or SE. Note that the SE of a flat sheet of material will not be equal to the SE of an enclosure made from the same material [18]. The reasoning behind the use of a screened room is to create a measurement environment that is entirely separate from changing external conditions, and that can be modeled and understood, but most importantly is repeatable between differing sites. The two forms of screened rooms used in this research are reverberation chambers and anechoic chambers.

2.8.1 Measurements in Reverberant Environments

As previously shown, (see section 2.3 and equation 2.4) the SE of an enclosure can be expressed as a simple ratio of powers. A more accurate measure of the SE than that expressed in equation 2.4 can be used when the shielding of an EUT is being examined. The so called corrected SE can be obtained by using the $S11$ reflection parameters from the measuring antenna, both inside and outside the EUT. This relationship is shown in equation 2.20 [7], and allows the reflections from cables, connectors and antennas to be accounted for in the calculation of the SE, and as such is more accurate.

$$SE_{dB} = 20 \log_{10} \left(\frac{< |S12_R|^2 > (1 - | < S11 > |^2)}{< |S12|^2 > (1 - | < S11_R > |^2)} \right) \tag{2.20}$$

The simple SE calculation assumes that, in both the chamber and the enclosure, the reflection coefficients and input impedances of the two measurement antennas are the same. The act of taking the ratio of the received powers will cancel any systematic errors out if they are indeed the same. This only works if the same antenna is used in both the chamber and the enclosure. Note that in a correctly calibrated VNA any cable reflections will be accounted for. In a measurement such as the ones performed in this thesis, for the different reverberant environments, i.e. a small enclosure and a large chamber, the reflection coefficients for antennas are not necessarily the same. The antennas are also sometimes not the same, e.g. an external horn antenna and an internal monopole antenna, hence the use of the corrected SE. A well matched horn antenna is used as the transmit antenna in the outer chamber in the majority of the work here.

In equation 2.20, the setup (shown in figure 2.6) is such that the receive antenna is assigned to Port 1 of the Vector Network Analyser (VNA), with $S11_R$ being the reflection coefficient from the reference monopole and $S11$ the reflection coefficient from the EUT monopole. $S12$ is the transmission into Port 1 from Port 2 via the EUT monopole, and $S12_R$ is the transmission into Port 1 from Port 2 via the reference monopole. This is shown in figure 2.12. Wherever possible, this corrected SE equation is used in this work as it gives more accurate results. This corrected measure of SE cannot be used with measurements that use a separate source, as the reflection coefficient data is not readily available when using a spectrum analyser.

Equation 2.20 is more accurate than the simple SE power ratio calculation because it takes into account the reflection from the antenna, and therefore takes into account the antenna mismatch. This is important because the monopole antennas that are used inside small enclosures can be more reflective than expected due to the enclosure influencing the input impedance [7].

The way that equation 2.20 is obtained is covered in detail in [7], and summarised here. Figure 2.12 is included for clarity. The starting point is to establish that the measurement of an unmatched monopole antenna $< |S21_m|^2 >$ will be less than the measurement of a well matched horn antenna $< |S21_h|^2 >$ because energy is lost in the mismatch between the monopole antenna and the cable that feeds the antenna. This necessitates a correction factor on the measured monopole signal in order to mimic a well matched antenna. The correction factor is shown in 2.21 and is obtained using the free space reflection coefficient of the monopole antenna $S1_m1_m$, measured as $< |S1_m1_m|^2 >$ in a reverberation chamber.

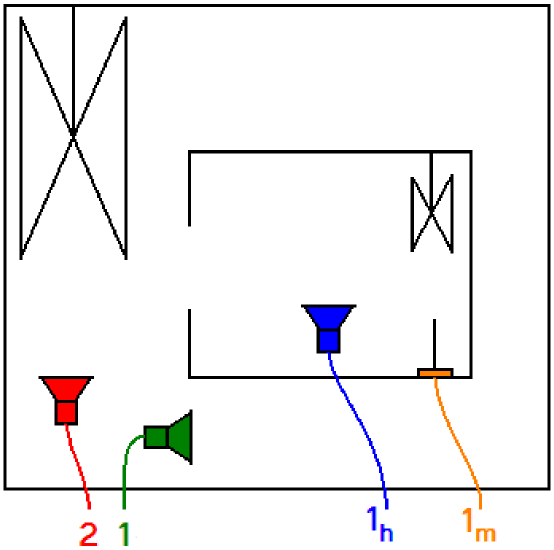

Figure 2.12: Nomenclature of ports for reference when considering corrected S parameters for the calculation of SE. Power is transmitted into the chamber on port 2, the unshielded measurement on port 1, and the shielded horn on port 1_h and monopole on 1_m

$$C = \frac{< |S1_m 2|^2 >}{1 - |S1_m 1_m|^2} \tag{2.21}$$

Using this correction factor to make the monopole measurement equivalent to the well matched horn measurement results in two comparable equations for SE, 2.22 and 2.23:

$$SE_{horn} = \frac{< |S1_h 2|^2 >}{< |S12|^2 >} \tag{2.22}$$

$$SE_{monopole} = \frac{C}{< |S12|^2 >} \tag{2.23}$$

Equation 2.22 is equivalent to 2.2, and equation 2.23 can be seen to be the corrected SE when using one monopole, in this case the monopole in the enclosure.

Applying the mismatch correction to the antenna at Port 1 as well (which in the measurements used here, is sometimes a monopole on a ground plane) results in the equation shown in 2.24, which can be seen to be equivalent to equation 2.20.

$$SE_{dB} = 20 \log_{10} \left(\frac{< |S1_m 2|^2 > (1 - | < S11 > |^2)}{< |S12|^2 > (1 - | < S1_m 1_m > |^2)} \right) \tag{2.24}$$

The naming convention used in equation 2.20 is used throughout this thesis, however it is easier to see the how the application of the correction works with the different nomenclature used in this section.

In an enclosure, it is useful to examine the functionality of a wall mounted monopole, as these are used to measure the field inside the EUTs used throughout this work. Measuring the received power on a monopole attached to an inside wall of an EUT (i.e. outside the working volume) is shown to be equivalent to a monopole in the working volume of the EUT in [7].

It is shown in [31] that the average power $< P_r >$ received by an antenna is independent of position and orientation within an electrically large enclosure, and can be written as equation 2.25,

$$< P_r >= \frac{1}{2}\frac{E_0^2}{\eta_0}\frac{\lambda^2}{4\pi} \tag{2.25}$$

in which E_0^2 is the mean square electric field, η is the free space impedance and λ remains the wavelength. In [7] it is shown that the average received power measured using a wall mounted monopole is equivalent to that shown in 2.25. This is also true for an electrically short monopole.

Chapter 3

Separate Source Measurements - Uniformity, Shielding Effectiveness and Frequency Modulation

3.1 Chapter Introduction

This chapter looks at the development of an instrument that could be used to create statistically uniform electric fields within an electrically large but physically small conducting enclosure. The rationale behind this aspect of research was to arrive at the situation where this instrument would be sold to an end user as a complete instrument with the ability to create uniform electric fields within enclosures. Currently, York EMC Services produce and market a range of instruments for test site calibration and certification, one of which is the Comb Generator Emitter (CGE-02), a generator that is designed to produce a ‘comb’ of discrete frequencies with switchable frequency spacings of either 250MHz or 256MHz from 250MHz to 26GHz [63]. There is scope for this instrument to be used alongside YES’s existing lineup to allow customers to carry out calibrated testing of field uniformity within small equipment enclosures. In this Chapter, the CGE is mechanically stirred inside an enclosure of brass construction which is 120mm x 120mm x 40mm, and has 4 SMA (Sub-Miniature revision A) monopoles mounted on the internal walls that can be used to monitor the field inside the enclosure. It is worth noting that here, the enclosure is empty of any intentionally absorbing contents, the only contents being the CGE, the stirrer and the measurement antenna(s). In addition to the instrument development, this chapter lays down some groundwork for the rest of the work to be based on when considering the measurement of shielding in enclosures.

3.2 CGE-02 and Experiment Setup

The CGE-02 can be used in two modes with different spacing between frequency peaks, either 250MHz (mode 1) or 256MHz (mode 2). This is simply selectable by using a switch on the bottom of the CGE-02 [63], and allows the CGE to ‘fill in’ parts of the spectrum at higher frequencies if both modes are measured. This results in a lower power requirement when compared to generating a continuous spectrum. The lower power requirement stems from the fact that a relatively small number of evenly spaced frequencies have to be excited to the level required, rather than the many frequencies needed for a continuous spectrum. The comb output of the CGE-02 can be seen in figure 3.1 [63]. The CGE-02 can be powered either by its own internal batteries or from a separate 5V source, and this version, available as CGE02KIT02, comes with an integral monocone antenna and battery pack; the battery pack can be removed and the CGE-02 run on a separate 5V system. The CGE and the battery pack (BP-01) can be seen in figure 3.2. The monocone antenna allows the CGE to be used for radiated measurements, and emits a comb up to 26GHz. This is the transmit antenna used for this experiment; other versions of the CGE come with SMA connectors that allow a user specified antenna to be added, however the height restrictions present while measuring small enclosures mean that the integral monocone used here is the best option.

The small stirrer used here is a simple twisted brass stirrer paddle (seen in Figure 3.4) and a DC motor, both installed inside the enclosure. The relatively large length of the DC motor is due to an internal planetary gearbox that substantially reduces the rotational speed, allowing more accurate positioning of the stirrer paddle when using the motor in ‘stepped’ mode; stepped mode simply being that the DC motor is turned off while the result is taken, then given a 5V pulse to move the stirrer on a ‘step’. Continuous operation of the DC motor resulted in one rotation taking 78 seconds, therefore for 60 steps in one rotation a 1.3 second pulse moved the stirrer 6 degrees. To get more steps it is necessary to reduce the pulse time, or decrease the voltage to slow the motor down. The brass stirrer paddle was 150mm in diameter, so a 6 degree step resulted in a radial stirrer movement of 3.9mm at the extremity of the paddle.

It has been mentioned in the previous Chapter that frequency stirring is quicker and experimentally easier than mechanical stirring (note that a noise source has been used for frequency stirring in [64]), however in this first instance mechanical stirring is used. This

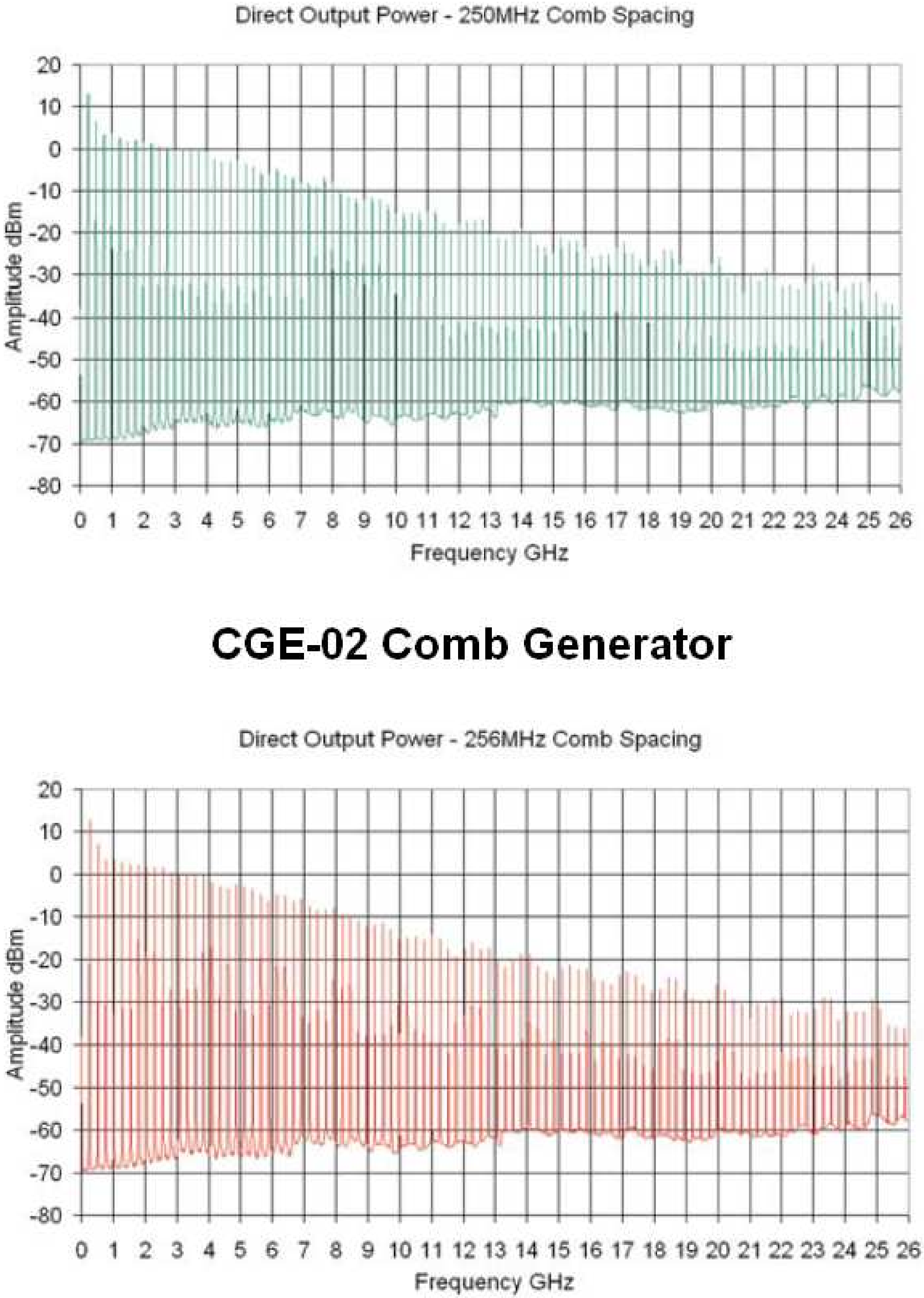

Figure 3.1: Direct Output Power for the CGE-02 comb generator in both modes from 250MHz to 26GHz.

Figure 3.2: Comb Generator Emitter CGE-02 and battery pack BP-01. The monocone antenna is inside the plastic cover.

is because the spectral lines seen in figure 3.1 are too far apart to be used for frequency stirring. This arises due of the bandwidth limitation imposed on stirring methods (recall equation 2.10, shown again in equation 3.1 for clarity), combined with the number of frequency points needed to average over to provide satisfactory stirring. The bandwidth limitation is described by equation 3.1, which for an enclosure of dimensions 480mm × 480mm × 120mm at the minimum frequency below which 60 modes are present [14] results in the frequency stirring bandwidth required to be much larger than 10MHz (using Equation 3.1).

$$BW >> \frac{c^3}{8\pi V_e f^2} \tag{3.1}$$

The spectral lines produced by the CGE-02 are 250MHz apart, this combined with the minimum bandwidth means that just two points will satisfy Equation 3.1, which is designed for use with a continuous spectrum. However, it is immediately obvious that two points are not going to provide enough measurement points to be statistically significant. In order to obtain enough points to enable statistical significance (for example, 60, to match the mechanical stirring points used later) the bandwidth would have to be extended to an unrealistic size, of the order of 10GHz. This problem does not arise in the situation where a continuous spectrum is used, as the relationship given in equation 3.2 can be used to obtain the number of points needed for post processing of the spectrum from the frequency range f_r and the number of modes below f, N_m [41].

$$N_{avgBW} = \frac{f_r}{N_m} BW \tag{3.2}$$

With such a large bandwidth needed to encompass sufficient measurement points due to the spacing of the spectral lines, the problem outlined by Holloway in [7] becomes a concern. In [7] the maximum bandwidth of frequency stirring is mentioned, with the proviso that the $Q-$factor of a reverberation chamber will change significantly over too large a bandwidth. This means that the frequency stirring method will become invalid when used with the CGE-02 due to the large bandwidth needed to encompass sufficient frequency points. This point is illustrated by considering a chamber that has some aspect that becomes more lossy as the frequency increases, thus substantially reducing the $Q-$factor at the frequencies that the aspect is sensitive to. A simple example of this could be a ventilation grid in a chamber that is 'invisible' up until a certain frequency dictated by the grid size, at which point it will become an aperture loss and the $Q-$factor will be affected.

As the standard method of frequency stirring could not be used, the CGE-02 was combined with a small mechanical stirrer to investigate the possibility of a new YES instrument. Data is measured using a spectrum analyser at spot frequencies from 1GHz to 6GHz, facilitated using the 250MHz inter-peak frequency setting. Due to the statistical nature of the mechanical stirring, any particular resonant modes present at each of these frequencies should not be dominant, so any measurements of received power should be representative of the average power within the enclosure, after the results are averaged. The mechanical stirring process used here is described in the following paragraphs.

In this first case, the CGE-02 was powered from an external 5V supply, which was shared with the DC motor and is brought through the wall of the enclosure using a fully shielded BNC (Bayonet NeillConcelman) bulkhead connector and cable. The reason this was done was to minimise the cutting of holes in the enclosure, something that would be important in the real world testing customer enclosures. The inset in Figure 3.4 shows the DC connection powering both the DC motor and the CGE-02. Also visible is the DC stirrer, which is situated parallel to the base of the enclosure. This drives through a 90 degree drive unit constructed from Meccano (TM) to allow the long motor to operate the stirrer paddle. As this particular setup was designed as a proof of concept experiment, to see if such a small stirrer would be effective, it was decided to use existing motors and location options that were as cheap and as fast as possible, hence the DC motor that was physically too long to fit vertically inside the enclosure, and the nature of construction of the right-angled drive, which can be seen in figure 3.3. The CGE-02 can be seen nestled under the stirrer paddle in figure 3.4 to further reduce the size of the proposed instrument. This also has the advantage of reducing the possibility of a direct path from source to receive antennas, by having the source antenna directly illuminate the stirrer. This setup proved to be beneficial in minimising the direct path component in the large reverberation chamber, as can be seen in later chapters, and results in good KS (Kolmorogov Smirnov) test agreement, as can be seen later in this Chapter.

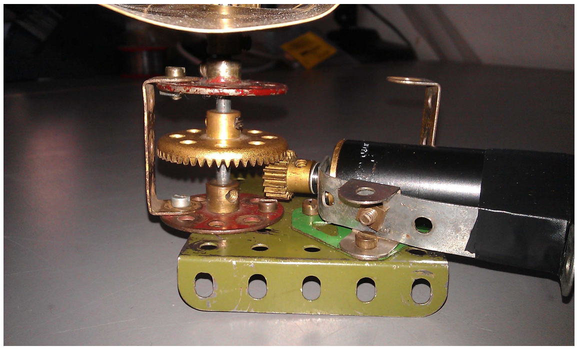

Figure 3.3: Right angle drive constructed to allow the tall DC motor and gearbox (inside the black tube) to drive the small stirrer.

Figure 3.4: The CGE-02 and DC stirrer present in the test enclosure. The inset shows the cable layout providing 5V DC to both the motor and the CGE via a BNC bulkhead connector

It was found that the presence of the DC stirrer on the same 5V supply as the CGE-02 (as shown in figure 3.4) resulted in very slight changes in the frequency of the spectral lines from the CGE-02, resulting in the detected peaks of spectral lines produced by the CGE-02 not staying on the same frequency for repeated runs. This may have been due to noise emitted by the DC motor on the 5V feed causing problems with the comb generation electronics present in the CGE-02. This problem has been potentially exacerbated by using a ‘pigtail’ method of connecting the 5V supply to the bottom of the CGE-02; a method which although very simple and easy, is known to cause problems with radiated emissions and immunity. The movement of the spectral lines led to problems when analysing the measured data, as the program written to obtain the peaks from the spectral lines was dependent on the spectral lines staying in the same position with respect to frequency, and also led to problems with the scientific rigour of the experiment, as the electrical nature of the enclosure is dependent on frequency. The MatLab program used to obtain the data points at the spot frequencies can be found in the appendix, Chapter 10. The stepped DC stirrer was an improvement on the continuously run DC stirrer that was investigated previously, however, which not only changed the positions of the spectral lines but also the baseline of the whole CGE-02, as can be seen in figure 3.5.

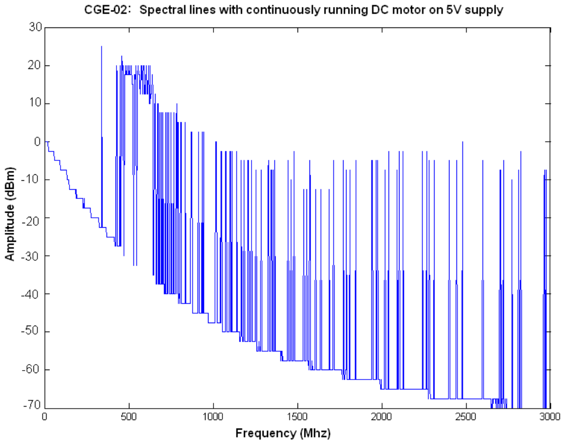

Figure 3.5: CGE-02 output suffering from interference on the 5V supply caused by the continuous running of the DC motor.

To solve the issue, the small stirrer was further developed into a more robust system, with the brass paddle inside the enclosure and a stepper motor, rather than a DC motor, mounted externally to the enclosure. An image of the CGE-02 on a PCB plate can be seen in Figure 3.6. The PCB plate was originally designed to allow the CGE-02 to mimic an emitting source on a motherboard, and is essentially a ground plane and a conducting plane separated by PCB substrate. In the experiments here, the top plate is used as the conducting plate, and the bottom plate is left alone. The PCB plate is supported 2mm from the base of the enclosure using a thin cardboard layer, which is just visible in figure 3.6. In the background of this image can be seen the grey shielded stepper motor control cable used to carry the signal to the stepper motor from a bulkhead connection on the wall of the large chamber: the stepper control is external to the large chamber. This setup completely removed the frequency variation of the spectral lines caused by the interference on the 5V input, allowing the CGE-02 to operate as intended. Removal of the shared 5V DC shared supply meant that the CGE-02 could be used either with the battery pack, or by connecting it to the top layer of the PCB plate, which is powered by a 5V supply. This setup is used in experiments in [18]. The CGE-02 on the PCB plate is shown in figure 3.6.

When this experiment was run in the reverberation chamber, 60 steps were used on the outer stirrer and 100 on the inner; this strikes a reasonable balance between enough statistical points and time constraints. More stirrer positions than this result in better statistics due to the increase in sample size, but result in a measurement taking longer than a day. On that subject, the time taken for a result using this twin stirring method has the potential to be very long indeed, of the order of tens to hundreds of hours. this is due to the fact that the outer stirrer is stepped independently from the inner stirrer; the procedure is that the outer stirrer is moved one step, then the inner stirrer is stepped and data taken over one full rotation before stepping the outer stirrer again. Therefore the number of outer stirrer positions have to be correspondingly reduced from those used in a single stirring measurement; with the settings above a single set of mechanical stirring results can be obtained in around 4 hours.

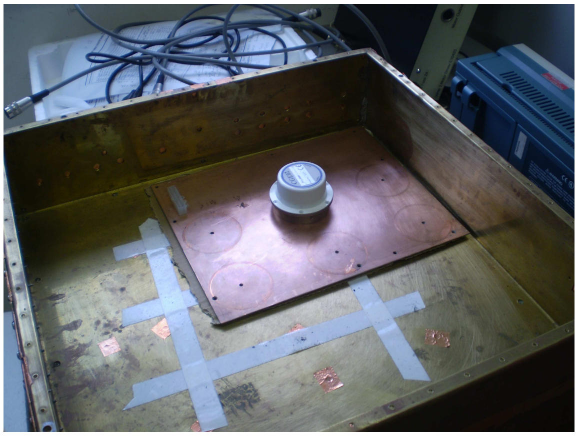

Figure 3.6: The CGE-02 present in the test enclosure. The 5V PCB supply plate can also be seen, separated from the enclosure by an insulating layer.

3.3 Mechanical Stirring and the CGE-02

The electric field distributions were examined using a spectrum analyser at both 250MHz and 256MHz frequency spacings and the KS test used to investigate whether field uniformity was present at spot frequencies between 1GHz and 6GHz inclusive with this combination of the CGE-02 and the small mechanical stirrer. The KS test results are shown in Figure 3.7.

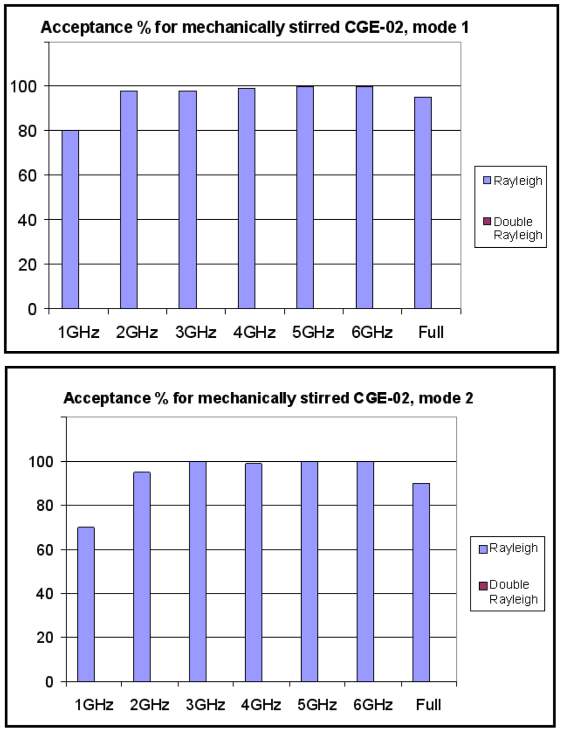

Figure 3.7: KS test results for both modes of the CGE-02 comb generator. Where no bar is shown the distribution is wholly rejected.

It can be seen from Figure 3.7 that Rayleigh distributions are well established at all frequencies tested with both frequency spacings. The experiment setup here involved putting the CGE-02 and mechanical stirrer inside the EUT and testing on a bench. The outer reverberation chamber is not needed in this case as both the source (CGE-02) and the receive antenna (19mm monopole) are inside the EUT, there are no EUT apertures and therefore there is no need for uniform external field illumination. This also is the reason why the distributions are classed as Rayleigh and not double Rayleigh, as the EUT is acting analogously to the large single chamber. Due to the separate source, the analyser used is a spectrum analyser, with the spectral lines of the comb generator being recorded at each stirrer position.

The results here show that a bench-top method for obtaining uniform field statistics within a reverberant enclosure is viable. Equally this could be useful for a standardised SE measurement technique where the internal averaged power density in an enclosure is required to be the same throughout all measurements, and where the same measurement technique could be applied irrespective of the size of the enclosure used. With this in mind, the shielding effectiveness method can be updated to work in a slightly different way, detailed in the following section.

3.4 Shielding Effectiveness Measurements using the CGE-02

The normal measurement procedure for obtaining the SE of an enclosure is detailed in Chapter 2 and also in the IEEE 299 standard [5]. In essence this involves comparing the received power both inside and outside the EUT. In this section the results of an investigation to see if there is a difference between a source placed inside the EUT transmitting out into the chamber and the source external to the EUT transmitting in to the EUT are presented. The CGE-02 is a perfect instrument for such a task. Three methods are used and can be seen in figure 3.8.

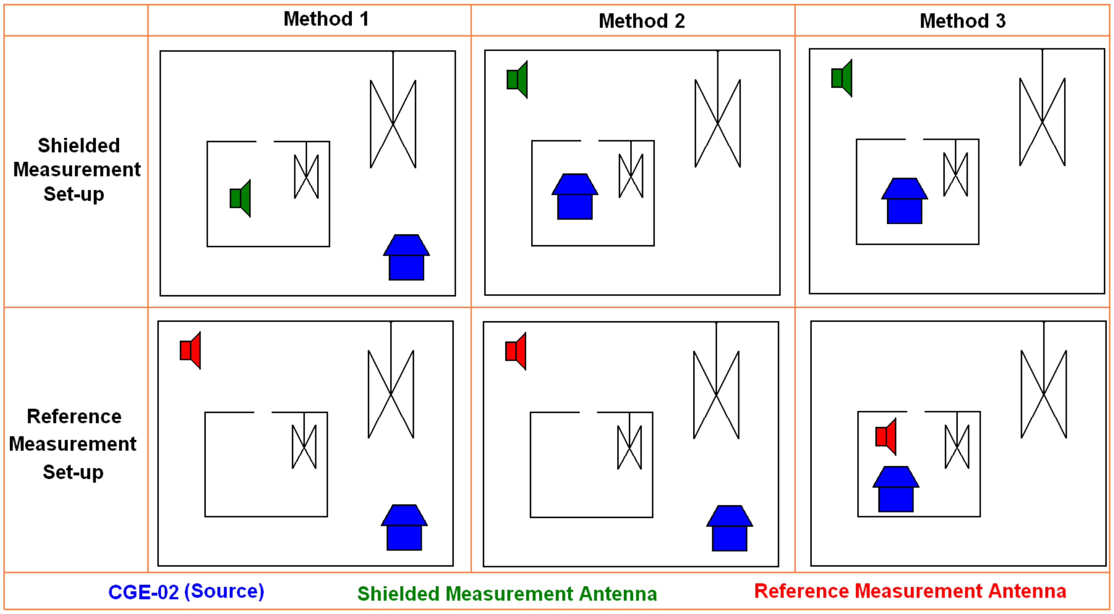

Figure 3.8: Schematic of the three different methods used to compare measurement techniques for shielding effectiveness measurements using a separate source.

As can be seen from Figure 3.8 the three methods are slightly different in setup, but all involve a shielded measurement, where the enclosure is between the source (blue) and the shielded (green) antenna. The reference (red) antenna is always kept in the same reverberant volume as the source, and is used to obtain the reference measurement. The SE equation requires a reference measurement that is higher than the shielded measurement in order to obtain a meaningful value for the SE. The three measurement methods provide that. The measurements are taken with a spectrum analyser, with 60 steps on the outer stirrer and 100 steps on the inner stirrer, and a 120mm x 4mm slot present in the front panel of the EUT. Both enclosure and CGE-02 (when it is external to the EUT) are within the working volume of the chamber, and the CGE-02 is powered from its own battery pack. The results are shown in figure 3.9. Also present in this figure is a set of results taken using the normal nested chamber method using a network anlayser.

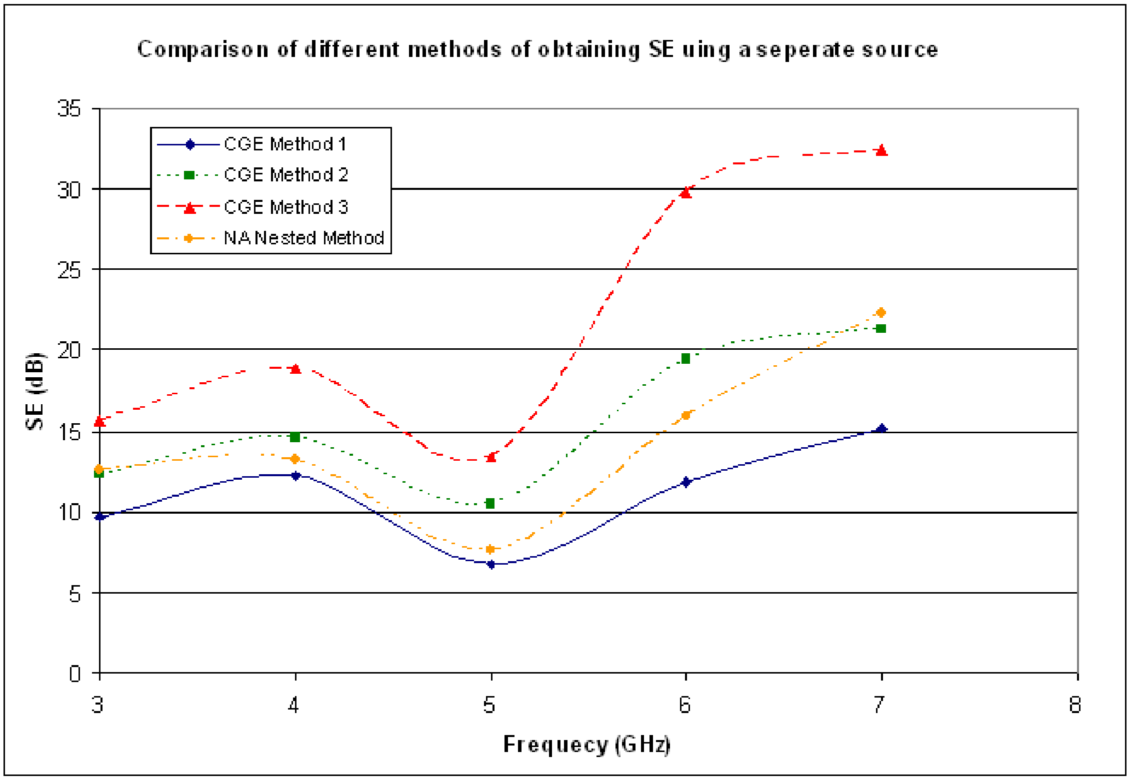

Figure 3.9: Results of the three different methods used compared with a data set measured with a network analyser.

3.4.1 Method 1

The first method applied here is analogous to the nested chamber method using a network analyser. This involves using the CGE-02 as the source in the same location as the transmit antenna in the IEEE 299 measurement, i.e. outside the EUT. Using this arrangement, the equation used for obtaining the SE is the same as that currently used in the 299 standard, repeated in equation 3.3

$$SE1_{dB} = 20\log_{10}\left(\frac{P_{CGE_u}}{P_{CGE_{s1}}}\right) \tag{3.3}$$

In this case, the SE from method 1 ($SE1_{dB}$) is expressed as the log of the ratio of unshielded power received directly from the CGE-02 (P_{CGE_u}) to the shielded power received ($P_{CGE_{s1}}$). In this case the shielded measurement represents the power received with the

CGE outside the EUT with the receive antenna inside the EUT. P_{CGE_u} is obtained from a monopole on an electrically large ground plane within the working volume of the chamber. The power is measured inside the EUT with a wall mounted 19mm monopole, shown as analogous to a working volume probe in [7]. This experiment setup follows the same outline as the ‘standard’ method outlined in [5], the difference being the use of a separate source and spectrum analyser rather than a vector network analyser. The closeness of this method to the ‘control’ method using the network analyser can be seen in Figure 3.9, with the solid line with diamond points being the CGE method and the dash-dot line with circular dots being the NA method. The two methods (control and Method 1) are within 3dB to 4dB for the frequency range used, except for the top end at 7GHz. Repeatability of around 4dB should be expected between runs (see Chapter 4) meaning that these two methods can be considered equivalent within the uncertainty of the experiment.

At 7GHz, the difference can be partly explained by the fact that the calibration kit used for the network analyser is only valid up to 6GHz; it can be seen in Figure 3.9 that all of the CGE traces are roughly the same shape over the higher frequency points, compared to the NA trace, which is significantly higher at 7GHz. A higher than expected loss in a cable or connector will be measured as an increase in the SE of the enclosure if the same cables are not used for reference and shielded measurements. Due to the design of the UoY Chamber a long cable was used to connect the transmit antenna to the wall behind the stirrer; this cable was not used for the receive measurement. If exactly the same cables are used for the transmit and receive measurements then there is no need to calibrate the NA, as the ratio calculation causes any factors to cancel out.

It is for this reason that the corrected SE equation detailed in Chapter 2 is beneficial, as it will take account of differing antenna factors. In this section, however, the uncorrected SE equation is used in order to compare with the SA results, the SA being incapable of measuring reflection coefficients. It needs to be noted that the SA is not calibrated in the same way, in that the calibration for the NA can take account for cable losses whereas the SA does not, however with good quality cables and connectors the losses should be very small.

3.4.2 Method 2

This method involves keeping the receive antenna in the same place for both the reference and shielded measurements. The shielding measurement is obtained by placing the CGE inside the EUT while measuring outside. Using this setup, the SE equation becomes equation 3.4.

$$SE2_{dB} = 20\log_{10}\left(\frac{P_{CGE_u}}{P_{CGE_{s2}}}\right) \tag{3.4}$$

This equation is very similar to equation 3.3, used for Method 1. In fact, if the method of measuring SE using just the ratio of powers is to be believed, as would be reasonable when following the IEEE 299 or 299.1 standard, then the two methods should be interchangeable. Examining the schematic of the different methods this would seem to be the case, as the level of shielding due to the aperture between the CGE and the antenna measuring $P_{CGE_{s1}}$ is the same, as the apertures in and the stirring mechanism within the enclosure are the same. However, looking at Figure 3.9 and comparing the lines for Method 1 and Method 2 reveals a 3dB to 5dB variation between the two methods. It has been noted previously that one of the problems with the current SE method used in [5] is that there is no capacity for contents or other loading of the enclosure, the method only being applicable to empty enclosures.

In this experiment, the enclosure is not empty, as a proportion of the volume of the enclosure is taken up by the CGE-02. The transmit antenna is also present in the enclosure, albeit joined to the CGE-02. Both of these aspects combine to lower the $Q-$factor and therefore give a lower field power within the enclosure, meaning less power emitted by the apertures, and therefore less power received by the external measurement antenna.

This has the effect of making $P_{CGE_{s2}}$ less than $P_{CGE_{s1}}$, which, combined with the same reference measurement P_{CGE_u} results in a larger measured value for the SE. It is very important to note that the actual level of the SE due to the aperture is not changed - the enclosure is identical throughout, and that the measurements done in different ways yield measured SE values of differing magnitude.

3.4.3 Method 3

A more extreme example of the above statement regarding the change in measured SE is highlighted when the results from Method 3 are analysed. This method involves the CGE and the recieve antenna both in the enclosure at the same time, to obtain the unshielded measurement $P_{CGE_{u3}}$ The shielded measurement is obtained in the same way as Method 2; and therefore equivalent to $P_{CGE_{s2}}$, but labelled as $P_{CGE_{s3}}$ to avoid confusion. The main point here is that the measurement inside the enclosure is now the reference/unshielded measurement, meaning that the numerator and denominator in the original SE equation, (equation 2.4)P_{out} and P_{in}, are switched. When looked at from the point of view of shielded and unshielded power this makes perfect sense, in all the SE equations the unshielded (larger) power is on the top; the shielded (lower) power being on the bottom. The equation for Method 3 is shown in Equation 3.5. Again, as the SE is expressed purely as a ratio of powers, and as the real shielding performance of the enclosure has not been changed, then the value for the SE should remain unchanged.

$$SE3_{dB} = 20\log_{10}\left(\frac{P_{CGE_{u3}}}{P_{CGE_{s3}}}\right) \tag{3.5}$$

As can be seen from Figure 3.9, using this method results in a much higher value for SE than the other 2 methods and the NA control method. This is down to a higher measured value of $P_{CGE_{u3}}$, and the fact that the large chamber is not equivalent to the small one. If following the reasoning behind the SE measurements stated in the standard and disregarding the contents and the $Q-$factors of the chamber and enclosure under test, then $P_{CGE_{u3}}$ should be equivalent to P_{CGE_u}. This is not the case, because of how the $Q-$factor behaves in different sized enclosures at the same frequency, and the dependence of the $Q-$factor on the loading of the chambers due to antennas. In the following chapters, using the Q-factor to obtain a value for the SE is investigated, and a more detailed study of the various aspects of the Q-factor are carried out; this can also be found in Chapter 2. However it is worth examining the $Q-$ factor when measuring the SE.

If the SE is viewed as dependent purely on the aperture then the three methods outlined here should be interchangeable. However, as the SE is calculated a ratio of powers, then anything that changes the measured power, either inside or outside the enclosure, will change the measured SE. Recalling the composite $Q-$ factor (equation 2.13) the loss mechanism in a chamber includes an antenna loss and an absorber or contents loss. Looking at figure 3.9 it can be seen that the $Q-$ factor of the EUT changes between the three methods. In method 3, the EUT contains both the the CGE-02 body with battery, the source antenna and the measurement antenna, which all reduce the $Q-$ factor within the EUT, and thus reduce the power in the enclosure when compared to method 1.

This reduced power on the reference measurement means that the measured SE is larger, which is reflected in figure 3.9. Method 2 falls between method 1 and method 3 in figure 3.9. The difference in measured SE between method 1 and method 2 suggests that the CGE-02 affects the power level in the EUT more than the receive antenna, resulting in a higher measured SE due to the power inside the EUT is less. This result highlights the need for consideration of the $Q-$factor in shielding effectiveness measurements. Unfortunately due to a change in the research direction, there was insufficient time to further investigate why the network analyser method follows an upwards trend at the higher frequencies where the three CGE methods do not.

3.5 Frequency Modulation of a Separate Source

Frequency modulation (FM) of a separate source spectral line at specific frequencies is investigated in this section, with the aim of obtaining an alternative method to the frequency averaging method outlined in section 2.5.4. Frequency modulation can be used as a method of obtaining statistically independent frequency peaks, which can then be used for frequency stirring, and works by applying a modulating signal to a spectral line. The CGE-02 spectral lines are too far apart to use the traditional frequency stirring method; the frequency modulation of the CGE-02 spectral lines allows generation of smaller amplitude and closer spaced spectral lines on top of the spread spectrum which can be used. In this case mechanical stirring is not used while using this frequency modulation method, as the spectral lines change in amplitude as the stirrer rotates, moving the modulated signal up and down and therefore affecting the base used for the frequency modulation. This method of frequency stirring requires stable amplitudes of the small spectral lines on top of the spread spectrum.

The best possible outcome of the frequency modulation is the creation of a spread spectrum that has a wide, flat top and steep sides. This is because, using this method, data is taken from the smaller spectral lines created by the FM that are present in the top of the spread spectrum. The ideal outcome of the modulation is a series of spectral lines that are far enough apart to be statistically independent but with a large enough number of them on the top of the spread spectrum. This ensures that both the statistical independence of individual points and a statistically significant sample size are retained. This is analogous to the stirrer position discussion mentioned previously. The width of the spread spectrum is, in this case, similar to the stirring window used in other frequency stirring methods.

It is possible to create different shapes of spread spectrum by using different modulating waveforms, for example square, sine or triangle. As this method requires data to be taken from the peaks that form on the top of the modulated trace, the width and flatness of the top of the spread spectrum is important. The best modulating waveform to use in order to spread the energy out as much as possible, and therefore obtain the widest and flattest top, is known as the 'Lexmark Kiss' shown in figure 3.10 [65]; this provides the 'squarest' output trace, with a reduction in the higher side lobes present in the results shown in figure 3.11 and figure 3.12.

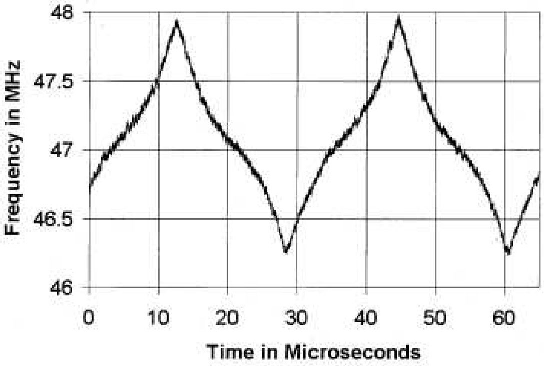

Figure 3.10: Lexmark Kiss waveform

The 'kiss' was originally used to spread a spectral line that would have otherwise have failed an EMC test by being above the limit for allowable emissions. Application of the Lexmark Kiss results in the spectral line being spread out so that the maxima is below the limit line. This process is frowned upon as the device in question still emits the same power, but over a wider frequency bandwidth, therefore allowing it to pass an EMC test for emissions (as the original spectral line would exceed the limit line) but still potentially emitting enough power to cause interference. The process used to create this effect is known as clock dithering [66][67][68]. The process of clock dithering, i.e. spreading out the original spectral line, is of possible use for frequency stirring.

The following figures demonstrate the spread spectrum obtained by frequency modulation using different modulating waveforms. Figure 3.11 shows an example of a 3GHz carrier modulated by a sine wave and figure 3.12 the same carrier modulated by a triangle wave. The traces are measured using a spectrum analyser. It can be seen that the widest spread is achieved by the triangle wave, for equivalent deviation values. Note that the triangle is the closest waveform in shape to the Lexmark Kiss. If a square wave modulation waveform is used, the output trace is unusable for this method as there is no 'flat' area between the edges of the raised section. This makes it difficult to analyse the frequency modulation peaks, as the amplitudes of the small spectral lines are not uniformly based. The frequency stirring uses the spectral lines on the top of the modulated trace, and as such it is necessary to have all of the spectral lines at the same amplitude. If amplitude correction is not used, and here it is not, then the flattest spread spectrum is the best to use. The spectral lines for stirring are taken from the raised areas in the following Figures, after 'zooming in' on the centre frequency area the peaks become apparent. This is shown schematically in figure 3.13.

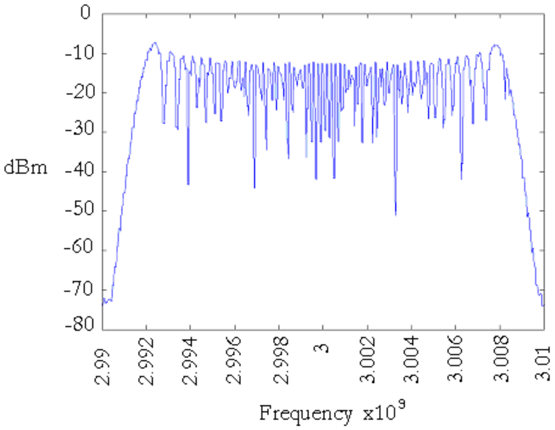

Figure 3.11: A 3GHz carrier modulated by a sine waveform

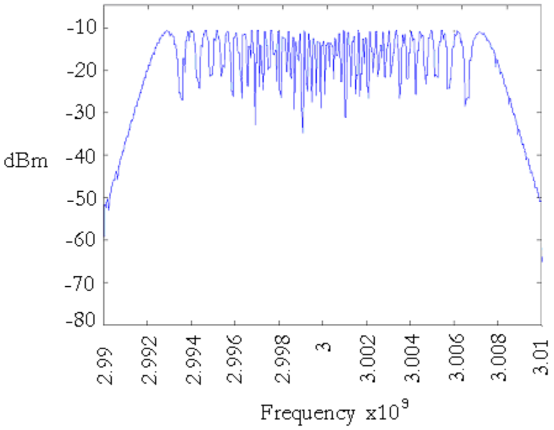

Figure 3.12: A 3GHz carrier modulated by a triangle waveform

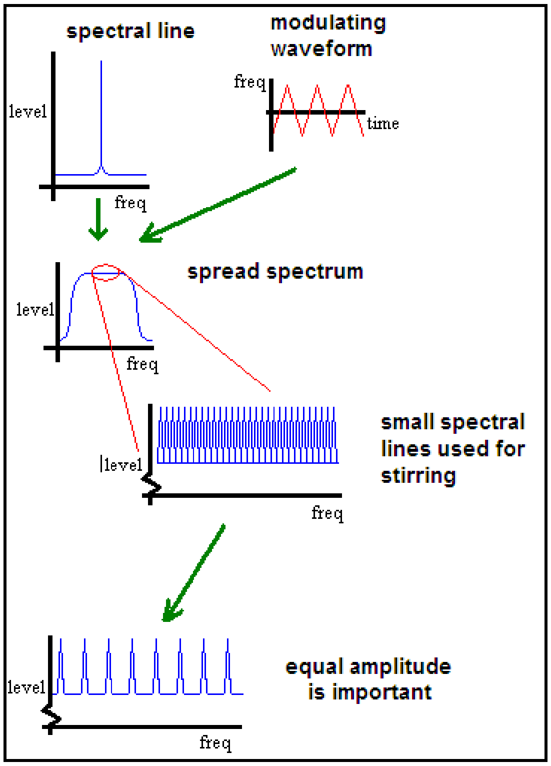

Figure 3.13: Schematic of FM trace and discrete peaks

The triangle wave modulation (see figure 3.12) gives a much flatter peak than the sine wave modulation seen in figure 3.11. This makes it easier to process the results, as the baseline is flatter. A totally flat top can be achieved with the application of the 'Lexmark Kiss' trace. It is worth noting that the measurable bandwidth of these traces is actually less than the actual bandwidth because of the way that the trace falls off at the edges of the raised section. This manifests itself as only being able to measure 15MHz either side of the centre frequency for a 16MHZ span modulation wave, for example. This is due to the way that the modulating waveform is created.

The deviation value of the frequency modulation governs the width of the peak. For a deviation of 16MHz, for example, the width of the peak is 32MHz. The rate of the FM determines how far apart the peaks in the data are: the deviation needs to be set so that the peaks are discrete and statistically independent without being too far apart, and the bandwidth (twice the deviation) needs to be set so that it satisfies equation 2.10. A point to note is that if the peaks are too far apart, the $Q-$ factor can change within the bandwidth of the modulated spectrum: this will lead to results that may differ from expected, as explained in section 2.5.4. It is often necessary to split up the frequency modulated peak (i.e measure the full trace in three or more sections) to allow enough data points to capture all of the peaks needed.

3.5.1 Frequency Stirring using Frequency Modulation

In order to investigate the feasibility of frequency modulating the spectral lines produced by the CGE02, frequency stirring using a separate signal generator that applied frequency modulation internally was implemented. The measurement points need to be spaced close enough together to ensure that the $Q-$factor of the chamber does not change within the bandwidth of the FM trace, and far enough apart to be statistically independent. An Anritsu spectrum analyser was used to obtain the data for the FM results. This particular instrument is limited to a maximum of 501 data points across its measurement window, so the data had to be split into three parts to get sufficient resolution of spectral lines. This was done by taking three sets of measurements across the bandwidth of the frequency response and then combining them in the analysis program. Spot frequencies from 1GHz to 6GHz were used.

This means that the final data set was 1503 points across rather than just 501, meaning that more independent peaks could be used to improve the statistics. A MatLab program was written (which can be seen in the Appendix, Chapter 10) to extract the frequency peaks from the data set; these were then plotted as a histogram and compared to a Rayleigh distribution for the outer chamber and Double Rayleigh for the inner enclosure using the KS test method.

The signal generator used for these experiments was a Rohde & Schwarz SMB100A, which gave an output up to 6 GHz with its own internal options for FM. This generator could produce square or sine wave generation using its own internal generator. As seen previously in this Chapter, a triangle waveform is the best for this procedure, so an external function generator was used to apply a triangle waveform. The generator used was a simple Instek function generator, and although capable of generating the correct shape modulating wave, it was found that it was not stable enough. This instability manifested itself in the frequency-modulated trace on the SA; the spectral lines created by the FM did not stay the same height (power) and varied in position (frequency) each scan.

Movement in the frequency position of the peaks is undesirable, so the R&S generator with higher quality internal generation was used, as this produced the most stable results. The R&S generator was not capable of generating a triangle wave, so a sine wave was used instead. As the baseline is not as flat as the FM spectrum created by the triangle waveform, the peaks have to be larger to ensure that the side lobes of the frequency waveform are not included in the peak count. To stop the side lobes being included, the peaks were only taken from the central, flattest, area of the modulated spectrum, effectively reducing the bandwidth over which the measurement can be taken.

It is worth noting that neither the outer chamber nor the inner enclosure needs to be mechanically stirred in this experiment to ensure a uniform incident field on the EUT as the frequency stirring should do this job, as long as the conditions are met. If it is not working correctly, then this can be seen in the distributions: the distribution of the electric field will not follow the Rayleigh shape.

An FM signal was transmitted into the chamber at spot carrier frequencies between 1GHz and 6GHz. The data obtained from the SA was run through the MatLab program seen in the Appendix, Chapter 10, which outputs a histogram of the electric field in mV and a simulated Rayleigh curve. The simulated Rayleigh curve is calculated using the Rayleigh parameter (seen in table 2.1, parameter b), which is obtained from the data. These simulations were then compared to the data using the KS test.

Figures 3.14 and 3.15 show the acceptance probability of the distribution in question for the chamber and enclosure respectively. Blue represents Rayleigh distribution acceptance and red represents double Rayleigh. What this shows is the likelihood of the distribution under test matching the simulated distribution. The distributions tested against are Rayleigh and double Rayleigh. If the acceptance level is 100%, it means that the KS test is 100% sure that the distribution under test matches the simulated distribution. If the acceptance level is 50%, the KS test is saying that it is a 50% chance that the distribution under test matches the simulated distribution, and a 50% chance that it is not. If the KS test is sure that there is no relationship between the distribution under test and the simulated distribution then the acceptance level drops to 0%.

The KS test results for the chamber using frequency modulated frequency stirring 3.14 clearly show that the Rayleigh distribution dominates, with near 100% acceptance at all frequencies tested. The double Rayleigh distribution is fully rejected (0% acceptance rate) at all frequencies. As should be expected, this shows there are enough modes at all frequencies and the stirring is effective enough to establish the full Rayleigh distribution. This acceptance level shows that the chamber is working correctly.

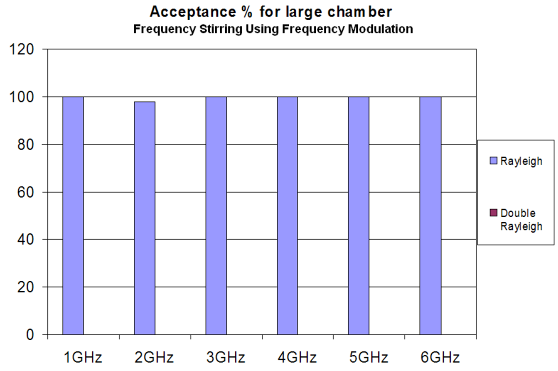

Figure 3.14: KS test results for frequency stirring using frequency modulation in the large chamber. Both distributions are tested; the double Rayleigh case does not show as it is fully rejected (0% acceptance) at all frequencies.

The enclosure used in this case is a brass box of dimensions 0.48m × 0.48m × 0.12m with a minimum frequency (below which 60 modes are excited) of 1.9GHz, calculated using the minimum frequency equation specified in equation 2.10. The KS test results from the twin chamber setup are shown in 3.15. The enclosure is set up with a single long slot (120mm × 40mm) as an aperture.

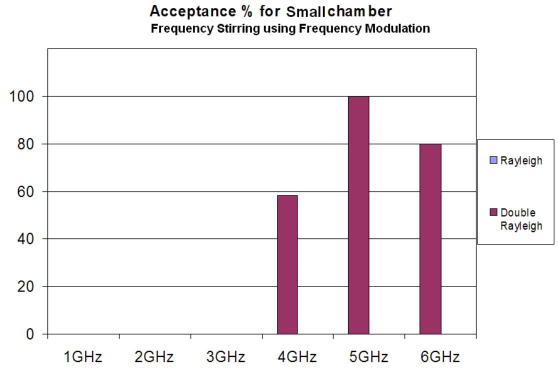

Figure 3.15: KS test results for frequency stirring using frequency modulation in the inner enclosure. Note that no Rayleigh distributions are established throughout.

It can be seen from figure 3.15 that neither type of distribution for the lower frequencies are well established i.e. they have a 0% acceptance level. This highlights the need to adhere to the minimum frequency criterion as there are not enough modes in this situation to fully establish the overmoded state and allow the statistical approach to be valid. As the test frequency increases, the double Rayleigh distribution becomes accepted while the Rayleigh distribution continues to be rejected. This is to be expected, as the aperture acts as a transmit antenna into the interior of the EUT, resulting in the combination of the external Rayleigh distribution with the internal Rayleigh distribution to create a double

Rayleigh distribution in the inner of the twin chamber environment. What may have been expected was that the double Rayleigh distribution becomes established as soon as the minimum frequency is passed, however in this case the distribution is established above 4GHz. This leads to the possible conclusion that a minimum of 60 modes is perhaps insufficient when using this type of frequency stirring, and that the number needs to be increased to 100 or 150 for more applicable statistics.

3.6 Frequency Modulation and the CGE-02

The previous section suggests that frequency modulation of the peaks of the CGE-02 may be beneficial at higher testing frequencies than would normally be used for an enclosure of a given size. The latest version of the CGE has the potential capacity to apply FM internally, unfortunately there was not time to pursue this line of investigation. However, frequency stirring using a separate modulated source does work, and would potentially be more easily implemented by an end user than a stepped stirrer method.

3.7 Chapter Summary

This Chapter has presented results obtained when a separate source and spectrum analyser is used to measure the shielding effectiveness of enclosures. The CGE-02 has been shown to be effective at establishing statistically uniform fields inside enclosures when used in conjunction with a small, stepped stirrer, however it does need to be powered by a separate power supply from the motor used to operate the stirrer. It has been shown that the SE is measurable in a number of different ways using the CGE-02 as the source. If the simple SE equation is examined then the methods at first seem to be equivalent, as the same enclosure with aperture separates the source and receive antennas. These methods prove not to be experimentally equivalent due to the effect of the antenna changing the $Q-$ factors in the enclosure and the chamber and therefore affecting the measured received power. This highlights the need to involve the $Q-$ factor in the calculation of SE, or at the very least consider it in order to have representative measurements. It is also shown in this Chapter how it is possible to use frequency modulation to stir an enclosure and chamber setup using a frequency stirring method. It appears that this method is more sensitive to the number of modes in the enclosure

Chapter 4

Comparing Reverberation Chambers Using a Shielded Enclosure

The contents of this chapter include the measurement techniques used on and results taken from an EUT that was designed to allow cross-chamber acceptance testing by being tested in a number of reverberation chambers around the world. The intent behind this piece of work was to help standardise measured results in differing reverberation chambers, in much the same way as site attenuation measurements do for Open Area Test Sites (OATS). Even though chamber design varies, the verification enclosure should provide a useful measure of chamber performance. So far results have been returned from Franco Moglie and Valter Mariani at the Università Politecnica delle Marche, Ancona, Italy, and the enclosure has been returned to the Physical Layer group as of January 2013.

4.1 Enclosure Design

This verification enclosure is a zinc galvanised steel box that incorporates three 19mm monopole antennas with SMA (SubMiniature version A) connectors and has the dimensions of 0.3m $\times$ 0.3m $\times$ 0.15m . It can be seen in figure 4.1. As this enclosure is to be used to compare reverberation chambers in different labs in different countries, it has to be able to have high measurement repeatability so that any change in the results could be attributed to the test chamber not the enclosure. Previous round robin chamber comparison attempts had been influenced by inconsistencies in the electrical sealing of the lid of the box, which used a simple method of sticky-backed compressible copper tape to seal the edges after the lid had been screwed on. Although many screws were used, this system was found to give a variation of up to 15dB in the SE of the EUT between tests, as the lid was removed, replaced and resealed at each test lab and between tests. This was masking any differences that may have been present between the different test chambers.

A new system was developed for this enclosure. Finger strip is used as the electrical contact between the lid and the rest of the enclosure, and the Allen head lid bolts are all torqued down to the same torque as the SMA cable connectors (8lbin/0.9Nm) using a standard calibrated SMA spanner. The sliding nature of the finger strip as the lid is closed ensures a good electrical contact between the lid and the rest of the enclosure, shown in figure 4.2. This contact will remain constant when the lid is reattached even after repeated removal and re-bolting. Finger strip is used on the doors of both anechoic and reverberation chambers for these reasons of low wear rate and high shielding performance. When measuring from any single port of the three available in this EUT, the other two ports are terminated with SMA shielding caps.

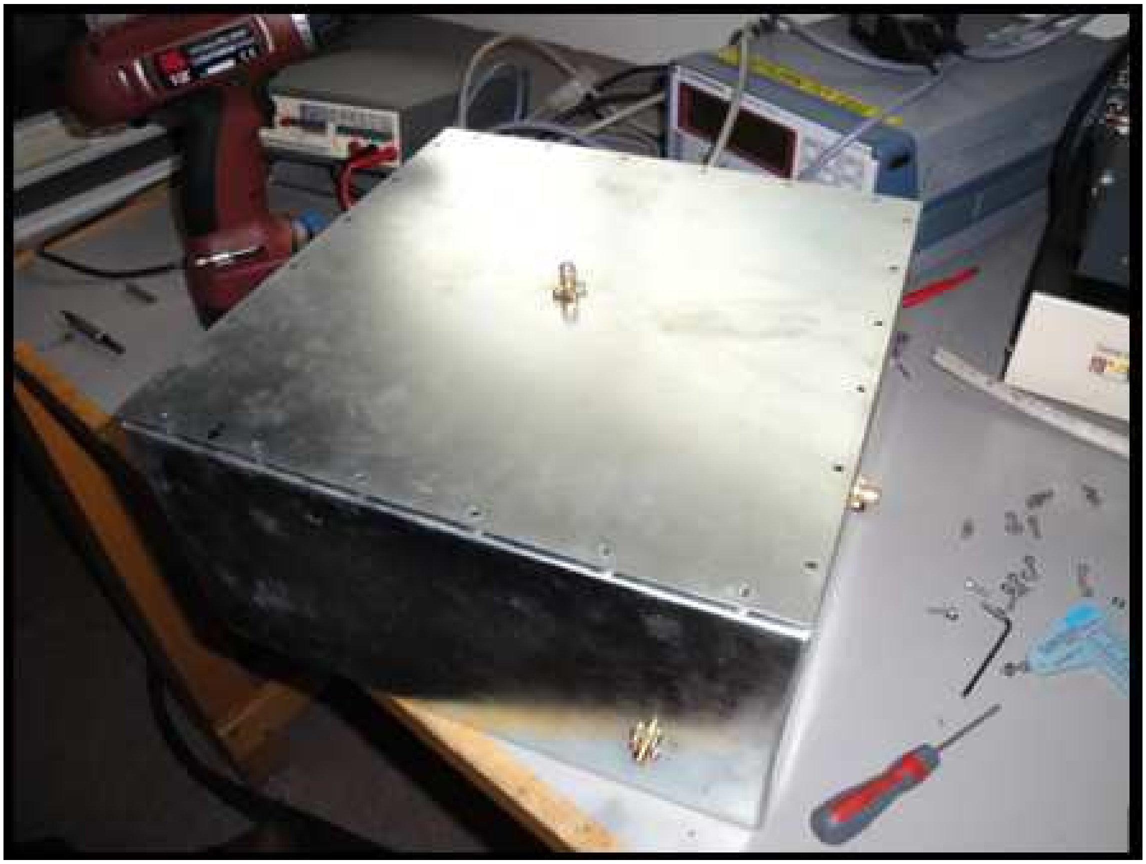

Figure 4.1: Verification enclosure showing the position of the three SMA monopole antennas

There is no mechanical stirrer present in the EUT, as the stirring is done using the post processing FS method. The EUT is placed in the reverberation chamber and the

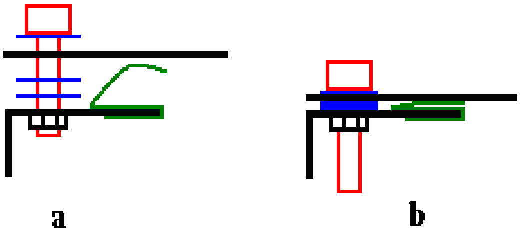

Figure 4.2: System of washers and finger strip used to ensure good contact; (a) is just before good contact, (b) is tightened to standard SMA spanner torque of 8 lbin. Spacing washers are included to avoid crushing the finger strip.

measurements are taken with a vector network analyser scanning 3GHz to 8GHz with 1601 measurement points and 100Hz IFBW. The stirring window is 50 points and the minimum frequency for 60 modes in this enclosure is 2.9GHz. The measurements are presented as SE with the $S11$ correction applied, as detailed in section 2.8.1 (see equation 2.20). The reference measurement for the SE value is obtained from the standard 19mm monopole antenna on a ground plane; the same reference measurement is used throughout. The power is transmitted into the reverberation chamber using a 1GHz to 8GHz ridged horn antenna.

4.2 Repeatability of Results

As one of the criteria is for this enclosure is to have the lid taken off and put back on again many times the repeatability of the measurement of SE is of interest. The lid was reassembled in the same orientation each time and the same port was used for the four runs shown in 4.3. Two different people did two runs each in order to look at the possibility of human error during the test. The SE is calculated using the corrected SE equation (see equation 2.20), using a 19mm monopole on a ground plane as the reference measurement and a ridged horn antenna as the source. The same port is used each time, and the SE is calculated for each run and the 4 runs are shown in figure 4.3.

As can be seen in figure 4.3 the port repeatability is high, within 7dB for most of the frequency range. It could be said that there are two different sets of lines, the light blue and red forming one set and the dark blue and green lines another set. It is of interest that each person doing the experiment produced one of each, suggesting that this is a feature of the enclosure rather than the operators. The port repeatability is better at the higher frequen-

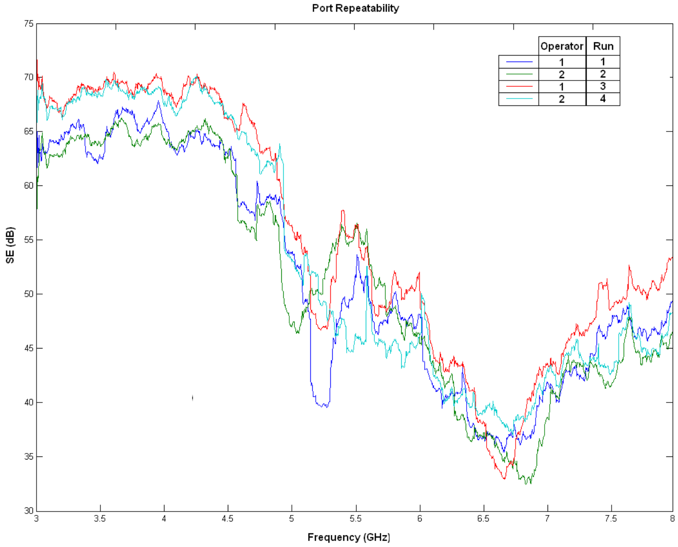

Figure 4.3: Port repeatability over 4 runs

cies, this is possibly due to the fact that the number of modes is much larger. Noticeable in the middle of this plot, on the spectrum for the first run (dark blue), at around 5.25GHz, there is a sharp dip in the SE of around 10dB. This is not present in the results from another test chamber in Italy at the Università Politecnica delle Marche, Ancona by Franco Moglie and Valter Mariani, shown in 4.4. This feature is present only in traces obtained by 'Operator 1', highlighting the need for using different people to highlight the possibility of human error. The difference in operator traces is slightly unexpected, however, as the two operators carried out the experiment together under the other's supervision, and alternately. Despite this, the finger strip method can be considered as a better method for enclosure lid sealing as the repeatability is around 7dB, compared to 15dB repeatability using copper tape to seal the lid.

Figure 4.5 shows two selected runs from both the UoY (UK) and the UoA (Italy). Agreement between the SE measured by the two labs is better at higher frequencies, averaging around 10dB above 5.25GHz. Below this frequency, there are variations of up to 25dB between the higher measured SE at UoY and the lower measured SE at UoA, for example at 4.75GHz. The actual SE of the enclosure should remain unchanged, as the experiments were carried out using the same measurement plan; any differences are down to the operator (as identified in figure 4.3) or difference in reverberation chambers. It is not clear from these results what could be causing the difference between the measured SE in the different labs.

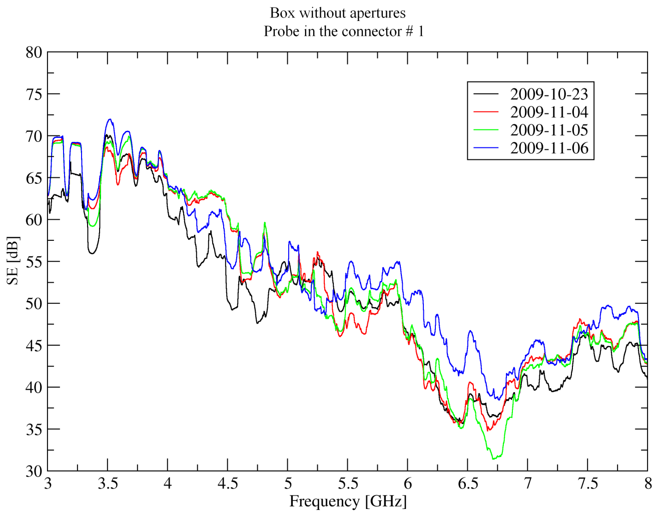

Figure 4.4: Port repeatability over 4 runs, results taken by Franco Moglie and Valter Mariani

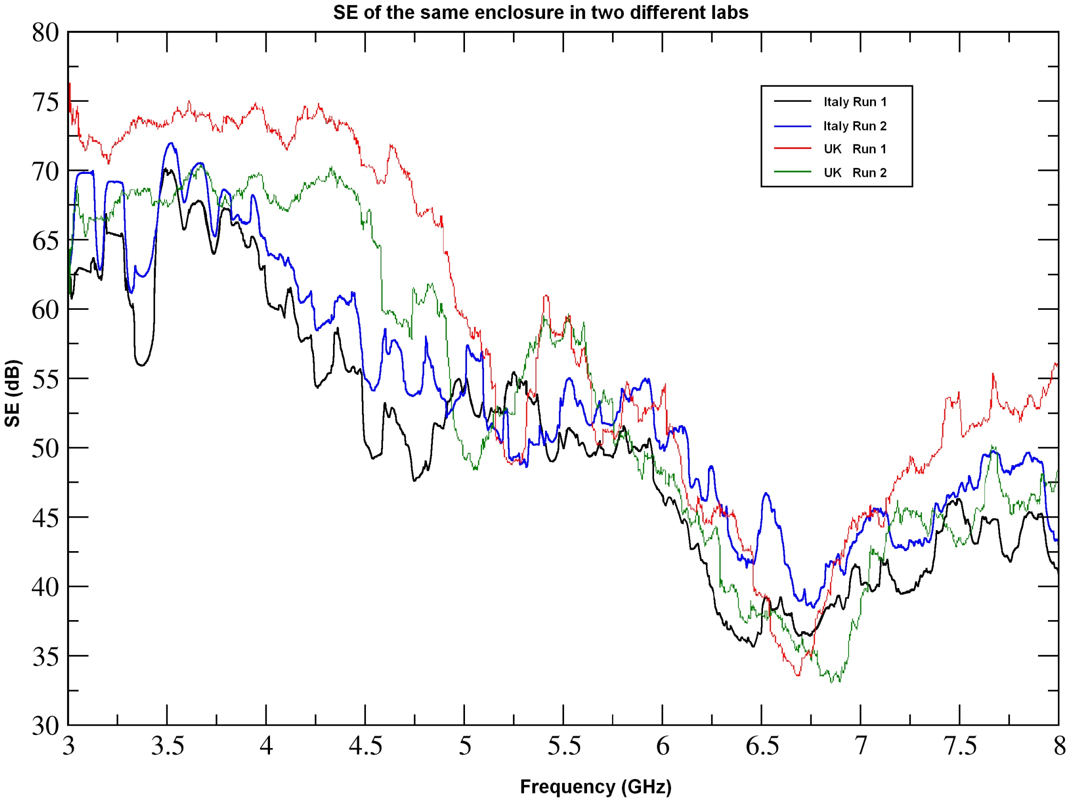

Figure 4.5: Measured SE using comparable methodology in two different labs.

4.3 Changing the SE

The finger strip around the lid of the enclosure is designed so that sections could be removed to create repeatable apertures in the enclosure. The aperture configurations are as follows: (A_s) all the finger strip in place, (B_s) take out a short piece to have a short slot, (C_s) replace the short piece and remove a long piece to create a medium slot, and lastly (D_s) to take out both pieces to have a long slot. The configurations (B_s) figure (4.6), (C_s) figure (4.7) and (D_s) (figure 4.8) give high, medium and low shielding respectively. Configuration (A_s) is used for the repeatability measurements.

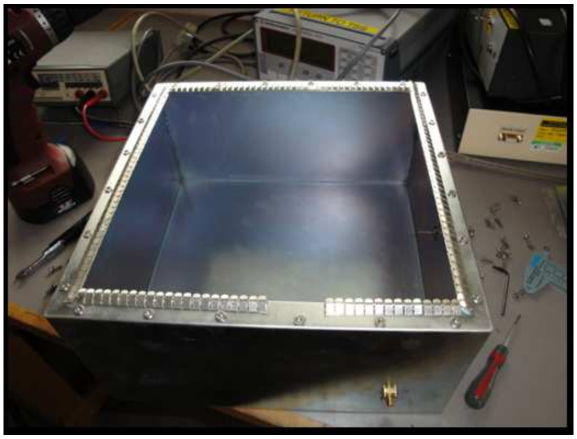

Figure 4.6: Short slot configuration, with lid removed for clarity. Note spacing washers still in place to prevent distortion of the lid. Two of the measurement monopoles can be seen, the third is in the lid.

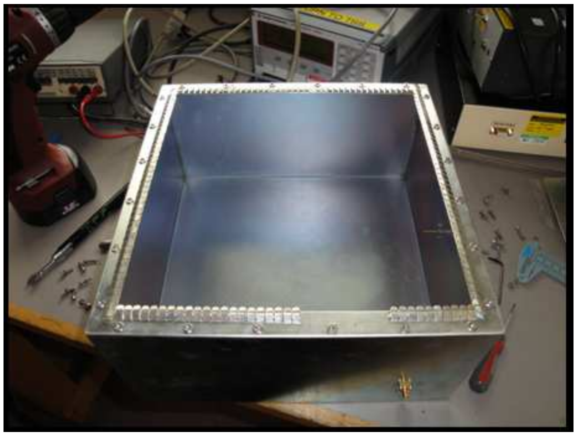

Figure 4.7: Medium slot configuration with lid removed for clarity. Note spacing washers still in place to prevent any distortion of the lid which may reduce finger strip effectiveness, and also to prevent crushing of the finger strip.

The SE of the enclosure is measured using the standard nested reverberation chamber method used in [5], but using the post processing stirring mechanism detailed in section

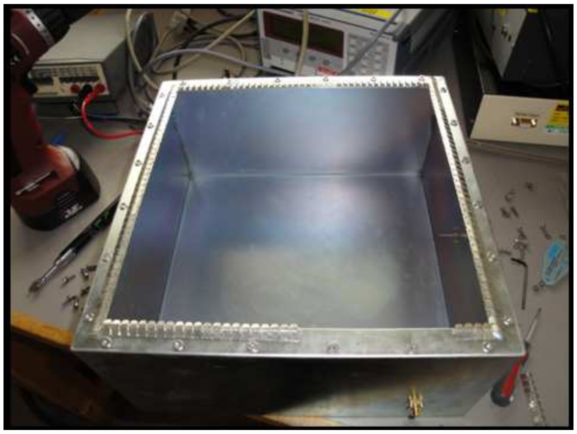

Figure 4.8: Long slot configuration with lid removed for clarity. Note spacing washers still in place to prevent distortion of the lid, which was more pronounced when using the long slot without the spacing washers.

2.5.4. The two 19mm monopole antennas visible on the left hand enclosure wall and the enclosure wall closest to the camera in figures 4.8,4.7 and 4.6 plus a third monopole in the lid are used to measure the internal power. In between measurements the finger strip is changed to give the long, medium and short variations. The lid bolts are torqued down using an SMA spanner and an Allen key adapter between each change. This was part of the repeatability modifications as it allows the same clamping force to be used over all the lid bolts. The received power is measured from each of the three ports, with the electrically sealed blanking pieces being moved to the two unused SMA connectors. The reference value of received power is taken from the chamber using a 19mm monopole antenna on an electrically large ground plane. The data is collected using a network analyser using 1601 points and a 100Hz IF bandwidth.

The stirring method used is the post processing type, and is implemented in MatLab (see Appendix, chapter 10) after the results have been taken. One frequency sweep on the network analyser is carried out at each port, which is then stirred using a 50 point stirring window, giving a 31.2MHz stirring bandwidth. Three ports are used to compare the internal field distribution which also helps to give more information on the post processing system as a method of obtaining uniform internal fields. The averaged powers obtained after the stirring from the three ports should be within the limits specified by IEC 64000-4-21 for a reverberation chamber above 400MHz, which is 3dB. This ± 3dB limit on the measured electric field power translates to an allowed variability of ± 6dB in the measured SE, when using the simple power ratio SE equation.

The results for each slot are shown in figures 4.9, 4.10, 4.11, the three traces being from the three different 19mm monopole antennas.

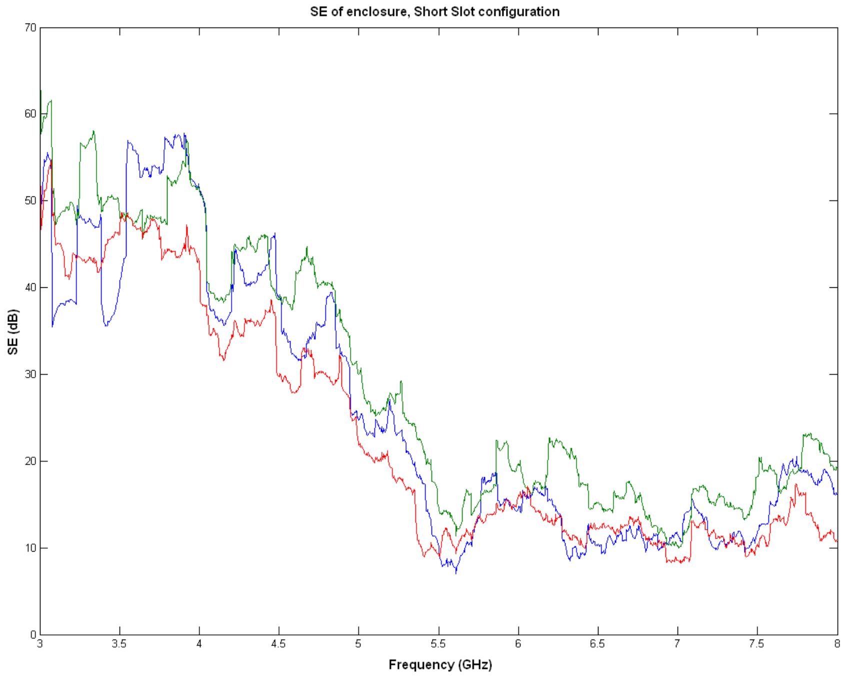

Figure 4.9: SE of enclosure using short slot apeture. All ports are shown.

The Figures 4.9, 4.10 and 4.11 show that the port agreement is not as good as could have been expected, as it was expected that the the field uniformity would be within the limit (3dB limit for powers, 6dB for SE) [17], in figures 4.9, 4.10 and 4.11 variations up to 12dB can be seen. Also present in the SE plots are large spikes that are more examples of similar peaks and troughs noticed in the repeatability plot in figure 4.3. In an attempt to reduce these peaks and troughs following the train of thought that resonances in the EUT cause large variations in field strength, results were taken with an absorber inside the EUT. The absorber is a carbon-impregnated foam block designated AN79 that is designed to absorb electromagnetic waves and therefore dampen resonances. The EUT is shown in figure 4.13 and the results for the three slots with the absorber present are shown in figures 4.14, 4.15, and 4.16.

It can be seen from figures 4.14, 4.15, and 4.16 that the large spikes in the previous SE results have been somewhat flattened by the addition of an absorber, suggesting that the absorber has helped to dampen some of the resonances present in the enclosure. However, some of the spikes are still present. These spikes should not be present in a statistically uniform field, however when tested the field distribution remains Rayleigh. This situation has been encountered before [41], with no conclusive outcome. A comparison between the SE measured with and without the absorber present can be seen in figure 4.17. Here

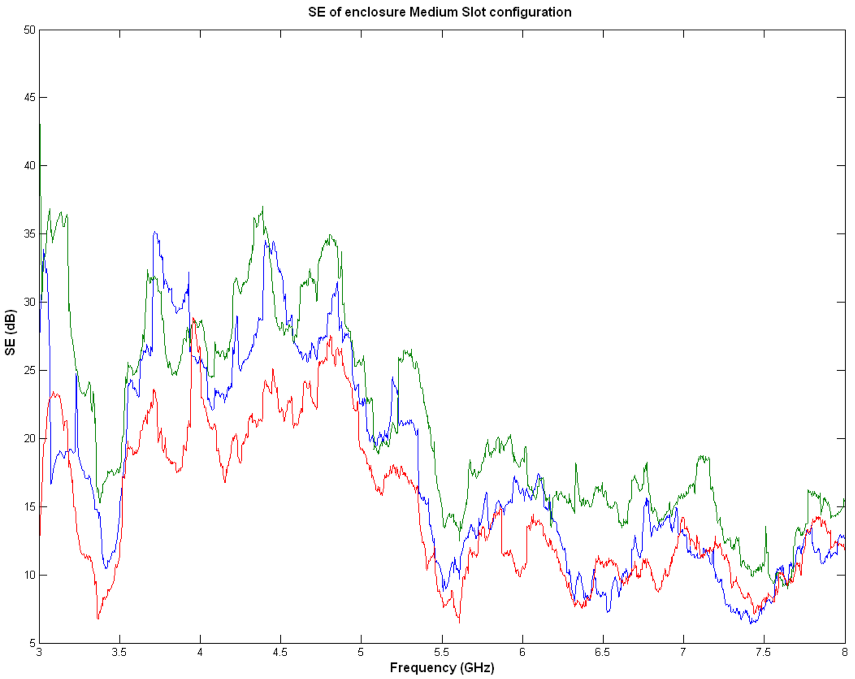

Figure 4.10: SE with medium slot. Note the SE is generally lower than that of the short slot.

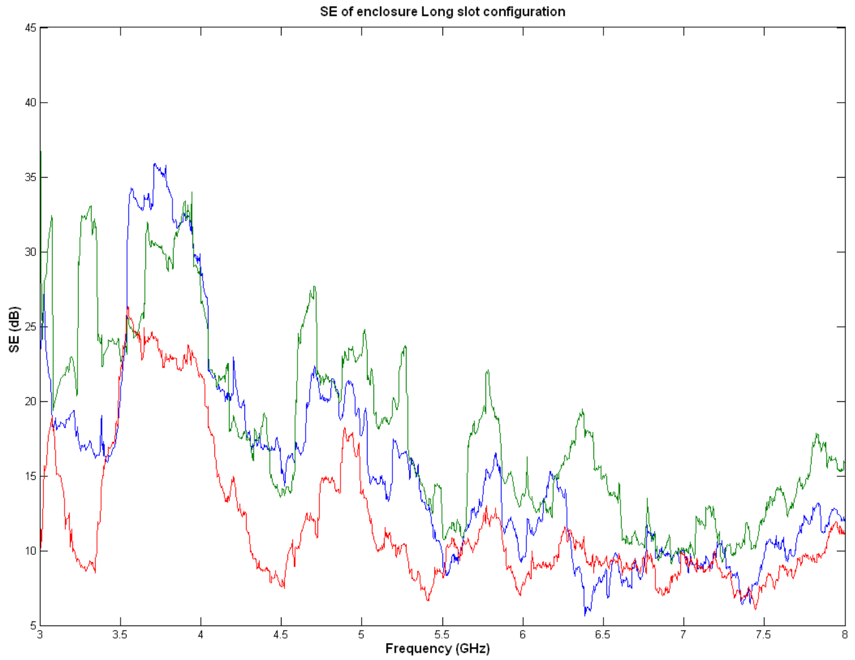

Figure 4.11: SE with the long slot. Note that this is generally less than both the medium slot and short slot SE value.

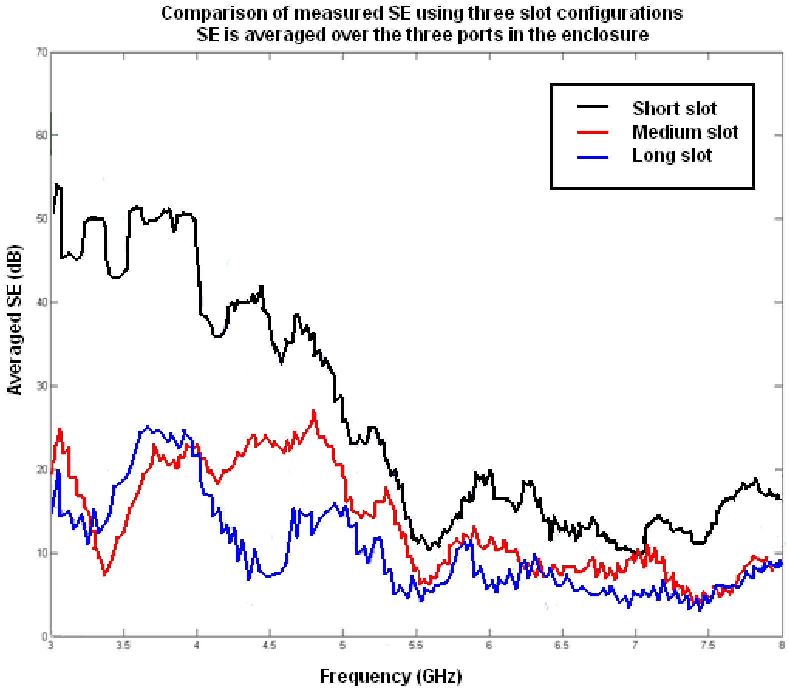

Figure 4.12: Comparison of the measured SE averaged over the three ports. The difference in SE is less at higher frequencies as the efficiency of the finger strip decreases.

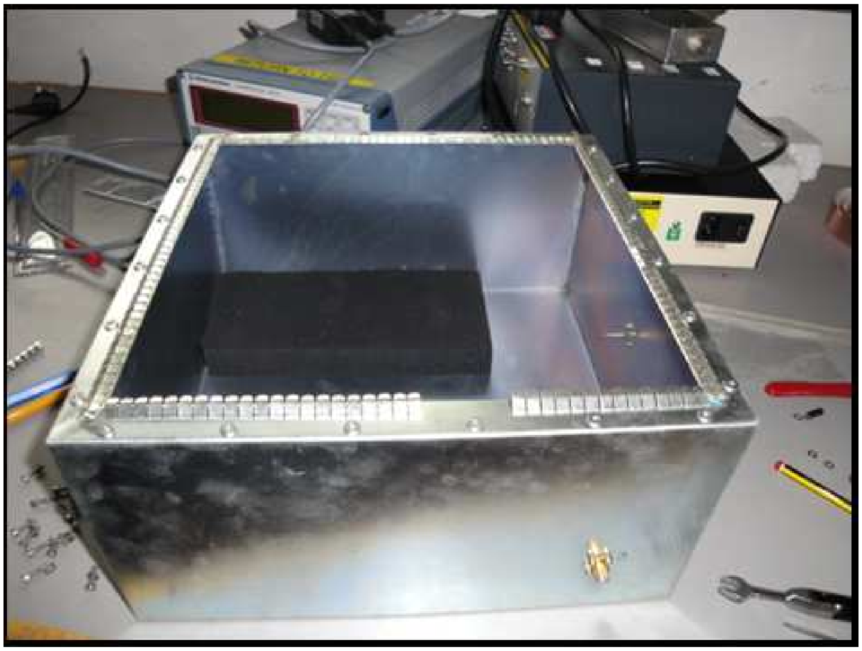

Figure 4.13: Internals of the EUT showing the added absorber block

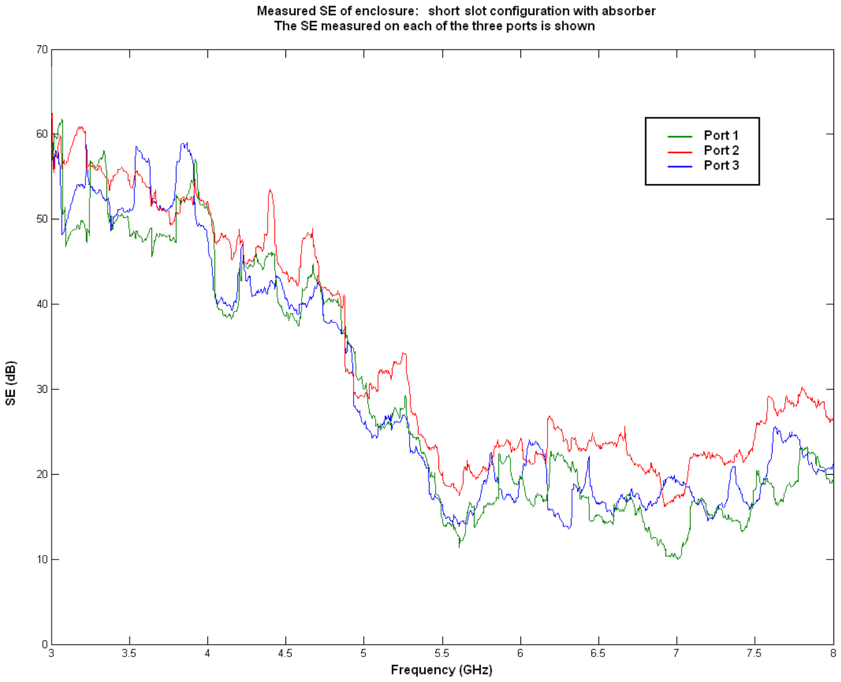

Figure 4.14: Short slot SE with absorber present.

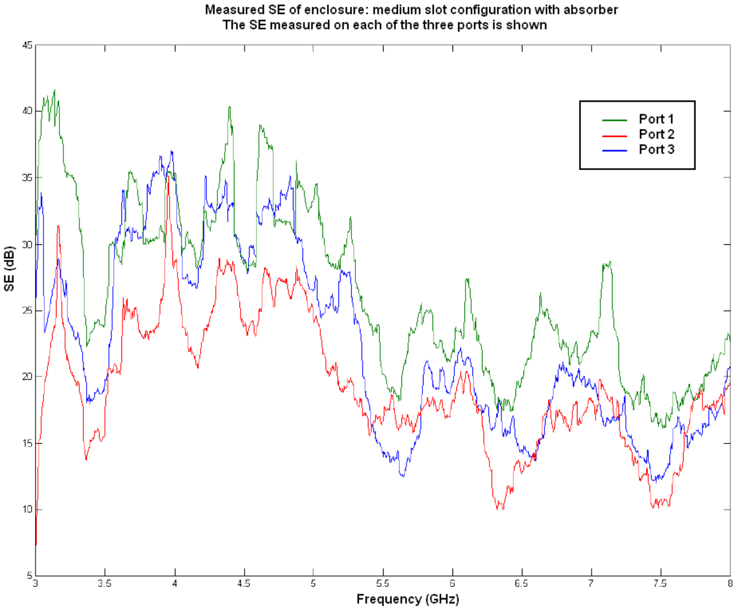

Figure 4.15: Medium slot SE with absorber.

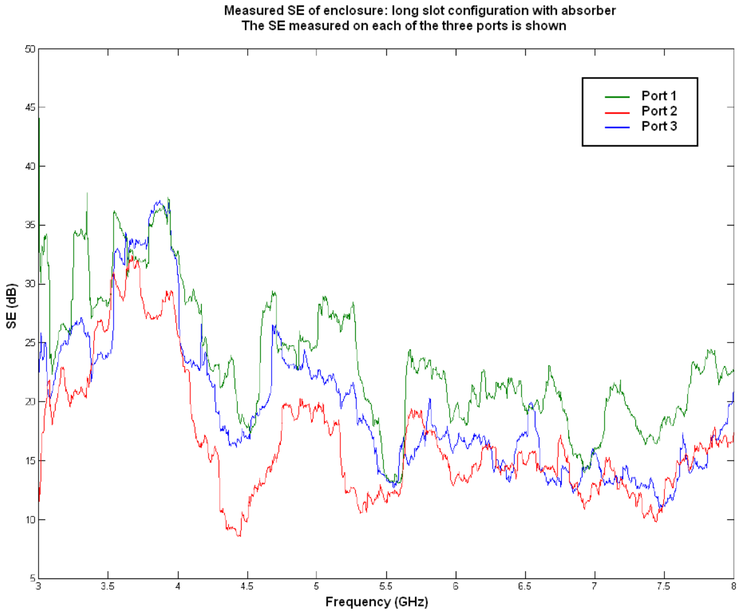

Figure 4.16: Long slot SE with absorber.

the absorption of large resonances at the lower end of the measurement frequency can be seen. The absorber has less damping influence at higher frequencies (above 6GHz), but can be seen to be increasing the measured SE by around 10dB. This is due to the fact that the presence of the absorber will reduce the power inside the enclosure and therefore result in a higher measured SE.

To check that the field statistics of the enclosure are behaving correctly, a DC mechanical stirrer was implemented. Using a DC motor as opposed to a contolled stepper motor allows the 5V supply powering the motor to be fed into the enclosure through an existing SMA bulkhead port, adaptors and BNC coaxial cables. Using this method of powering the stirrer removes the need for large holes in the enclosure that would be needed for the large shielded connectors used for the stepper motor. More holes in the enclosure are undesirable as they will have to be sealed off in a repeatable manner to ensure the enclosure can still be used in a round robin fashion; with less holes present the likelihood of errors involved in the resealing the EUT is reduced. The DC mechanical stirring method will also inform if the large changes in measured SE over small frequency ranges present in the previous results is a characteristic of the enclosure or an issue with the processing, data collection or post processing frequency stirring method. The DC stirrer is stepped in that results are taken while the DC motor is off, otherwise the electromagnetic noise from the brushes in the motor interferes with the desired data, as found in Chapter 3. The DC stirrer in the enclosure complete with 5V supply can be seen in figure 4.18. As this enclosure is

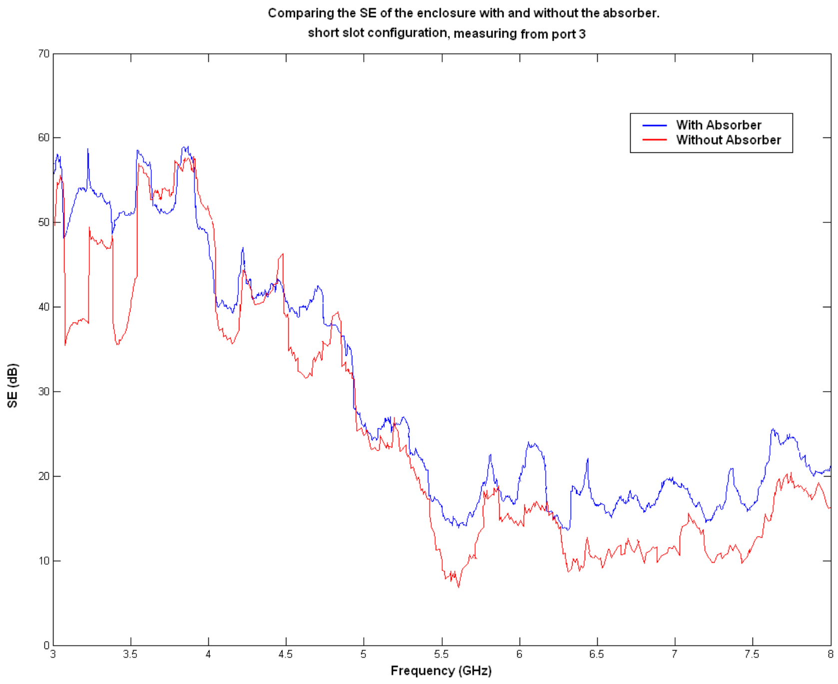

Figure 4.17: Comparison of the measured SE using port 3 with and without the absorber block present. The short slot configuration is shown.

taller than the enclosure used in Chapter 3 then there is no need for a right angle drive; the motor can be mounted vertically.

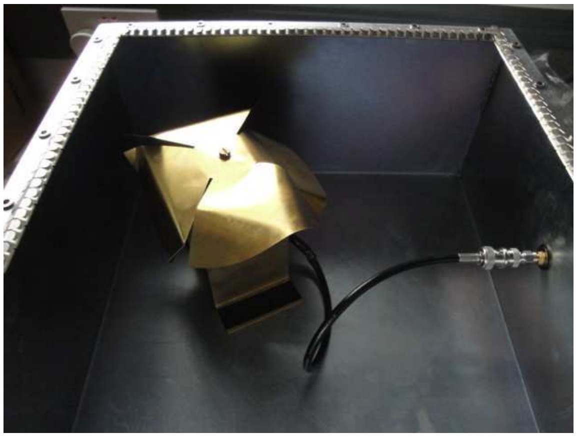

Figure 4.18: DC stirrer present in the enclosure. A similar stirrer paddle is used in chapter 3

The SE result from the DC stirrer can be seen in figure 4.19. The two traces are frequency stirring (without absorber present) and mechanical stirring; the frequency stirring is obtained from one of the mechanical stirring traces. It can be seen in figure 4.19 that the two traces for the SE from both methods mostly lie on top of each other. The first 50 results of the frequency stirring trace are ignored due to the way that the averages are calculated

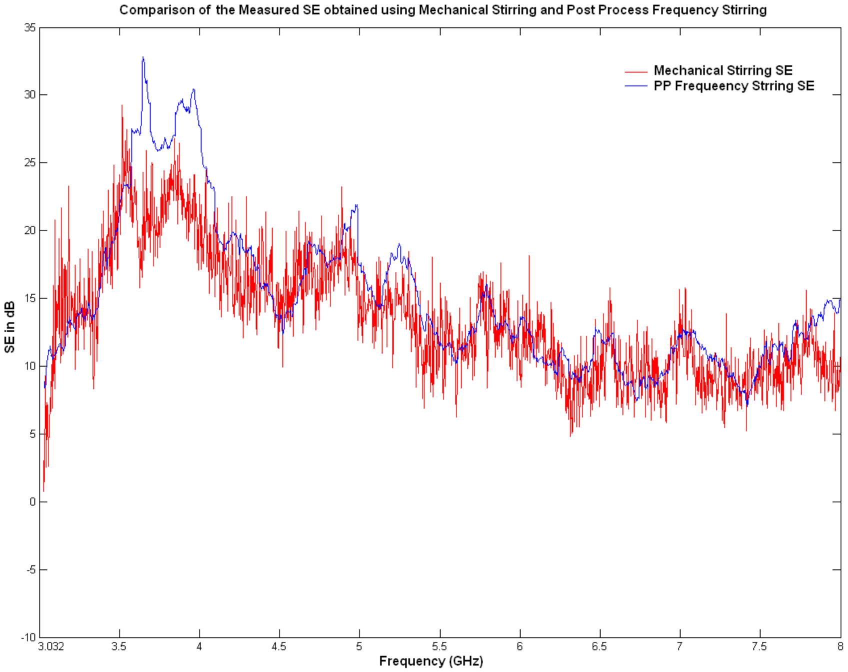

Figure 4.19: DC stirring compared to post process frequency stirring.

using the frequency stirring window. The 50 point stirring window within which the data points are averaged does not give the correct value until it is 50 points into the data, hence why the plot begins at 3.032GHz (recall the 31.5MHz stirring window). The large changes in SE at adjacent frequencies are also still present but lessened on both traces, suggesting that the presence of the stirrer, motor and associated wires provides some electromagnetic damping of resonances. A point of interest is that even though the overall shape of the two traces is similar, there are variations of around 15dB (for example at 3.8GHz). At other frequencies (4.2GHz and 7.3GHz) the difference is very small. This is possibly down to the large changes in levels around these frequencies observed in the previous figures. Figure 4.19 proves that the mechanical and frequency stirring methods are equivalent to each other, due to the fact that only at a couple of frequency areas around 3.8GHz and 6.75GHz is the difference between the mechanical and frequency stirring traces larger than the 7dB repeatability limit obtained earlier with the port repeatability data. The spikes present in the post processing method perhaps indicate that the mechanical stirring method is better at coping with the large resonances present in empty enclosures with a very high $Q-$factor. This is due to the fact that the stirrer, motor and associated cabling all have an effect on the loss inside the enclosure, and reduce the $Q-$factor. As seen in figure 4.17 the addition of absorbent contents reduces the resonance within the enclosure; it is likely that the stirring components are having a similar effect.

4.4 Chapter Summary

This chapter has provided a useful insight into the repeatability of enclosure measurements. As can be seen, it is possible to get good agreement between measurements with the application of finger strip to the enclosure lid. This repeatability of 7dB between runs has been replicated at the UoA, showing that this sort of enclosure could be used to check different chambers in different labs are capable of producing the same results. As seen, however, the results are not the same between the two labs, and reasons for this are not deducible from these results. A comparison between stirring the enclosure using the post processing method and using a stepped small internal mechanical stirrer is also shown, this shows good agreement (within 5dB for the majority of the frequency range) between the two methods. Further development of this method may result in an additional check when building and testing reverberation chambers.

Chapter 5

Rician Statistics and the $K-$factor

5.1 Introduction

This Chapter details the effect of a Rician distributed statistical environment on the measurement of received powers in enclosures. The method of testing outlined in IEEE 299 [5] assumes that stirring in both the outer reverberation chamber and the inner EUT is fully effective and that the field is uniformly distributed within the working volume. There is no mention of testing the distributions in the methods used in [5] to ensure that this is the case. The work done in this chapter looks at how the change in the magnitude of a direct path in a reverberation chamber has an effect on the measured power and therefore on the measured SE. Also investigated is how the Rician $K-$factor can be used as a measure of field uniformity. A direct path in a reverberant environment is measured as a Rician distribution of electric field values. A summary of the distributions and how they are created is given in section 2.6.

5.2 Reverberation Chambers - Required Field Uniformity

It is important when using using reverberation chambers to check that the internal fields are statistically uniform, as all calculations of SE of enclosures are dependent on the statistical uniformity of the received power. The uniformity can be tested in a number of ways, although it is not deemed necessary if following IEEE 299.1 directly. When using [5], it is assumed that, for a well-stirred reverberation chamber, that the probability density function (PDF) of the magnitude of one component of the electric field follows a Rayleigh distribution [31][41]. This is due to the in-phase and phase-quadrature components of E_x, E_y and E_z being normally (Gaussian) distributed and having a mean of zero [31]. If the distributions of these components of the field are centered on zero, then it follows that the resultant PDF of the magnitude of the electric field will follow the predicted Rayleigh distribution.

The above statement relies on the fact that the reverberation chamber has sufficient modes present inside it to enable the stirrer to stir successfully. Measurements in this section are carried out with more than 100 resonant modes excited below the lowest testing frequency in both the EUT and the chamber.

A problem can potentially arise in a reverberant volume if the Gaussian distributions of the in-phase and phase-quadrature contributions have non-zero means. This indicates that there is a direct path present between the source antenna and the measuring field probe. A direct path in a reverberation chamber refers to the situation where the transmission antenna can directly illuminate the receive antenna with no reflections from the stirrer (in the case of a mechanical stirrer) or the chamber walls taking place. This is illustrated in figure 5.1.

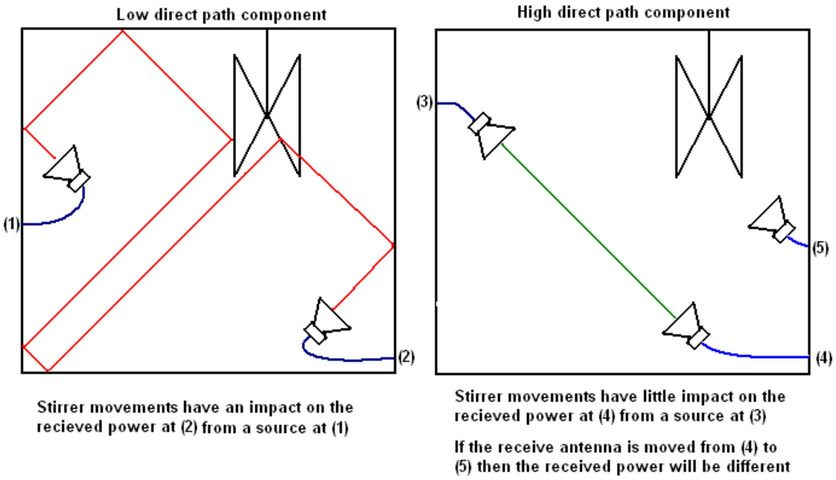

Stirrer movements have an impact on the recieved power at (2) from a source at (1)

Stirrer movements have little impact on the recieved power at (4) from a source at (3)

If the receive antenna is moved from (4) to (5) then the received power will be different

Figure 5.1: Illustration of a direct path in a reverberation chamber. It can be seen that the power received on (2) will change as the stirrer rotates, and also that the power received on (4) will not. In addition, the power received at (5) will be different from the power received at (4)

Referring to figure 5.1, it can be seen that moving the receive antenna from (4) to (5) will result in a different level of received power, whereas the average received power on (2) will be statistically the same throughout the chamber due to effective stirring and antenna placement. A direct path such as the green straight line between source and receive in figure 5.1 results in a non-zero mean, due to the dominance of the unstirred component over the stirred component [69]. Distributions with non-zero means are statistically representative of a direct path [69] [70] meaning some areas of the reverberant volume have higher average received power than others. The result of this is that measurement of electric field is now dependent on the position within the chamber of the receive antenna. This means that the reverberation chamber is no longer working as intended or assumed, which will increase the measurement error and decrease the reliability (in that the measured SE cannot be relied on to be representative of the actual SE of the enclosure) and repeatability of any measurements made of the shielding effectiveness of enclosures. The assumption that within the working volume the average received power is statistically uniform is no longer valid, making the power received with a monopole or at an EUT aperture dependent on its position. For larger EUTs, this can result in non-uniform illumination, a problem that is exacerbated when more than one aperture is present. A reverberant environment without a direct path ensures that every aperture on the EUT is equally illuminated; equal aperture illumination may not occur if there is a direct path present.

In the case where the Gaussian distributions have non-zero means, the resultant field statistics can be described by a Rician distribution, the form of which can be seen in table 2.1 in section 2.6. The measurement of a Rician distribution in a reverberation chamber indicates that a direct path is present and the internal fields are not statistically uniform, with the associated consequences to the quality of the measurement. An acceptable level of offset is established in this chapter, allowing categorisation of a Rician distribution that will significantly effect the measurement.

It has been shown that the field inside an EUT in a nested reverberation chamber setup can be measured with a small monopole probe antenna mounted on the inner wall of the EUT [7]; this approach is widely used to measure the SE of enclosures. Unfortunately, this approach may not be applicable if there is a Rician component large enough to render the field uniformity assumption untenable in the chamber, as average received power is used in [7] to confirm that the wall mounted monopole is equivalent to a monopole in free space. Due to the fact that the average received power is reliant on efficient stirring (in order to retain the independence from position), and an absence of direct path components, this means that the average received power on a wall mounted monopole is also dependent on efficient stirring. In the analysis in [7], it is assumed that the field components are

Gaussian distributed random variables with zero means, and there is special attention paid to the experimental results in [7] to ensure that is the case. If the field components have a non-zero mean, then a wall mounted monopole cannot be relied upon to give results that are equivalent to those obtained with a working volume probe.

Due to the effect that a Rician distribution of electric field can have on the measurement, the distributions of the in-phase and phase-quadrature components need to be examined and used to help build a picture of how large the magnitude of a direct path has to be in the reverberant volume before it starts influencing the uniform field assumptions. To achieve this, a simulated environment was created to test for direct paths in any physically small electrically large EUT. The workings of this simulation are detailed in the following section and can be seen in the Appendix (Chapter 10). The simulation can be set up to examine both single or multiple apertures.

The possibility of a direct path between the source antenna and an aperture in an EUT is increased when more than one aperture is present in the EUT, because the coupling between the source antenna and the receive antenna has a choice of paths, one or more of which may have a large direct or unstirred component. For example, if the stirring is not particularly effective, (if the paddle is too small) then the direct path in the chamber can be minimised by pointing the aperture away from the transmit antenna when carrying out measurements on enclosures. Unfortunately real world enclosures rarely have only one well defined aperture, meaning that a multiple aperture EUT is more susceptible to direct paths in an under-performing chamber. Even if the outer chamber is correctly stirred, there is a possibility of a direct path inside the EUT. If this is the case, it means assumptions of field uniformity are no longer tenable inside the EUT. This results in the measurement antenna being dependent on position inside the EUT and means that a wall mounted receive monopole is no longer representative of a receive monopole in free space. These points highlight the need to stir effectively inside the EUT.

As seen previously, (section 2.3) the of SE of an enclosure can be defined as shown in equation 5.1,

$$SE_{dB} = 20 \log_{10} \left(\frac{P_{out}}{P_{in}} \right) \tag{5.1}$$

where P_{in} and P_{out} are the average received powers, measured by monopole antennas inside and outside the EUT respectively. The magnitude of the average received power is dependent on the distribution of the received power. As the level of shielding given by equation 5.1 depends on the magnitude of the received powers, it can be said that the SE is dependent on the statistical distribution of the averaged received powers that make up both P_{out} and P_{in}, which are in turn dependent on the distributions of the electric fields.

If the electric fields inside and/or outside the EUT are not Rayleigh distributed, then the SE will have a statistical distribution different from that which is expected, and therefore the measurement of the SE will also be dependent on the position of both the location of the EUT within the chamber, and also the location of the receive antenna and/or any contents present in the EUT. With a well-stirred (in both chamber and EUT) nested chamber setup, the external (to the EUT) monopole measures a Rayleigh distribution of electric field while the internal EUT monopole measures a double Rayleigh distribution of electric field [56]. This is due to the fact that the Rayleigh distribution generated from the Gaussian distributed phase and phase quadrature components present in the chamber combines with the Rayleigh distribution that exists in the EUT at the point where the two reverberant volumes join, i.e. at the aperture(s). It is important to note that the assumption of a double Rayleigh distribution might not hold true if there is a Rician component involved in either the chamber or the EUT.

5.3 Direct Paths in Enclosures

The EUT is set up as in figure 5.2, with three apertures designated A, B and C. The apertures are created by monopole antennas mounted on bulkhead connectors on both sides of the enclosure wall to act as a penetration point. This novel method of aperture creation produces repeatable apertures that can be easily changed without disassembling the EUT. This arrangement can be seen in figure 5.3, with a single monopole visible in 5.4. The enclosure probe and the aperture monopoles are 19mm long and connected to SMA (Sub-Miniature revision A, 50Ω impedance) connectors. The SMA connectors on the apertures (monopoles) that are not being used are terminated with 50Ω loads. The 360^o shielding caps used in Chapter 4 were away with the enclosure at the UoA.

It can be seen in figure 5.2 that there are three options for a varying selection of paths. Path A is set up with a Rician distribution both outside and inside the enclosure, representative of a worst case scenario regarding inefficient stirring in a nested chamber setup. This is achieved by placing the source antenna close to the EUT aperture and the mea-

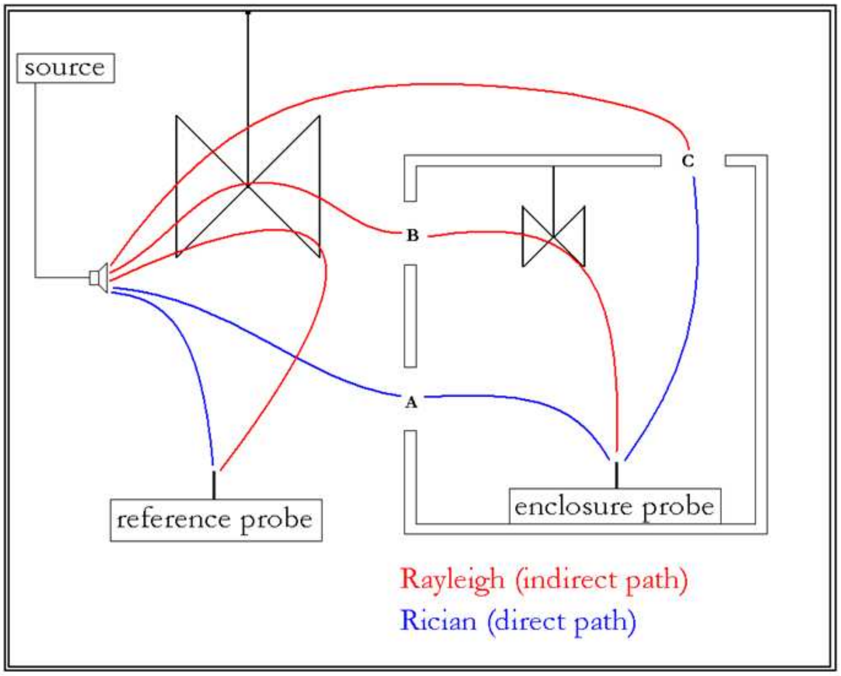

Figure 5.2: Schematic Diagram illustrating the various path options set up on the test enclosure

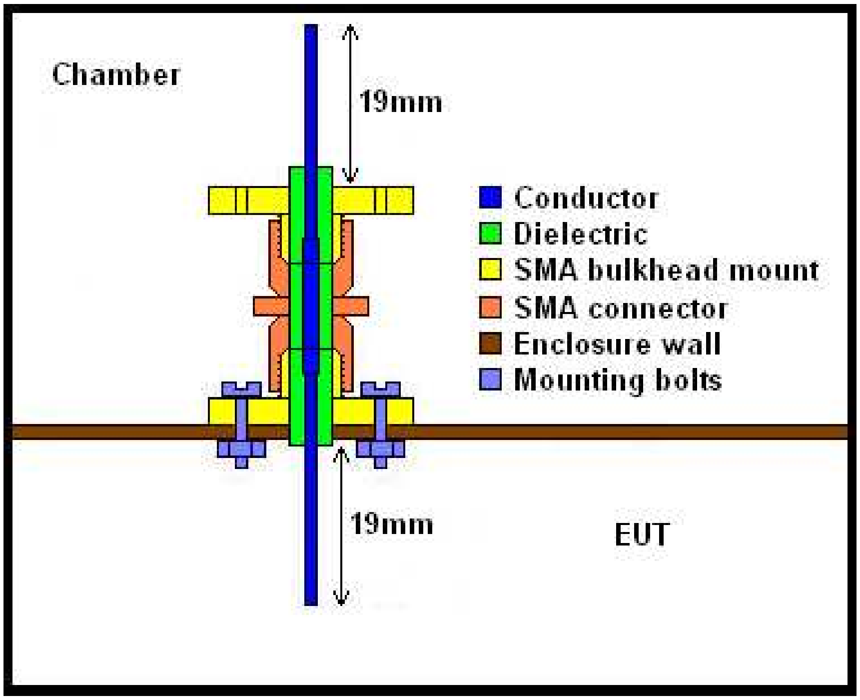

Figure 5.3: Diagram of the monopole arrangement used as apertures

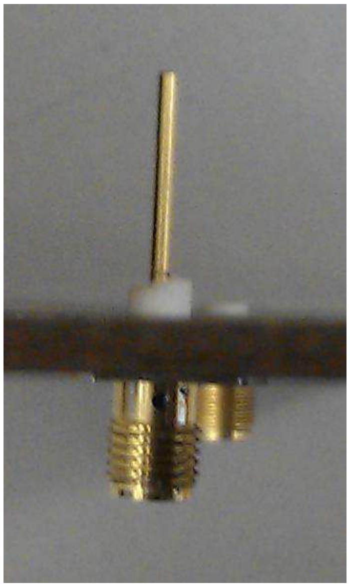

Figure 5.4: Close up of a single 19mm monopole with SMA connector. This one is on a ground plane, two are used with a female to female connector to create an aperture in an enclosure

surement antenna inside the EUT close to the aperture. The chamber and enclosure paths are engineered to emulate the right hand side of figure 5.1 and therefore bypass the stirrer to illustrate the effect of inefficient stirring. Path B is indicative of how the measurement is assumed to work, with a properly stirred Rayleigh distribution both inside and outside the EUT. This is set up by ensuring efficient stirring by placing the source antenna behind the stirrer pointing at the chamber wall, and measuring from an internal monopole that is placed such that the EUT stirrer is between the aperture and the measuring monopole. Path C is the most likely occurrence in a measurement situation where the EUT is unstirred, with a direct path present inside the EUT, set up with the source pointed at the chamber wall behind the chamber stirrer and no stirrer present in the EUT. It is likely that most measurements taken in the manner suggested by IEEE 299 (i.e. without an internal stirrer) have a direct component and therefore fall into the Path C category to some extent. In the situation where an internal stirring mechanism is not used, the size of the direct path inside the EUT depends on where the measurement antenna is in relation to the aperture(s).

5.4 The Rician $K-$factor

A useful measure of the magnitude of a Rician distribution is known as the $K-$factor [59]. The Rician $K-$factor is a measure of the relative size of a direct path between source antenna and the receive antenna compared to a situation with no direct path present, and is primarily used in a communications environment. A low $K-$factor (less than 1 [59]) indicates a well-stirred environment with no significant direct paths and therefore an expected Rayleigh distribution. Higher values of $K-$factor are indicative of a departure from statistical uniformity, with larger $K-$factors indicative of Rician distributions created from Gaussian distributions with larger offset from the zero mean. The $K-$factor is defined as the ratio of the direct path component to the scattered component [59], seen in equation 5.2.

$$K = \left(\frac{direct\ component}{scattered\ component} \right) \tag{5.2}$$

The $K-$factor can also be defined as a function of the unstirred (equivalent to the direct) component $E_{d\theta}$ and the associated variance of the field distribution σ as seen in equation 5.3

$$K = \left(\frac{|E_{d\theta}|^2}{2\sigma^2} \right) \tag{5.3}$$

From equation 5.3 [59] it can be seen that if the direct component is reduced to zero, then the $K-$factor also reduces to zero: therefore the $K-$factor is related to the direct component of the received field. If the direct component is significant, this can also be seen in the means of the in-phase and phase-quadrature normal distributions being offset from zero by some significant value. This value is termed ϕ. If ϕ is small, the distribution tends to Rayleigh. For simulated normal distributions here, the variance is set to 1, resulting in the $K-$factor being directly related to the unstirred component of the field. This leads to a relationship between the offset on the means of the normal distributions ϕ and the $K-$factor, shown in figure 5.5 and equation 5.4.

$$K_{\sigma=1} = \frac{\phi^2}{2} \tag{5.4}$$

The shape of figure 5.5 suggests that as the offset increases, the $K-$factor increases rapidly. It is said [59] that the distribution should be considered to be approaching Rayleigh if the $K-$factor is less than 1: this gives a value of ϕ of 1.4. If a value of ϕ is over 1.4 then the $K-$factor is over 1 and the distribution is likely to depart from the assumed Rayleigh distribution. The value of ϕ can be used as a measure of the magnitude of the direct path component, and therefore provide a cutoff point where $\phi_{min} = 1.4$, where values of ϕ larger than ϕ_{min} results in increasing Rician behaviour. This can be verified by examination of the distribution in question and the application of a goodness-of-fit test, while bearing in mind the limitations of tests such as the KS test.

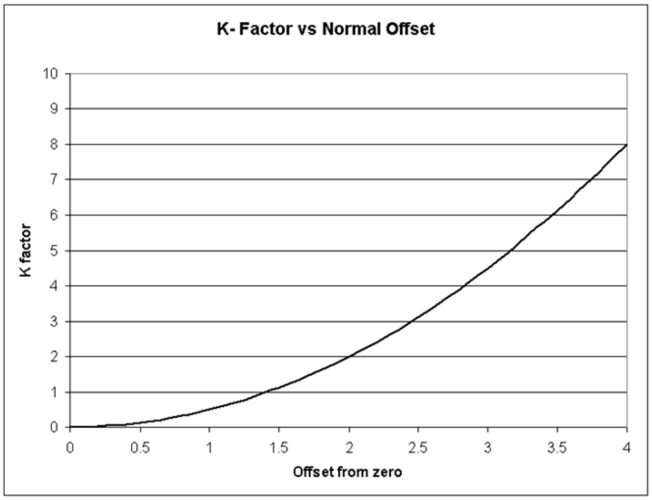

Figure 5.5: Plot of the Rician $K-$factor against the offset from zero of the mean of a Gaussian Distribution.

5.5 Simulation of the Test Enclosure

The simulations carried out in this section follow the paths A, B and C shown in figure 5.2. The simulation program was written in MatLab and can be found in the Appendix (chapter 10). The in-built Gaussian distribution generator in MatLab is used to specify Gaussian distributions with a variance of 1 and, for the simulation of a path with zero direct component, a mean of zero. Two Gaussian distributions are generated, then combined to achieve the desired distribution in the chamber. The simulation program allows input of Gaussian distributions with a definable offset mean ϕ and with a set variance of 1, meaning that different strength Rician distributions can be constructed. To explain the simulation program, Path A (see figure 5.2) will be followed. Path A is representative of the worst case scenario where stirring is ineffective in both environments, with a Rician distribution present both in the EUT and the chamber.

5.5.1 Simulation of Paths

Path A will be used to illustrate the workings of the simulation program. To simulate path A, first two Gaussian distributions with an offset mean of ϕ are generated. Note that if two Gaussian distributions of equal and opposite values of ϕ are combined, then the resultant distribution will be Rayleigh. The specification of two positive offset (the scatter plot is in the upper right quarter of a phase against phase quadrature plot) Gaussian distributions ($\phi > \phi_{min}$) simulates a direct path in a single enclosure and results in a Rician distribution when the two Gaussian distributions are combined. Two more Gaussian distributions of offset $\phi > \phi_{min}$ are generated and combined to create another Rician distribution, equivalent to a direct path present inside the EUT. The $K-$factors of both these Rician distributions are noted, being obtained from the specified value of ϕ and equation 5.4.

At this point in the simulation there are two separate distributions: the Rician distribution in the chamber and the Rician distribution in the EUT. Both of these distributions are made up of two non-zero mean Gaussian distributions. In a measurement, these two Rician distributions combine at the aperture, assuming a single aperture enclosure. The combination of the two Rician distributions at the aperture is calculated in the simulation by combining the matching in-phase and phase-quadrature Gaussian distributions from either side of the aperture using the root sum of the squares method.

When ϕ is set to zero, this simulation method results in Rayleigh outside the EUT and a separate Rayleigh inside the EUT. When the two are combined by the aperture, the resultant simulated distribution in the EUT becomes double Rayleigh, as found in [56][61]. The form of a double Rayleigh distribution can be seen in table 2.1. This simulated result is equivalent to the measurement obtained in a well stirred nested chamber setup. When the individual environments are Rician, a double Rician is formed when the two Rician distributions combine [71].

Figure 5.6 shows the resultant simulated distribution along path A with $\phi = \phi_{min}$ in both the chamber and EUT. It can be seen that the histogram (obtained by sorting the simulated field powers into bins) is showing deviation from the expected double Rayleigh distribution, which is outlined in blue.

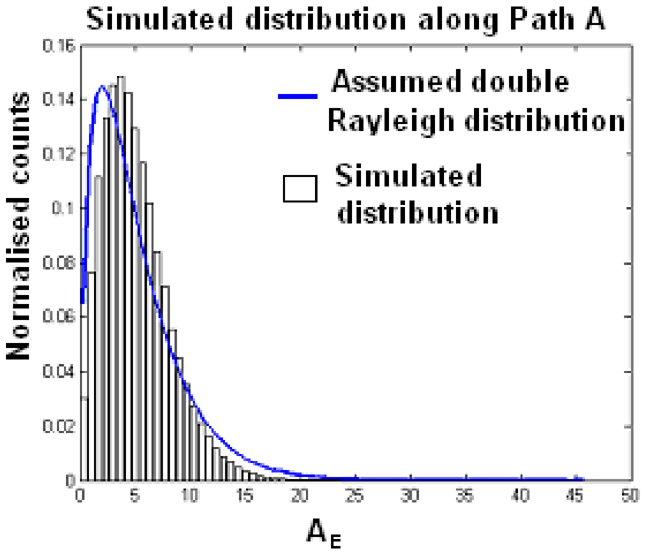

Figure 5.6: Histogram of the simulated distribution with ϕ = ϕ_{min} = 1.4 for all Gaussian distributions both inside and outside of the EUT compared with the assumed double Rayleigh distribution. This is representative of Path A.

Figure 5.7 shows the distribution along Path A (Rice-Rice) where $\phi = 5$ in each case. The histogram has become completely Rician in shape, which suggests a very large direct path component. This is known to be the case as it has been set in the simulation. In an experimental measurement, this situation could occur as a result of poor stirring effectiveness, bad experimental setup or an under-performing (high wall attenuation, high internal and/or antenna loss, or an unexpected aperture) chamber or EUT. The axis label A_E is representative of the electric field strength.

Figure 5.8 shows the distribution from Path C (Rayleigh-Rice), with the single Rician distribution in the EUT having $\phi = \phi_{min}$. It can be seen that the maximum of the histogram is slightly misaligned with the maximum of the expected double Rayleigh; this is due to the addition of the minimal Rician distribution. This becomes more apparent in Figure 5.9 where ϕ in the EUT Rician distribution has been increased to 5.

It is worth noting that the application of a relatively large Rician distribution in either the EUT or the chamber can result in a distribution being created that looks like a Rayleigh distribution instead of the expected double Rayleigh shape, as shown in Figure 5.10, where $\phi = 10$ in the EUT.

This is an important point, as confusion can arise while examining the distributions.

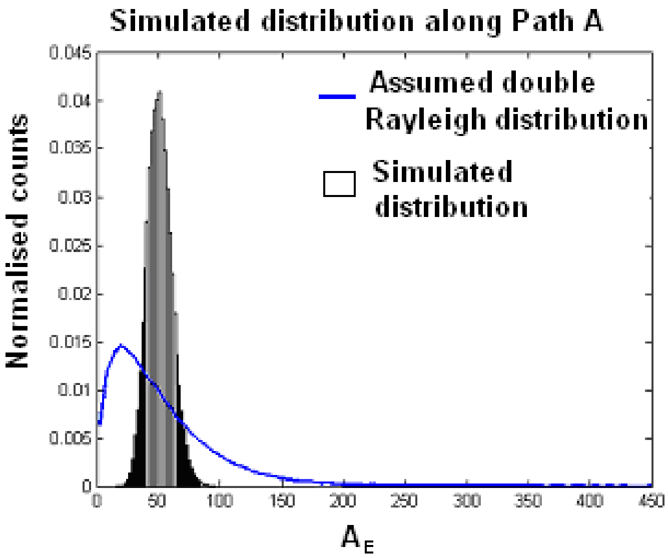

Figure 5.7: Histogram of the simulated distribution with ϕ = 5 for all Gaussian distributions both inside and outside of the EUT compared with the assumed double Rayleigh distribution. This is again representative of Path A, but with a larger direct path component than in figure 5.6.

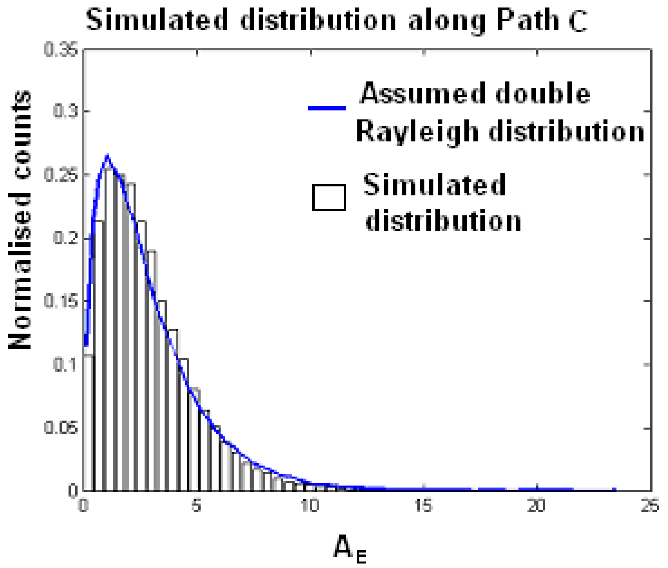

Figure 5.8: Histogram of the simulated distribution with $\phi = \phi_{min}$ = 1.4 for the two Gaussian distributions inside the EUT and with ϕ = 0 for the two Gaussian distributions in the chamber. Also shown is the assumed double Rayleigh distribution. This is representative of Path C

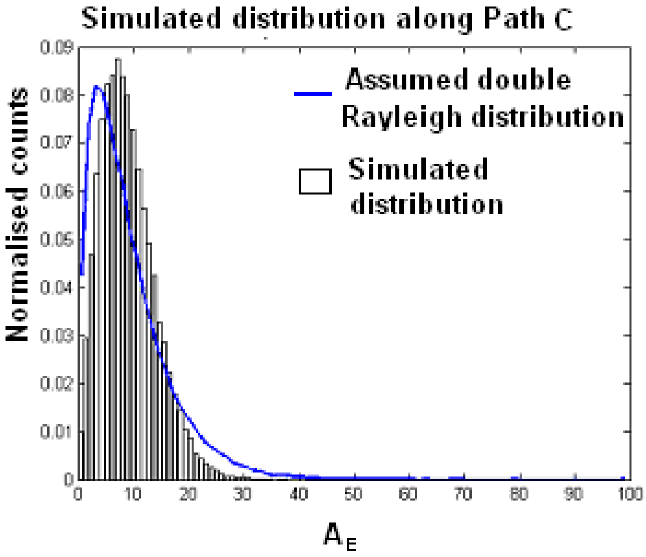

Figure 5.9: Histogram of the simulated distribution with ϕ = 5 for the two Gaussian distributions inside the EUT and with ϕ = 0 for the two Gaussian distributions in the chamber. Also shown is the assumed double Rayleigh distribution. This is representative of Path C with a larger direct component than in figure 5.8

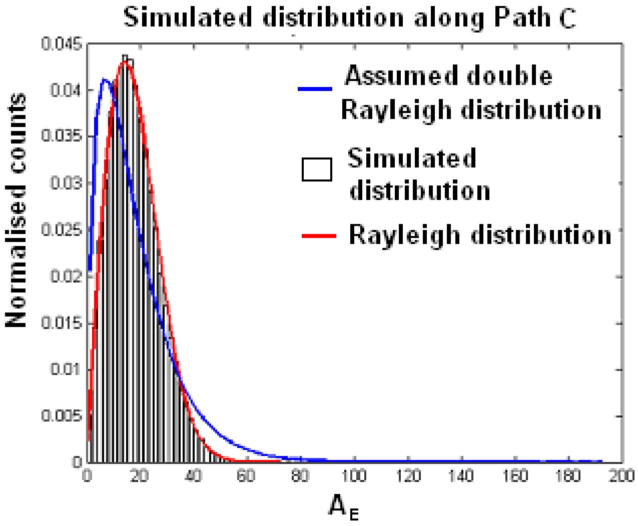

Figure 5.10: Histogram of the simulated distribution with ϕ = 10 for the two Gaussian distributions inside the EUT and with ϕ = 0 for the two Gaussian distributions in the chamber. Also shown is the assumed double Rayleigh distribution. Note that the simulated distribution follows the shape of a Rayleigh distribution due to the direct path.

This is due to the fact that the receive antenna in the EUT will also measure a Rayleigh distribution of electric field if the apertures are large enough to make the chamber and the EUT one reverberant volume. In the case of enclosures,where the change frequency between two statistically different enclosures and one single enclosure is close to the measurement frequency, a situation resulting in a 'fake' Rayleigh will cloud the point at which the chamber and enclosure become statistically separate. This case is more likely with an aperture dominated enclosure as the point where the chamber and enclosure behave as one occurs at a lower frequency due to the greater total aperture cross section.

If the Rician $K-$factor becomes very large, the form of the resultant combined distribution moves from a Rayleigh shape to a Rician shape, changing smoothly as ϕ increases. It is therefore possible to state that the stirring becomes ineffective as ϕ increases significantly above ϕ_{min}. As ϕ is defined by the variance of the data, the relationship between the $K-$factor and ϕ is different in a real situation rather than the simulated one shown here, as the variance will not necessarily be 1. The information shown in these simulated distributions also show how, if a Rician component is present, the distribution moves away from the expected double Rayleigh shape.

5.6 Experimental Setup - Creating a Direct Path

The main problem encountered while carrying out this particular set of experiments was being able to obtain a sufficiently large direct component in the reverberation chamber in order to prove the effects on the measured SE, and to obtain significant values for ϕ. Experiments were performed at 4GHz using the large reverberation chamber (dimensions 2.4m $\times$ 3m $\times$ 4.7m) with the EUT placed within the working volume. The EUT used is a 0.48m $\times$ 0.48m $\times$ 0.12m sealed brass enclosure with four bulkhead SMA ports each connected to a 19mm monopole antenna inside the EUT. The apertures are achieved by attaching a second monopole antenna to one of the existing SMA ports on the outside of the EUT, as shown in figure 5.3. One SMA port is used for the EUT probe antenna, and the other three are available as apertures, used to mimic the setup shown in figure 5.2 used in the simulation. The unused SMA ports are terminated with 50Ω loads. The direct paths within the reverberation chamber but external to the EUT are measured using a single 19mm monopole antenna on an electrically large ground plane. The direct paths within the EUT are measured between the internal probes. The setup showing the arrangement needed for the creation of a large Rician in the outer chamber is shown in figure 5.11. Due to the position-dependent nature of this experiment, when a reference and EUT measurement are needed the EUT aperture is aligned with the monopole on the ground plane (after the ground plane has been removed) as far as can be practicable.

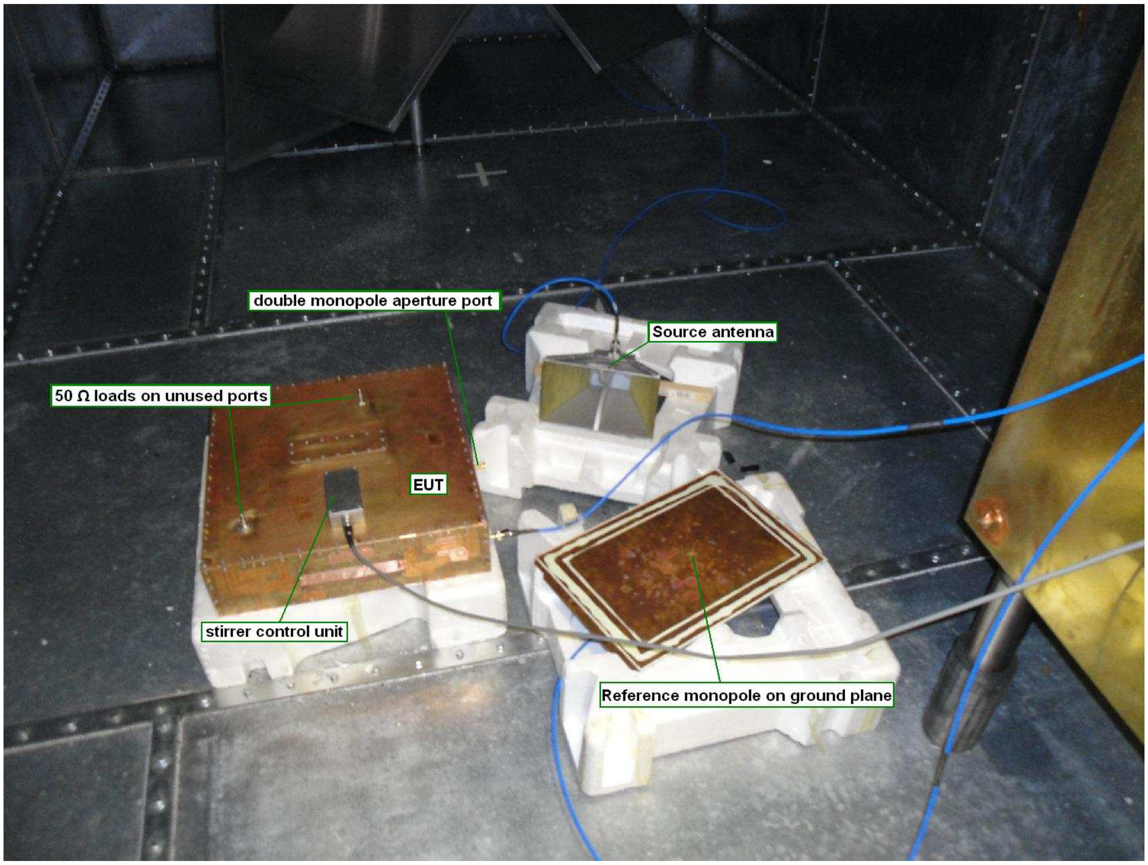

Figure 5.11: Experimental setup to obtain a large Rician component in the reverberation chamber

This setup shown in 5.11 would never be used in a measurement under testing conditions when following a standard; however the quality of the reverberation chamber at the UoY is such that obtaining a direct path is quite challenging, hence the very close proximity of horn antenna, EUT and reference probe. In a chamber that is not so effective at stirring, for example a poorly constructed chamber with a smaller paddle or with insufficient steps on the stirrer, a Rician environment is more easily obtained. In this experiment, the stirrer is used in the same way as it would be to obtain a uniform field measurement, as it was also of interest to see how effective the stirring was, to verify the quality of the UoY reverberation chamber.

The layout of the probes, apertures and stirrer within the EUT is such that either a Rician or a Rayleigh distribution can be established within the EUT. The varying paths used are shown in figure 5.12. Here it can be seen that there are a number of possible permutations to obtain varying strengths of direct path. A small stirrer is present inside the EUT, under the silver control box; in this image the large $K-$factor Rician path between port 3 and 4 is being tested, equivalent to the inner part of path A in figure 5.2. The 50Ω loads on the other apertures can just be seen on ports 1 and 2.

This part of the experiment can be carried out on the bench; there is no need to test inside the large chamber to establish the paths inside the enclosure as there are no apertures in the EUT. The inherent SE of the enclosure ensures a good test environment (all apertures are sealed) and the VNA uses one port to transmit and another to receive. The distributions obtained here are used to identify the $K-$factors of the various paths separate from the nested chamber arrangement. Resultant distributions that are compared to the simulated results are as per the simulation; i.e. tested in the reverberation chamber, in order to obtain the correct doubled distributions.

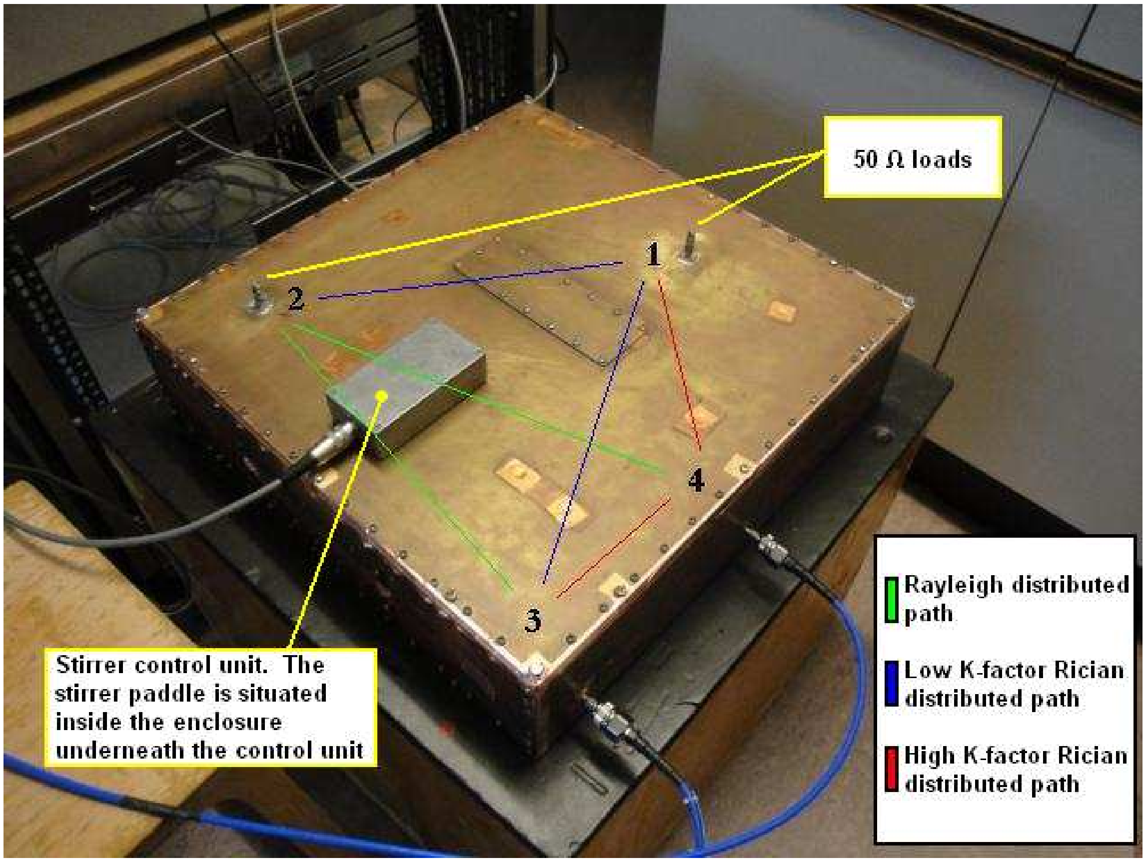

Figure 5.12: Experimental setup to obtain direct paths of varying $K-$factor within the EUT

With these two setups (figures 5.11 and 5.12, the paths inside and outside the EUT can be controlled separately, with the aperture configuration combined with the probe location allowing paths inside the EUT to be changed simply by changing the positions of the 'aperture' antenna and the measuring antenna. Using this knowledge, an experiment was carried out with the manufactured Paths A, B and C shown in figure 5.2 to see if the results obtained follow the relevant simulation. These results are taken at 5GHz using a receive port calibrated vector network analyser, with mechanical stirring in both the EUT and in the chamber.

It can be seen in figure 5.13 that when there is a large Rician component, in this case a Rician inside and outside the EUT, the distribution differs greatly from the expected double Rayleigh. As expected, the difference is less as the Rician component is reduced, as shown in figure 5.14, by only being present in the EUT in this case. The state where the direct path is minimised in either chamber or the EUT (figure 5.15) gives a result that is closer to the expected double Rayleigh distribution.

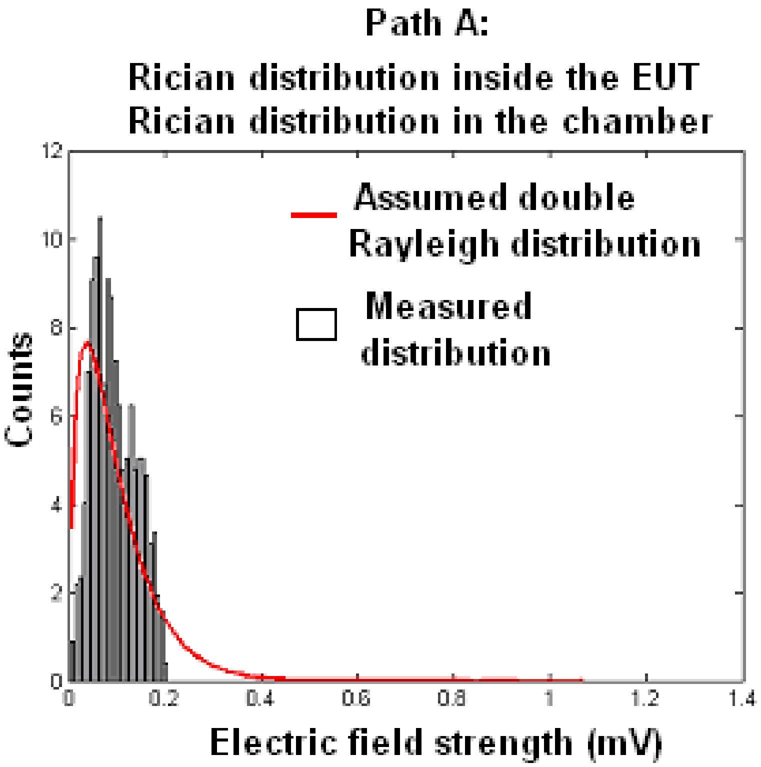

Figure 5.13: Histogram of the measured distribution along Path A compared with the assumed double Rayleigh distribution.

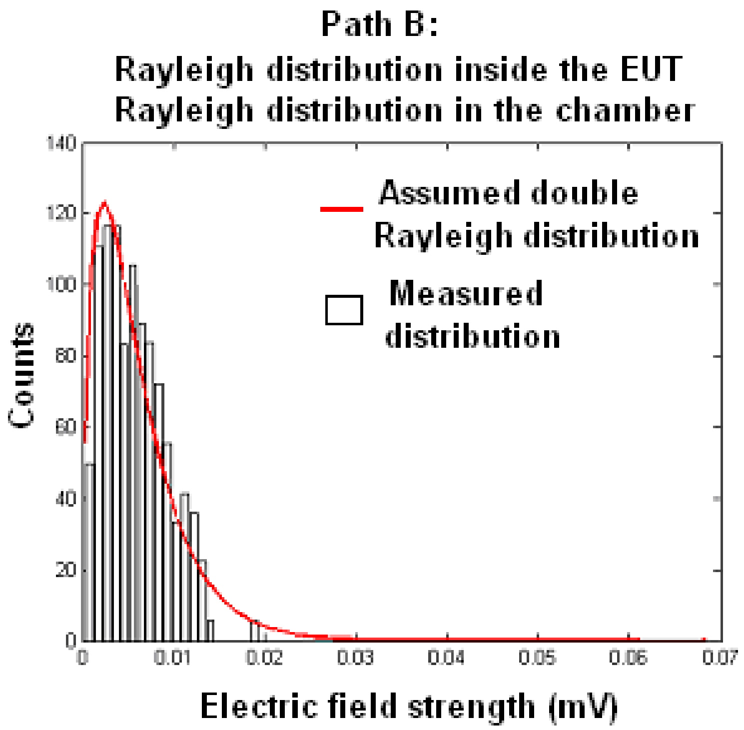

Figure 5.14: Histogram of the measured distribution along Path B compared with the assumed double Rayleigh distribution.

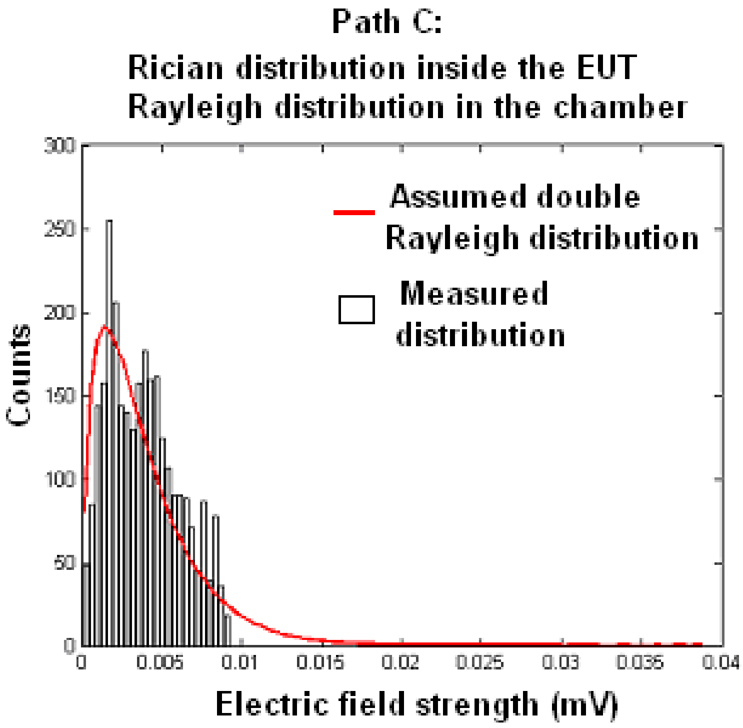

Figure 5.15: Histogram of the measured distribution along Path C compared with the assumed double Rayleigh distribution.

5.6.1 Experimental Results - Nested Chamber Measurements

It is useful to know if the presence of a Rician distribution and therefore a direct path alters the measured value of the SE. The internal field in the EUT is kept as a Rayleigh distribution using the knowledge obtained in the previous section during the bench-top EUT measurements. The external field is changed between being Rayleigh distributed and Rician distributed, obtaining a Rayleigh distribution, a small offset Rician distribution and a large offset Rician distribution. This is achieved with the layout of the chamber, using the setup shown in figure 5.11 to create a large Rician distribution, changing to a larger separation between horn and EUT for the smaller Rician distribution, and with the horn fixed to the wall behind the stirrer and pointing away from the stirrer for the Rayleigh distribution measurements, ensuring minimal direct path. For measurements not involved in investigating direct paths, this source antenna location is usually used. These different geometrical setups change the incident field strength on both the EUT and the reference; the magnitude of the Rician path can be seen by examining a histogram of the reference data. Three measurements were taken with different paths present in the outer chamber: a Rayleigh, a small Rician and a large Rician distribution. The histograms for the three measurements (taken from the reference probe) can be seen in figures 5.16 to 5.18.

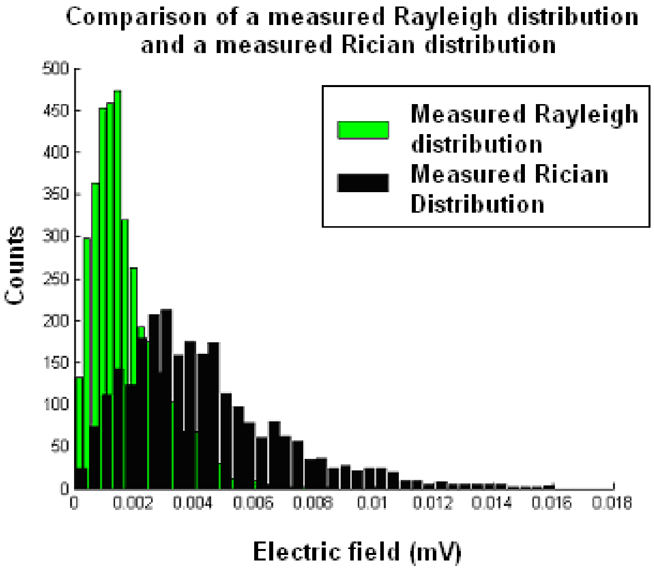

Figure 5.16: Rician distributed reference measurement (ϕ = 7.5 on both component Gaussian distributions) compared to a Rayleigh distributed reference measurement This Rician distribution is termed the ‘small’ Rician.

These reference measurements shown in figures 5.16 to 5.18 are used to calculate the SE of the EUT. The Rayleigh-Rayleigh situation (ideal measurement environment and an

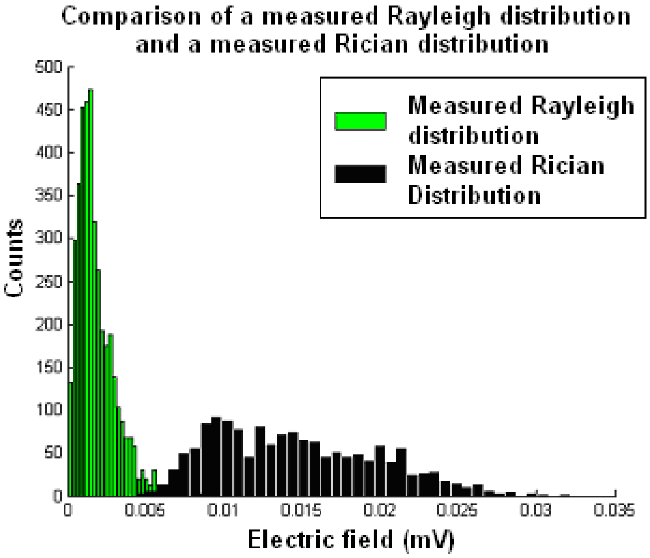

Figure 5.17: Rician distributed reference measurement (ϕ = 15.6 on both component Gaussian distributions) compared to Rayleigh distributed reference measurement. This Rician distribution is termed the 'large' Rician.

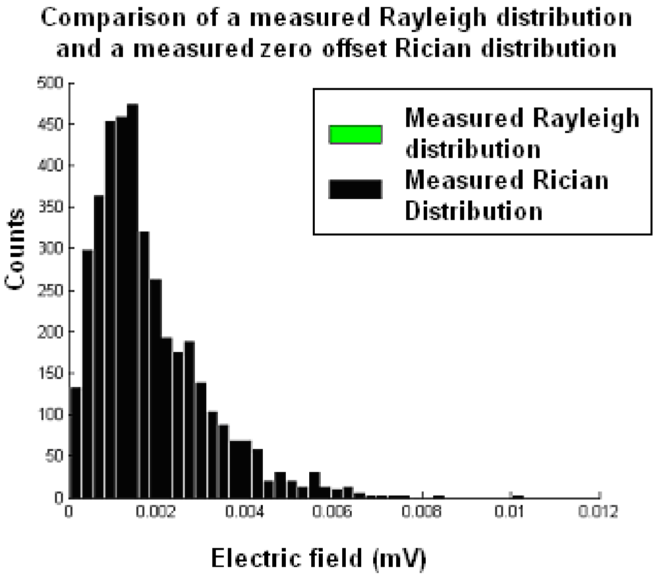

Figure 5.18: Zero offset Rician reference measurement compared to Rayleigh reference measurement. They are shown to be the same.

accurate representation of the SE) is shown on all the following SE plots (the red line) and the Rician-Rayleigh situations are shown by the blue line. The SE with a Rician distribution present is calculated using the power received inside the EUT under Rician path conditions as P_{in} and the various reference distributions shown in Figures 5.16 to 5.18 as P_{out}. The Rician distribution incident on the EUT has value of ϕ = 11.2.

5.7 Effect of Rician Statistics on the Measured SE

Figure 5.19 shows the SE plot when the Rayleigh distribution seen in figure 5.18 is used as the reference measurement. The path from the source to the EUT is Rician with $\phi = 11.2$ in the blue plot and Rayleigh ($\phi = 0$) in the red plot. It can be seen that there is a large difference between the SE obtained with Rayleigh distributions and the SE obtained with Rician distributions, around 15dB on average, with the Rician path SE being measured as much smaller. The $S11$ correction detailed in [7] is used here on both traces, but because of the large Rician distribution incident on the EUT, the Rician path SE shows negative dB values, which the antenna reflection coefficient compensation should not allow. If the fields are supposedly uniform, then it is impossible to have a higher value of average received power inside a well stirred overmoded EUT over the LUF than is present outside the EUT when using an external source. In figures 5.19 to 5.21 , the red line is always the SE obtained with Rayleigh field incident on both the EUT and the reference.

Also measured was the SE with a Rician reference measurement of ϕ = 7.5 (figure 5.16), shown in Figure 5.20. This Rician reference measurement was taken with the source horn antenna pointed at the EUT and the reference, this arrangement creates the black distribution shown in figure 5.16. It can be seen in figure 5.20 that the two SE traces are much closer together, with the Rician path SE being about 7dB less than the Rayleigh path SE.

The Rician distribution in figure 5.17 was measured with the horn antenna pointing directly at the reference monopole and has $\phi = 15.6$. The Rician distribution in figure 5.17 gives the SE trace shown in figure 5.21. Illustrative of the importance of a statistically uniform field for the measurement of SE, figure 5.21 shows that with the large Rician reference present, the measured Rician path SE is now actually larger than the measured Rayleigh path SE.

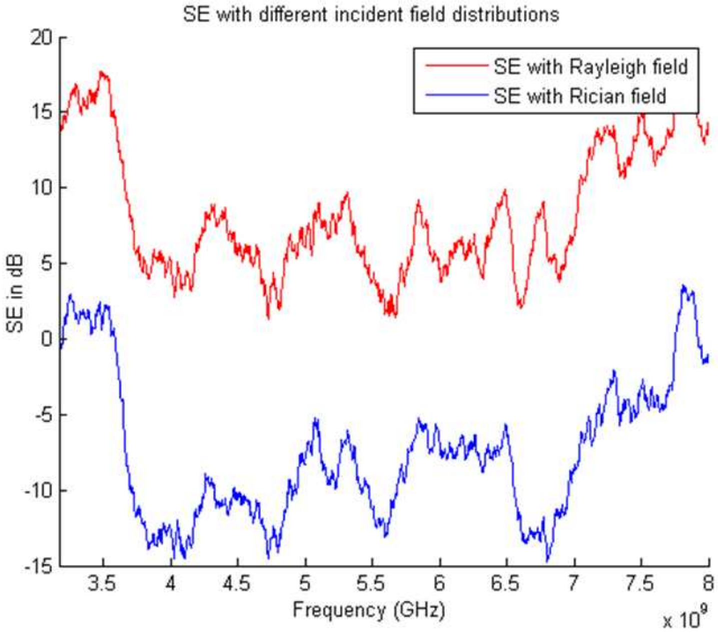

Figure 5.19: SE measurement with small Rician inside the EUT and Rayleigh outside

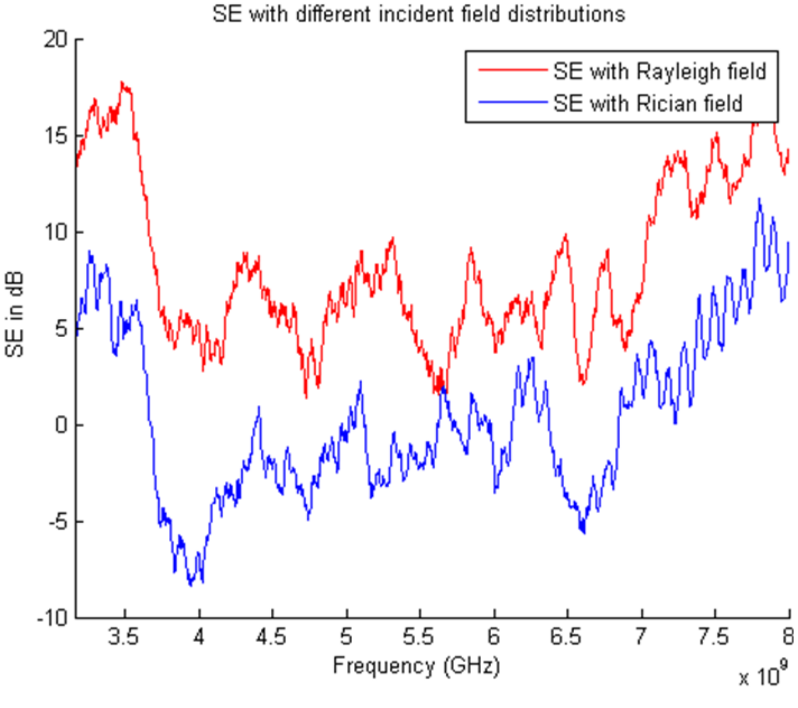

Figure 5.20: SE measurement with small Ricians inside and outside the EUT

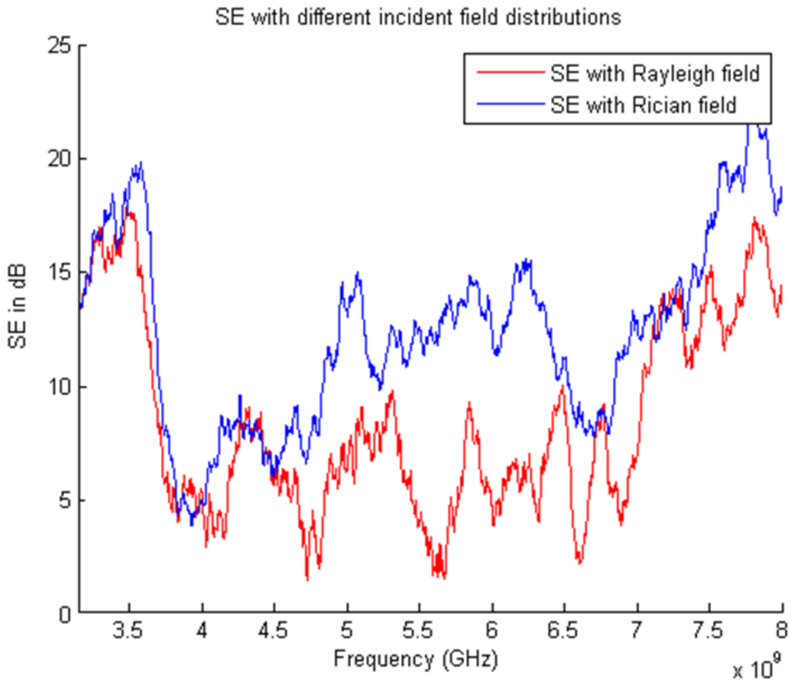

Figure 5.21: SE measurement with large Ricians inside and outside the EUT

5.8 Chapter Summary

It would seem important to check that the distribution within a chamber or enclosure being used for shielding measurements is indeed as assumed. There is no mention of such a check in the IEEE 299 standard, meaning that it is possible that SE measurements can be unreliable if the chamber and/or enclosure do not have a uniform field distribution. This chapter proves the importance of making sure the field is statistically uniformly distributed before making a measurement of the shielding effectiveness. A way to obtain this is to use the Rician $K-$factor to measure the stirring effectiveness and therefore give an indication of the chamber performance, leading to knowledge about the statistical uniformity and therefore the distributions of the fields. Both simulated and experimentally measured results show that if the offset of the mean of the Gaussian distributions ϕ is less than 1.4 then the chamber or enclosure is providing adequate field uniformity. In order to be sure of measurements in a reverberation chamber this check should be performed every time the experiment setup is changed.

Chapter 6

Estimating Shielding Effectiveness using Absorber Cross Sections

This chapter will present results obtained using a new method of estimating the SE of an enclosure. The concept is that an enclosure with a large proportion of internal absorber will reduce the $Q-$factor of both the EUT [72][73] and the outer test chamber. The reduction of $Q-$factor in the chamber should be dependent on the shielding performance of the enclosure. To investigate this, the enclosure used in chapter 3 with dimensions of 0.48m × 0.48m × 0.12m is used, which has a minimum frequency of 1.9GHz, below which 60 modes are excited.

6.1 Experiment Setup

The enclosure is placed within the working volume of the reverberation chamber on a polystyrene block. The source and receive antennas were placed within the chamber, with the source antenna behind the stirrer and the receive antenna mounted on a piece of rigid coaxial cable connected to the wall of the chamber. The enclosure was loaded with a 0.4m × 0.4m square of microwave anechoic chamber pyramidal wall absorber, and the transmission across the reverberation chamber is measured. There is no stirrer present in the enclosure during this experiment, and post processing frequency stirring is used in the outer chamber.

The experimental setup is shown in figure 6.1. It can be seen from figure 6.1 that the reference measurement is when the enclosure is absent, and the absorber is present in the chamber, and the shielded measurement involves shielding the absorber. The difference

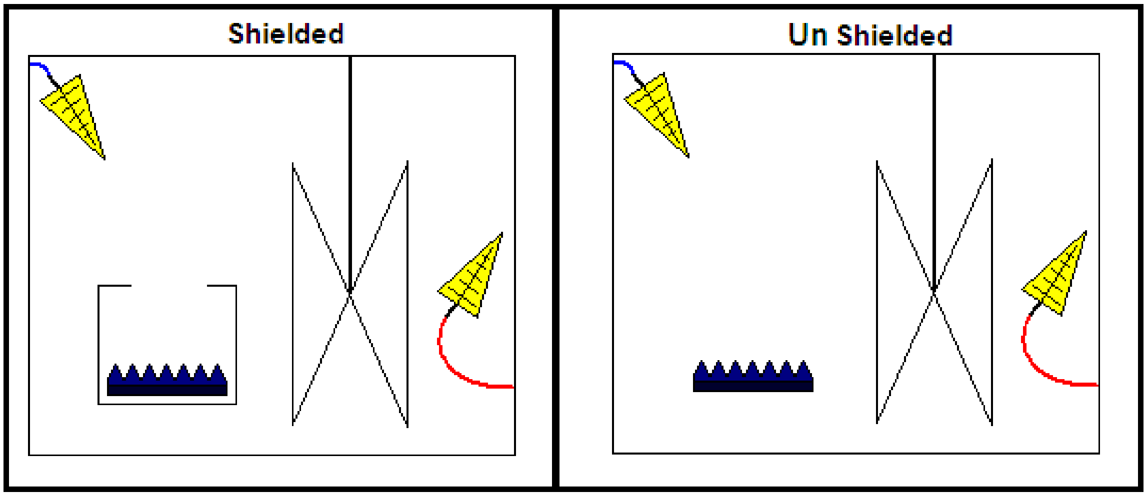

Figure 6.1: Experimental setup showing shielded and unshielded measurment arrangements.

in the measured power in the reverberation chamber is likely to be small, but should be representative of the shielding performance of the enclosure when the SE is predominantly influenced by aperture losses. The aim of this experiment was to see if this effect would be measurable in the large reverberation chamber.

No monopole antennas are mounted in the enclosure, however a single aperture is varied in size to test the sensitivity of the measurement. The four different apertures used are: (1) no front (2) a square hole of dimensions 40mm tall by 160mm wide (3) a long slot that is 4mm tall and 120mm long and (4) a short slot that is 4mm tall and 40mm wide.

6.2 Centralisation of Measured Distributions

As this measured effect is expected to be very small, some effort is made to ensure there is no direct path. As presented in previous chapters the presence of a direct path can influence the measurement of SE. In this experiment, the analysis suggested by [69] is followed, which involves centralising the measured electric field distribution to remove the direct path component.

The way that this is implemented is to first measure the received power across the chamber. The resulting distributions of the phase and phase quadrature are noted and the means calculated. In an reverberant environment with no direct path present then the means of the Gaussian distributions of the phase and phase quadrature will be zero. A non-zero mean therefore indicates a direct path. In order to remove any direct path component the mean of the measured distribution is centered on zero by obtaining the vector mean of the measured data, then subtracting this value from each measured data point. A diagram of how a Rician distribution appears on a phase vs. phase quadrature plot when measured in a reverberant environment is shown in figure 6.2. In figure 6.2, phase is plotted against phase quadrature, or, as measured using a Network Analyser, the real component is plotted against the imaginary component. This makes the centre of the distribution, i.e. the mean, $A_o + jB_o$. A_o and B_o are used to re-centre the distribution, in this case each data point would have the operation $-A_o$ and $-B_o$ carried out on it. Another way of looking at the centering operation is to consider the distributions of the phase and phase amplitude components. As mentioned, in a perfect reverberant environment the distributions of the two components are normally distributed with a zero mean. Figure 6.3 shows an extreme illustrative representation of non-zero means. The centering of the data is equivalent to centering the means of these two distributions on zero [69].

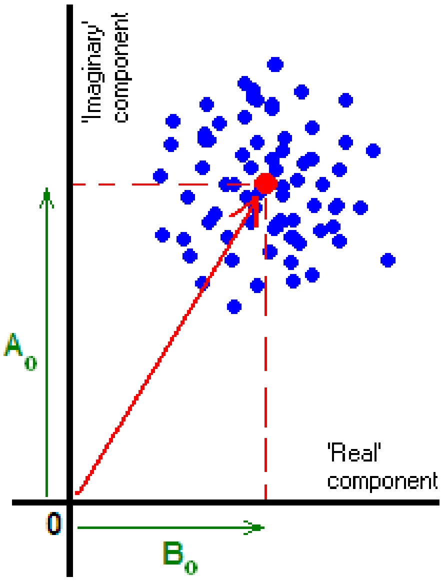

Figure 6.2: Schematic Diagram illustrating offset measurement centering

The centered measured distributions are now combined to obtain the Rayleigh distributed $S12$ parameter across the chamber. The distributions are centered for both the shielded and reference measurements, post-processing frequency stirring is used, then the SE is calculated using the corrected data.

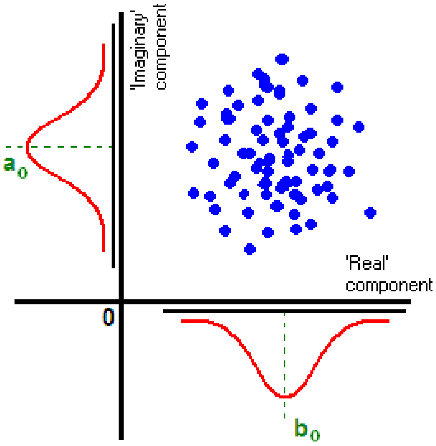

Figure 6.3: Exaggerated illustrative direct path with non-zero means

6.3 Comparing the measured results

The method outlined here is intended to give an indication of the possibility of using this measurement system to gauge the SE of the enclosure. The electric field data taken across the chamber is compared between the reference and the shielded measurements by using a ratio (here termed the loss ratio L_R) similar to the SE equation, shown in equation 6.1.

$$L_R = 20 \log_{10} \left(\frac{reference}{shielded} \right) \tag{6.1}$$

The loss ratio is representative of the aperture size of the enclosure. In an empty enclosure where the SE is governed by the aperture losses, this measure should be representative of the SE of the enclosure. In this case, the higher the loss ratio the larger the loss across the chamber and the lower the SE. A direct comparison of the loss ratio and the SE is not carried out, as it is found that the difference in reference and shielded measurements is not sufficient to make this a valid method of estimating the SE. It is misleading to refer to the SE directly, as in this case the enclosure expected to have a high SE has a near zero loss ratio.

6.4 Results

The unstirred transmission across the chamber ($S12$) is between 10dB at 2GHz to 7dB at 9GHz lower with the absorber placed within the working volume of the chamber. This is representative of the difference between a completely unshielded measurement and a fully shielded measurement, assuming that the enclosure completely shields and there is no absorption loss across the chamber with the enclosure in place with no apertures. This puts a limit on this measurement method, as there is only a 10dB window in which this method would work using this enclosure and chamber. Perhaps for larger enclosures where more absorber could be used this measurement window would increase.

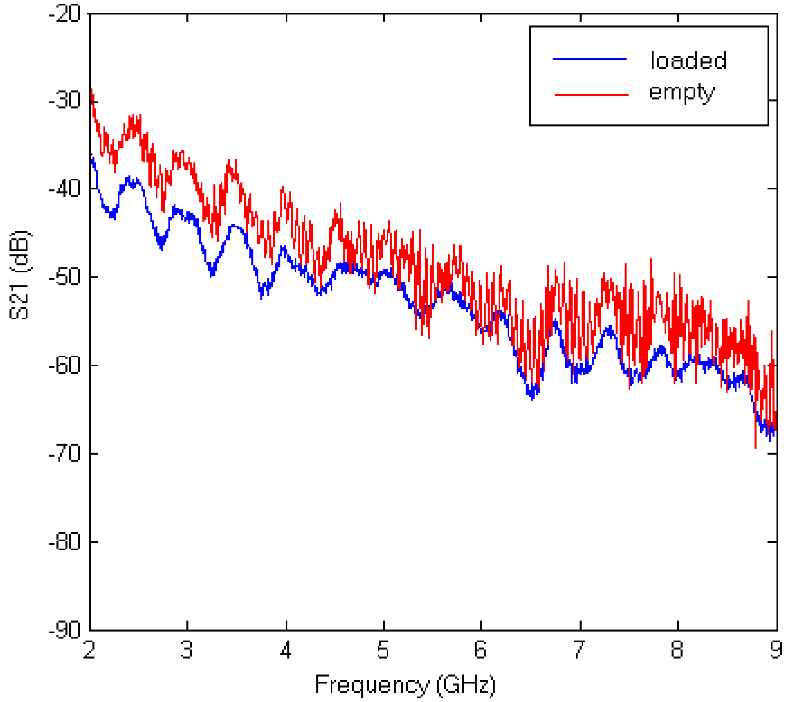

Figure 6.4: Transmission across the reverberation chamber with and without a 0.4m × 0.4m sample of pyramid absorber. Note how the absorber dampens the resonances evidenced by the smoother loaded trace

Figure 6.5 shows the loss ratio measured using the method illustrated in figure 6.1. The large aperture (aperture (1)), shown in red, has the largest difference between the reference and the 'shielded' measure, and therefore the largest loss ratio and the smallest SE. It can be seen that the difference between the loss ratios of the different apertures is very small, with a maximum difference of around 1.5dB. This is a very small difference between the reference and the shielded measurement considering that the enclosure has an entire side removed. The measurement with the short slot (aperture (4)) does not register any loss at all, hovering around a 0dB loss ratio. This is because the aperture is too small to allow much absorption; equivalent to having a very small amount of absorber in the chamber. Due to the fact that there is very little absorption potential with the smaller apertures, it can be said that this method works better for very large apertures. This is relative though,

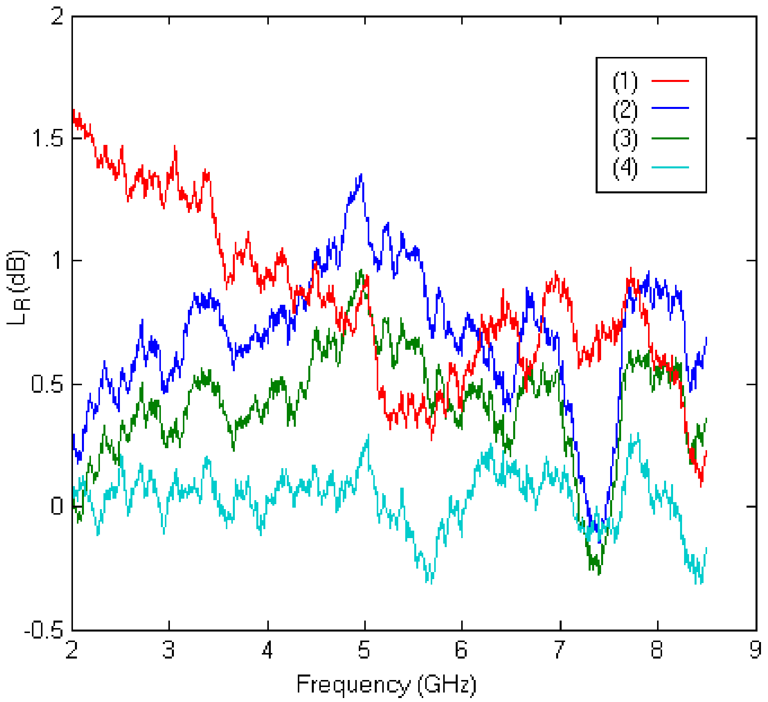

Figure 6.5: Loss ratio with using a loaded enclosure with different aperture sizes

as even the largest effect using this method is a lot smaller, and therefore more difficult to measure, than the usual measurement method using nested chambers. Due to the small size of this effect, this method is not very robust and is very susceptible to changes in field strength due to direct paths; this is why the distributions need to be centralised.

6.5 Chapter Summary

This short chapter has shown that using the absorption cross section of the reverberation chamber with a loaded EUT to estimate the SE of the EUT is not a viable method. The aim was to measure the differences in the received power across the chamber that occur due to a loaded enclosure with varying aperture sizes. This method works best for enclosures with large apertures, i.e. enclosures with very low SE. It has been found that for an enclosure of similar size to a standard 19 inch rack unit there is a measurement window of around 10dB, the narrowness of which results in a method that requires extreme sensitivity of measurement setup. The high sensitivity of the method results in poor resolution, as the differences between expected high SE and low SE enclosure setups is very small, of the order of 1dB. This is too small to be of any practicable use, as the effect can easily be eclipsed by the uncertainty in the chamber. The SE of the enclosure would have to be so low, i.e. the apertures so large, for this method to provide a large enough effect to be robust, that the enclosure would not be able to be classified as an ’enclosure’ any more. Further investigation into the relationship between the loss ratio and the SE of the enclosure was not carried out, as it was thought that the measurement technique was just too sensitive, and not applicable to moderate to high levels of shielding enclosure.

Chapter 7

Using $Q-$factor to estimate shielding effectiveness

7.1 Introduction

In this chapter, a relationship between the shielding effectiveness and the $Q-$factor of the enclosure under test (EUT) is investigated. Measurements are made in an anechoic chamber to obtain the $Q-$factor of the EUT and to assess the shielding effectiveness of the enclosure under test. A relationship between $Q-$factor and shielding effectiveness is shown, and possible uses of this relationship are discussed. The rationale behind such a measurement is to develop a technique that removes the need to alter the enclosure in any way. It may be possible to obtain the $Q-$factor without penetrating the enclosure with an antenna if the enclosure is aperture dominated, which would be a useful property of the measurement if used in real world EUTs. Previous enclosure shielding methods, both in this thesis and in IEEE 299 [5], involve measurement of the electric field both inside and outside the EUT.

7.2 SE and Effective Stirring

Recalling the corrected SE equation introduced in section 2.8.1, and reproduced in equation 7.1, it can be seen that an increase in the measured power inside the enclosure, for example as a result of any apertures present in the enclosure, reduces the value of the SE. Obtaining the SE of an enclosure using equation 7.1 involves a measurement of the field strength external to the EUT $S12_R$ and a measurement of the field strength inside the enclosure $S12$, and applying mismatch correction factors to the receive antenna. This equation holds true for an effectively stirred, electrically large EUT and test chamber. As a VNA is used in this experiment, the S-parameter antenna corrections on the reflection coefficients can be applied.

$$SE_{dB} = 20 \log_{10} \left(\frac{< |S12_R|^2 > (1 - | < S11 > |^2)}{< |S12|^2 > (1 - | < S11_R > |^2)} \right) \tag{7.1}$$

For the method outlined in [5] and the above equation to be valid, the EUT has to be classed as an electrically large reverberation chamber. Either mechanical or electronic mode stirring can be used to obtain statistical field uniformity; in this chapter the method is mechanical stirring, with a stirrer situated inside the EUT. With the stirrer paddle inside the EUT, the stepper motor is bolted to the outside of the EUT and the motor is controlled via shielded cables from the PC outside the outer chamber. The method of obtaining the $Q-$factor (see section 7.5) also results in narrow band frequency stirring over the measurement bandwidth, meaning that the end data set is double-stirred. Double stirring occurs when two methods of stirring are used, in this chapter mechanical stirring is used in the chamber and enclosure. The act of taking the autocorrelation has a similar effect to the post processing stirring method (see section 2.5.4 and chapter 4) in that an average over a bandwidth is calculated. Therefore the results obtained after the mechanical stirring and autocorrelation have been carried out have been averaged twice, hence the term double stirred.

For the stirring to be effective and to provide an adequately uniform field, the chamber must be of sufficient size to enable the LUF to be within the measurement capability of the VNA The LUF (f_{min}) minimum frequency below which 60 resonant modes should exist, as detailed in section 2.5.2[7][14]. For the EUT used here (dimensions of 0.48m × 0.48m × 0.12m) f_{min} is 1.9GHz. The experiments here are carried out at 4GHz to make absolutely sure there are enough resonant modes present below the test frequency for the EUT to be in an overmoded state. Previous work (see Chapter 4) and [4] suggests that over 100 modes is a more satisfactory limit for effective statistics. In this EUT, there are around 300 modes excited below the test freqency of 4Ghz, calculated using equations for the corrected Weyl's law (2.8) and the mode density (2.9). The actual number of modes depends on the ratio between the mode density and the mode bandwidth [32][22] and can be calculated using models as in [22]. Mechanical stirring is utilised in the EUT in this experiment, with 200 steps per rotation. This number of steps has been shown to give fully effective stirring in this EUT, as evidenced by the fully Rayleigh path present within the enclosure; shown in chapter 5.

7.3 $Q-$factor review and application to this chapter

Hill et all [49] show that the reciprocal of the total average $Q-$factor of an electrically large reverberant enclosure can be described as the sum of four contributions: Q_1 (7.3), the losses in the walls of the cavity, Q_2 (7.4), the absorption loss by means of any absorbing contents, Q_3 (7.5), aperture losses and Q_4 (7.6), the losses in the measurement antennas. This is expressed in Equation 7.2.

$$Q_{tot}^{-1} = Q_1^{-1} + Q_2^{-1} + Q_3^{-1} + Q_4^{-1} \tag{7.2}$$

$$Q_1 = \frac{3V}{2\mu_r S\delta} \tag{7.3}$$

$$Q_2 = \frac{2\pi V}{\lambda < \sigma_a >} \tag{7.4}$$

$$Q_3 = \frac{4\pi V}{\lambda < \sigma_l >} \tag{7.5}$$

$$Q_4 = \frac{16\pi^2 V}{m_a \lambda^2} \tag{7.6}$$

As this investigation has been expressly set up to achieve aperture domination, i.e. the main dependence of Q_{tot} is on Q_3. This means that equation 7.5 is the most interesting and useful part of equation 7.2 in this chapter. These experiments are carried out with nothing inside the enclosure other than the probe antenna (a 19mm monopole connected to a bulkhead SMA port) and the mechanical stirrer meaning there is little if no absorption loss inside the enclosure. This has the effect of making Q_2 very large, and therefore Q_2^{-1} vanishingly small. Thus the absorption $Q-$factor can be ignored in this case. The input from the wall $Q-$factor Q_1 is not needed, as the change in surface area between the different front panel arrangements is not large enough to merit investigation. The antenna

$Q-$factor Q_4 is the same throughout, as the same antenna is used and the VNA remains calibrated. As the $Q-$factor is measured and compared to a relative SE value, any antenna-dependent $Q-$factor will be the same throughout and therefore not have a bearing on this measurement.

If it was necessary to obtain a measurement of the actual value of the SE then the antenna $Q-$factor would have to be accounted for. It is worth noting that, with the exception of the 'small hole' configuration, (see Figure 7.1) , all apertures in these experiments are electrically large at 4GHz (wavelength of 7.5mm). The only value in equation 7.2 that changes throughout these experiments is that of the aperture losses Q_3. The other $Q-$factor contributions, can be assumed to stay constant over the small measurement bandwidth used for the $Q-$factor measurement. The $Q-$factor in relation to the walls of the enclosure, Q_1 will change slightly as the surface area of the enclosure is changed due to the addition of an aperture, though in this enclosure the change is small. The surface area term in Q_1 will become more significant when larger apertures are used, as the difference in surface area between a large enclosure with a large aperture and a large enclosure with no aperture is greater that the equivalent with a smaller enclosure. It is the relationship between the aperture dominated SE and the aperture $Q-$factor that is of interest in this chapter, and a comparison of the two is carried out.

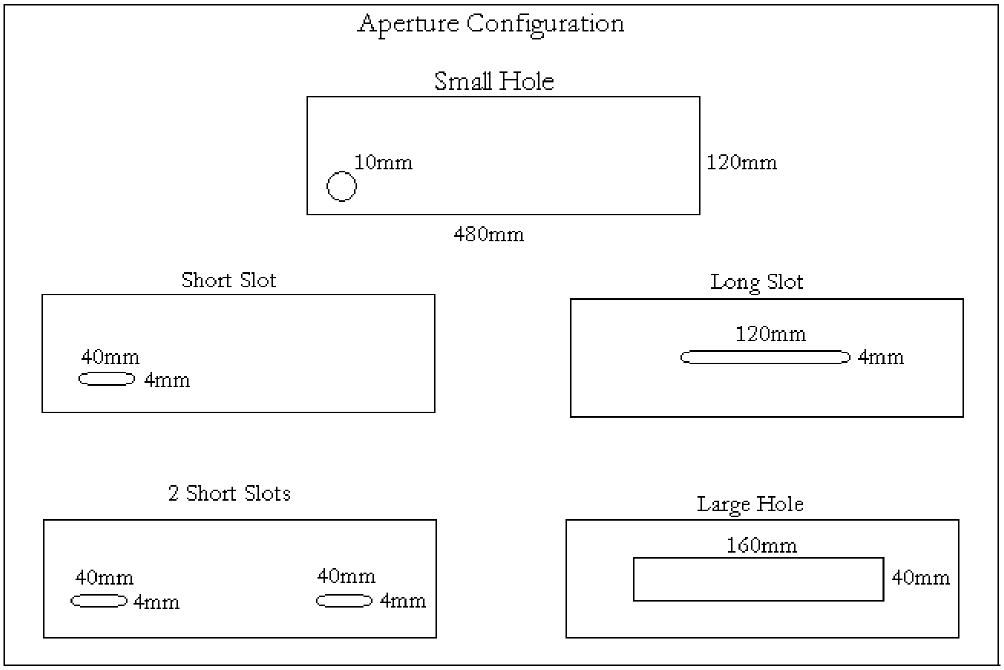

Figure 7.1: Aperture Configuration on front panel of test enclosure.

It is worth noting here that Hill in [49] also presents a relationship between the SE and the $Q-$ factor, seen in equation 7.7. In [49], an investigation into aperture excitation of lossy cavities is carried out, where results of $Q-$factor simulation and measurements are given with reference to the SE of the enclosure. The work in [49] looks at the SE of both lossy cavities (by loading with salt water filled spheres) and empty cavities and evaluates the $Q-$factor for both cavity loadings. The tests done in [49] are concerned with power density measuring the cavities with a single SE value over a frequency range, and are not involved with changing the SE of the enclosure as is done in this chapter.

$$SE = 10log_{10}\frac{2\pi V}{< \sigma_t > \lambda Q} \tag{7.7}$$

Equation 7.7 shows that the SE of an enclosure is dependent on the $Q-$factor, the volume and the transmission cross section of any apertures, and the wavelength of the test frequency. Equation 7.7 assumes that the chamber is well stirred. In [49] the time constant is used to obtain a value for the $Q-$factor rather than the different method used here, and a nested chamber setup is also used, again different from what is used here. Equation 7.7 is not directly applicable to the results obtained in this chapter due to the differing measurement environments and the different way of obtaining the $Q-$factor.

7.4 Enclosure Setup

The enclosure is placed in an anechoic chamber of dimensions 1.8m × 1.8m × 3m with the EUT situated 2m away from the transmit antenna, in this case a ridged horn waveguide antenna. The ridged horn antenna is connected to port 2 of the network analyser and the enclosure antenna (a single 19mm monopole with SMA connector) is connected to port 1. The EUT present in the chamber is shown in figure 7.2. The network analyser measures the S21 and S11 parameters at 4GHz. The S21 parameter refers to the coupling between the monopole antenna inside the stirred EUT and the external ridged waveguide horn antenna in the anechoic chamber.

The level of field coupling into the EUT from the horn antenna (and therefore the SE) is controlled by changing the layout and configuration of apertures on the front panel of the EUT. The different aperture layouts are shown in figure 7.1. Data from the EUT is measured using the network analyser around a 4GHz centre frequency using two different scan bandwidths, 50MHz and 100MHz, each with the maximum available 1601 data points. This is done to investigate the effect of the number of resonant modes seen by the NA on the average $Q-$factor; the 50MHz span will encompass fewer resonant modes than the 100MHz span.

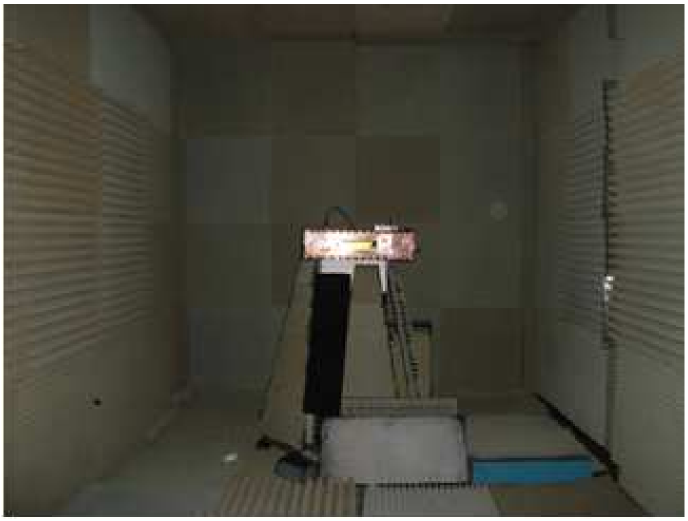

Figure 7.2: EUT in place in the Anechoic chamber. The front panel is facing the camera and the ridged waveguide antenna - current aperture configuration is ”Large Hole”.

To obtain an SE measurement, the average received power inside the EUT P_{in} (obtained from the $S21$ from the horn antenna to the internal monopole antenna) is compared to the received power outside the EUT P_{out} (obtained from the $S21$ between the horn antenna and the reference monopole), as per equation 2.20 in section 2.8.1. The antenna mismatch factors are used in the calculation of the SE, obtained from the reflection coefficients of the EUT and reference antennas ($S11$). As previously, the ridged horn is assumed to be well matched at this frequency. The EUT is mechanically mode stirred using a stepper motor and a small paddle stirrer to ensure that the P_{in} measurement is not dependent on the position of the measurement antenna inside the EUT. Data is taken while the stepper motor is stopped and the paddle stationary to ensure that there is no interference from noise on the motor, discovered in previous work detailed in Chapter 3. The paddle is inside the working volume of the EUT with the motor on the outside; the control hardware sits outside the chamber and is connected to the measurement PC via a shielded control cable. The stirrer has a maximum number of 400 steps per revolution; statistically independent data sets are taken every 2 steps, giving 200 measurement sets per full rotation of the stirrer paddles. The data sets are averaged over one full stirrer rotation to obtain the average field power inside the EUT. As the EUT is being effectively stirred, this makes the positioning of the receiving wall mounted monopole antenna irrelevant within the working volume of the EUT.

The P_{out} measurement is also taken using a 19mm monopole receiving antenna on an electrically large ground plane. The EUT is replaced with the ground plane for this measurement, with the P_{out} receiving monopole positioned where the centre of the working volume of the EUT would be, were the EUT present during the measurement. This is because the position dependent nature of the anechoic chamber means that the placement of the reference monopole is important. The SE is then calculated using these two values combined with the reflection coefficients measured with the VNA, following equation 7.1.

The main area of interest in this particular experiment is how the different aperture configurations change the SE and how the measurement method can be utilised, rather than the absolute value of the SE. The different aperture configurations (see figure 7.1) are only changed on the front panel facing the external ridged waveguide horn antenna, and the EUT is stirred internally: the turntable in the anechoic chamber is not used. The measured SE in an anechoic chamber with this set-up will depend only on the directional properties of the array of apertures in the front panel that can be considered as an antenna; the assumption is that the majority of power is transmitted into the enclosure via the aperture. As only one EUT orientation is used the results are comparative and indicate changes in SE as the aperture configuration is changed. This results in plots of the relative SE rather than an actual measure of the SE that could be compared with the SE of this enclosure that was previously measured in a reverberation chamber, for instance. However it is still undesirable to have a direct path present inside the enclosure, hence the enclosure stirring.

7.5 Autocorrelation and Width of Autocorrelation

The autocorrelation method is a statistical method that can be used to look for similarities in the frequency response of a reverberant volume. This allows the bulk electromagnetic properties of the reverberant environment inside the EUT to be examined without the need to look at the fine structure of the frequency response. In the case of an enclosure at this frequency (4GHz), the fine structure of the frequency response is complicated. The application of autocorrelation to a frequency response has the effect of transforming the frequency response into a single peak [74], the width of which is representative of the $Q-$ factor. The autocorrelation is applied to the frequency response in MatLab using the '$xcorr$' command, producing results normalised to 1. The $S21$ is measured as a number I

of spot frequencies with the same interval, this is set up on the VNA by spacing the 1601 frequency measuring points equally throughout the measurement bandwidth, something which the VNA does automatically. The autocorrelation of a sequence of I values x_i is defined as:

$$C[i] = \sum_{k=0}^{I-(i-1)} x_{i+k} x_k \tag{7.8}$$

where i is the lag, which is plotted against the correlation $C[i]$ in the autocorrelation plot. The range of the lag is $[-I+1,\ I-1]$, making the length of the autocorrelation $2I-1$, symmetrical around $i=0$. Studies of the autocorrelation results in [18] and [74] suggest that the width of the autocorrelation is related to the energy dissipation within the cavity. In these previous experiments, the energy dissipation due to absorber has been investigated, in this case the energy dissipation due to the aperture is looked at, hence the need for an aperture dominated EUT. An example autocorrelation plot is shown in figure 7.3, with the different cutoff levels shown.

The $Q-$factor is calculated using the frequency response from the stirred EUT at each stirrer position. It was found that obtaining the $Q-$factor from the averaged frequency response, i.e. after the individual response at each stirrer position had been averaged, resulted in a very low resolution. This means that it was difficult to tell the difference between EUTs with large apertures compared to EUTs with small or nonexistent ones. Computing the Width of Autocorrelation (WA) of the frequency response at each position results in a much greater capacity to distinguish between aperture sizes. The autocorrelation of the frequency response at each stirrer position is taken from the measured data using a MatLab program (see Appendix, chapter 10). The WA [18][74] is found for various cut-off levels, 1.2dB, 2dB, 2.5dB and 3dB at each stirrer position. The cutoff levels are defined with respect to the maximum value of the autocorrelation.

The original method of using the WA to link to $Q-$factor was simulated in [74] for a single stirrer position. This method used here leads to 200 values for WA (one for each stirrer position), which are then averaged over the full stirrer rotation. This results in an average WA for each cut-off level, and is carried out independently for both the 50MHz and 100MHz spans. This secondary averaging applied by the autocorrelation method (primary averaging being over the mechanical stirring positions) results in a double stirred situation.

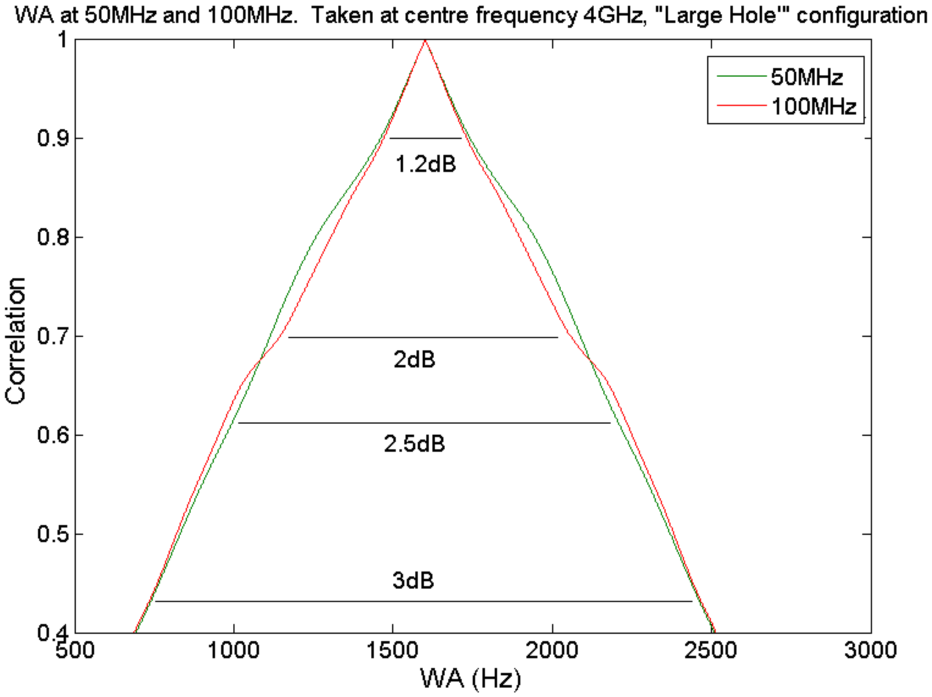

Figure 7.3: Autocorrelation plot for the ‘large hole’ configuration at 4GHz. 50MHz and 100MHz span widths are shown

It can be seen in 7.3 that a ‘shouldering’ effect of the 100MHz autocorrelation plot is occurring between the 2dB and 2.5dB cut-off levels. This shouldering effect moves around - note that the 50MHz shoulder is higher up on the autocorrelation plot - and highlights the need to look at the different cut-off levels. The shouldering effect is more apparent at higher frequencies, as can be seen in figure 7.4, taken at 6GHz.

The merits of the different cut-off levels are as follows. The 1.2dB cut-off level has the advantage of being clear of any shouldering effects, which tend to occur below this cut-off level. The disadvantage of the 1.2dB level being used as a measure of WA is that the sensitivity is not as good. By this it is meant that the WA will not change very much for a given change in autocorrelation plot width, simply due to the cut-off being higher. By contrast, it would seem that the 3dB cut-off level would be the best for obtaining the largest change in WA, or WA resolution. However, it can be seen from figure 7.3 that the traces for both 50MHz and 100MHz are similar at the 3dB level. This level is also very susceptible to the shouldering effects, as can be seen in figure 7.4, where the application of a 3dB cutoff could lead to unexpected results. The 2dB and the 2.5dB levels could be seen as a compromise between the low sensitivity of the 1.2dB and the poor resistance to the shouldering effect of the 3dB level. However, it can be seen in figure 7.3 that there

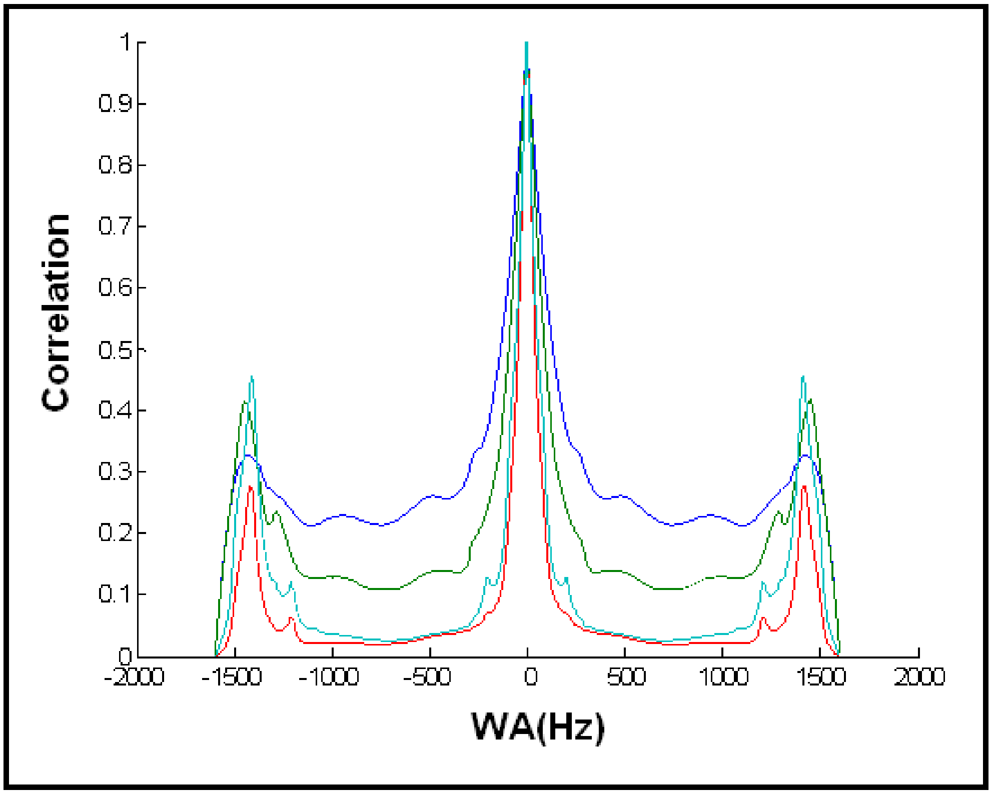

Figure 7.4: Extreme shouldering effect observed on autocorrelation peak with 6GHz frequency response. The different colours correspond to different aperture configurations.

are also shouldering effects present at both the 2dB and the 2.5dB levels. This would tend to indicate that the best cut-off level to be used at this frequency is the 1.2dB level, for reliable results albeit with reduced sensitivity. The act of averaging the plots does not seem to improve the shouldering effect; the effect was not noticed in previous work as the frequency was not high enough to produce shoulders in the autocorrelation plot. Note that the higher $Q-$factor at the higher test frequency used in figure 7.4 has resulted in a narrower central autocorrelation peak.

7.6 Obtaining the $Q-$factor from the Width of Autocorrelation

The first step to obtaining a value for the $Q-$factor from the WA is to simulate a WA for a given known $Q-$factor. A simulation program used in [74] computes the theoretical frequency response for any cavity for a given, known value of $Q-$factor. This theoretical frequency response is calculated by combining all of the many resonant modes present in the EUT. The modes are assumed to have Lorenzian line shape. The WA can then be calculated from the autocorrelation of this theoretical frequency response, giving a table of $Q-$factor against WA for each data set. This is done 200 times (to minimise computational error) for the two frequency spans, one of 50MHz and one of 100MHz, both centered on 4GHz. The $Q-$factor vs. WA data can then be used to calculate the $Q-$factor of the EUT by fitting a curve to the data set and rearranging for $Q-$factor. Both the 50MHz and 100MHz span give different curves, shown in figures 7.5 and 7.6 respectively. It is worth noting that each cut-off level has its own WA vs. $Q-$factor relationship, and that the curve used fits the higher cut-off levels better. The two curves can be seen on the same plot in figure 7.7. It is also interesting to look at $log_{10}(WA)$ vs $log_{10}(Q)$; this is shown in figure 7.8.

7.7 Experimental Results

The SE values for the purposes of this comparison are relative values. The SE values presented here are not representative of the actual SE of the enclosure, as the enclosure has not been illuminated on all sides. This is one of the reasons why the formulation in [49] is not applicable. The received power measured using the EUT monopole antenna is purely

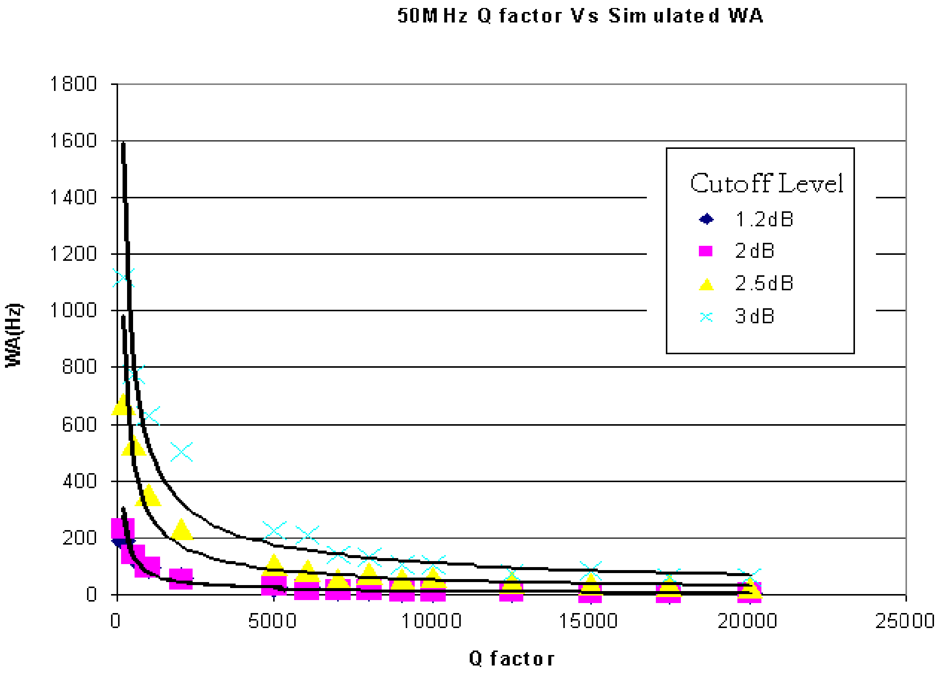

Figure 7.5: Simulated $Q-$factor Vs Autocorrelation width for measurement span of 50MHz

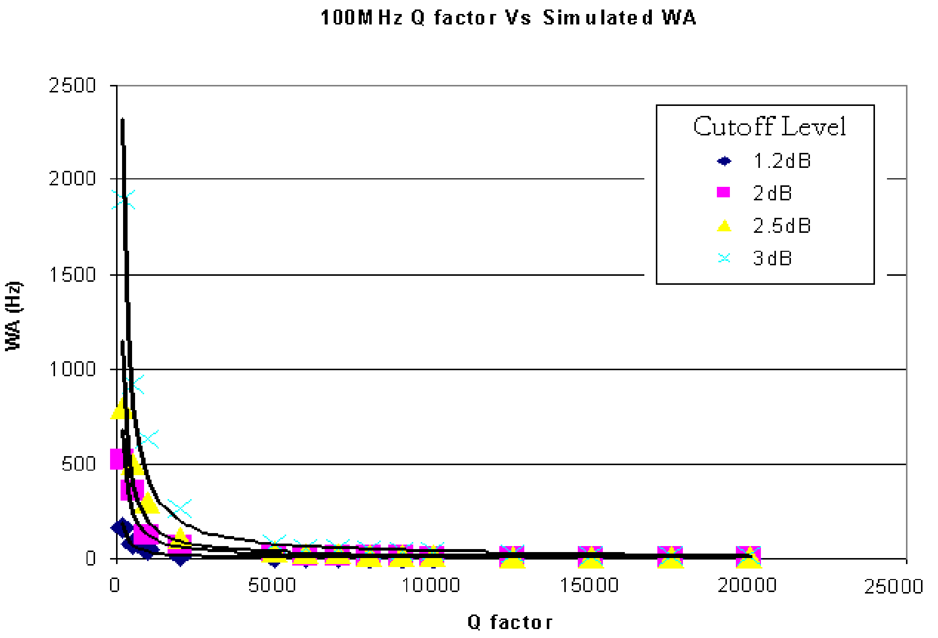

Figure 7.6: Simulated $Q-$factor Vs Autocorrelation width for measurement span of 100MHz

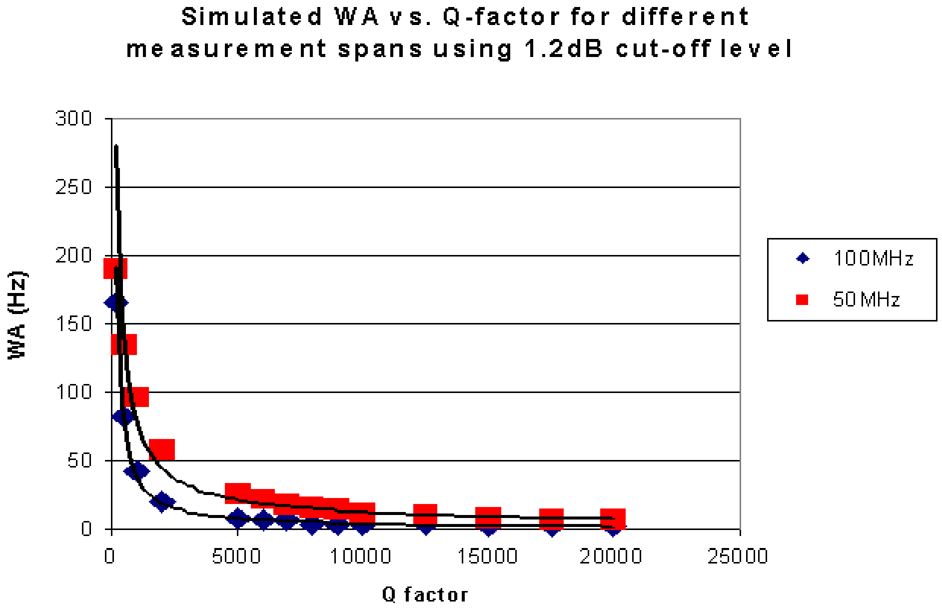

Figure 7.7: Autocorrelation width plotted against $Q-$factor for the 1.2dB cutoff level

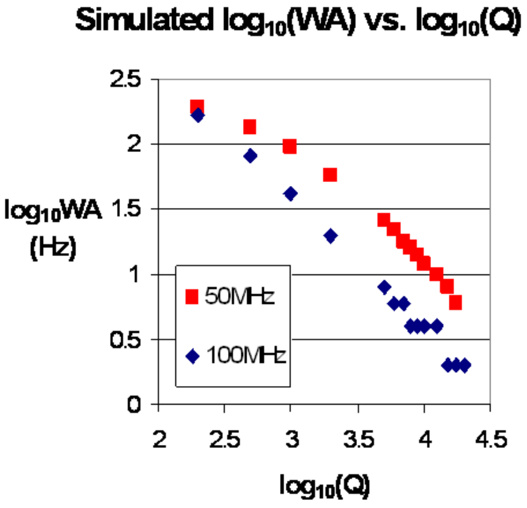

Figure 7.8: Log of the autocorrelation width plotted against log of the $Q-$factor for the 1.2dB cutoff level

defined by the aperture configuration in this setup. The different aperture configurations, in addition to a ‘no holes’ configuration, give 5 differing values of relative SE; these are then plotted against the measured $Q-$factor obtained from the WA. This can be seen in figure 7.9. The SE is termed relative SE to distinguish it from the true measured SE of the enclosure.

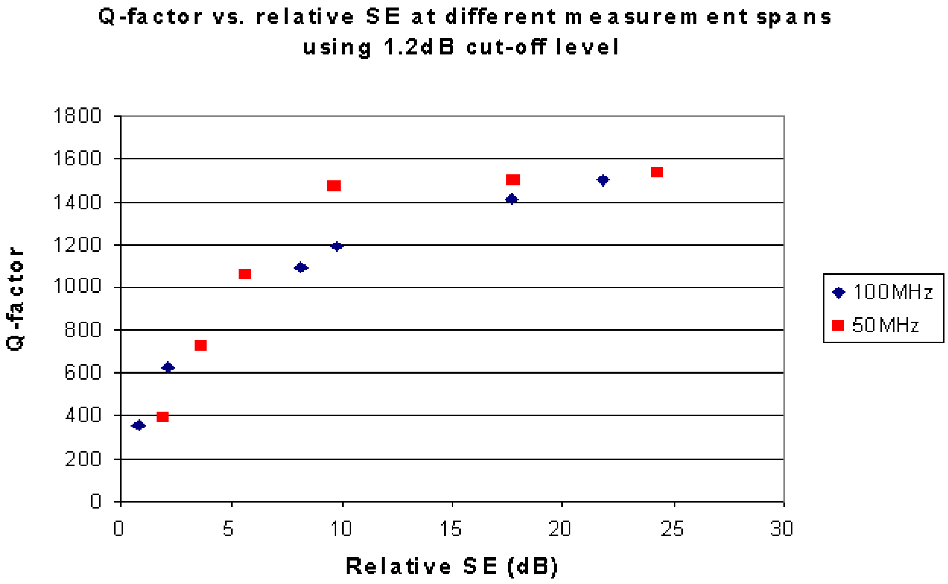

Figure 7.9: Measured $Q-$factor plotted against measured SE

It can be seen from figure 7.9 that there is a monotonic relationship between $Q-$factor and SE, as implied by examination of the SE equation (equation 2.4) and the knowledge that reducing the $Q-$factor reduces the stored energy in a reverberant environment [49]. There are differences between both the different measurement bandwidths and the differing cut-off levels. It is worth noting that the abscissa on figure 7.9 is relative SE rather than actual SE. The variations in the two figures are interesting as they indicate the variation between different scan bandwidths.

The shapes of the different scan bandwidth plots are also different. The 50MHz measurement bandwidth seen in 7.9 would not be so useful for use as a test method for enclosures exhibiting higher relative SE values as it levels off above 25dB of relative shielding, reducing the $Q-$factor sensitivity for a given change in relative SE. The 100MHz measurement bandwidth seen in 7.9 shows no such leveling effect within the range of relative SE values measured here, and could be seen as being a more accurate way of obtaining $Q-$factors at higher levels of relative SE as the $Q-$factor sensitivity is larger. The two plots can be seen separately in figures 7.10 and 7.11

From this it may be thought that the larger scan bandwidth is more beneficial as there are more resonant modes and therefore more information enclosed within the measurement span. However, the dependence of $Q-$factor on frequency could make having too wide a scan bandwidth detrimental to the results, as the $Q-$factor changes over the width of the scan.

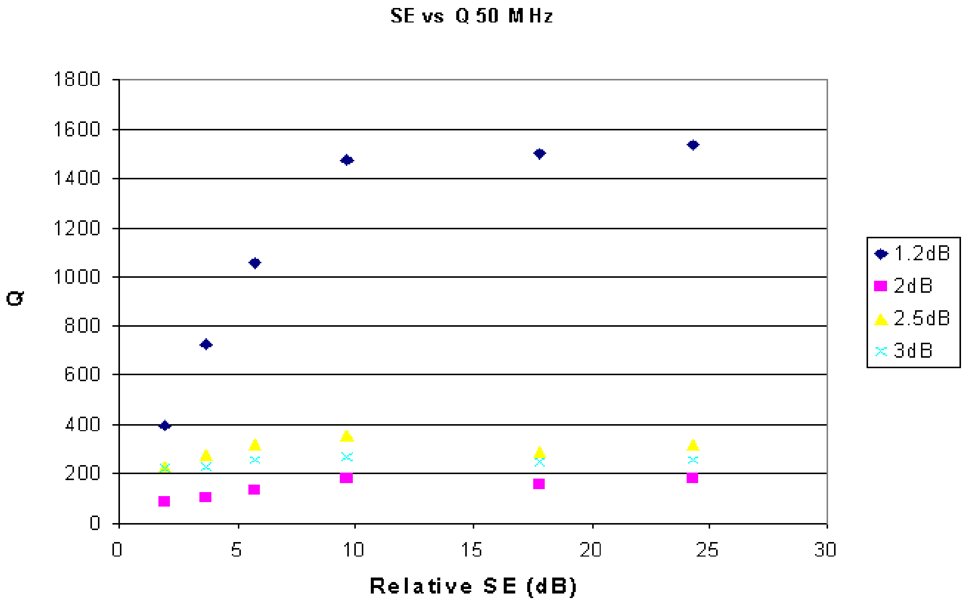

Figure 7.10: Measured $Q-$factor plotted against measured SE for 50MHz bandwidth

7.8 Desktop Setup and Results

Also measured was the $Q-$factor of the enclosure using two 19mm monopoles both situated on bulkhead connectors on the internal walls of the EUT. Power was transmitted into the EUT through one monopole and received on the other. Aperture configurations are changed on the front panel as previously, however this time the EUT is situated on the bench in the EMC lab. Due to the energy loss from the apertures being quite small, it is unlikely that any of the energy lost will return through the aperture, meaning that the lab will act in a similar way to the anechoic chamber, potentially removing the need for an externally benign electromagnetic environment provided by a chamber. However, this desktop method will only work at frequencies outside the frequencies used for intentional broadcast, for example the 900MHz and 1800MHz GSM bands. The plots for the different methods (inside the chamber using an external source antenna, and outside the chamber using an internal source) are shown in figure 7.12.

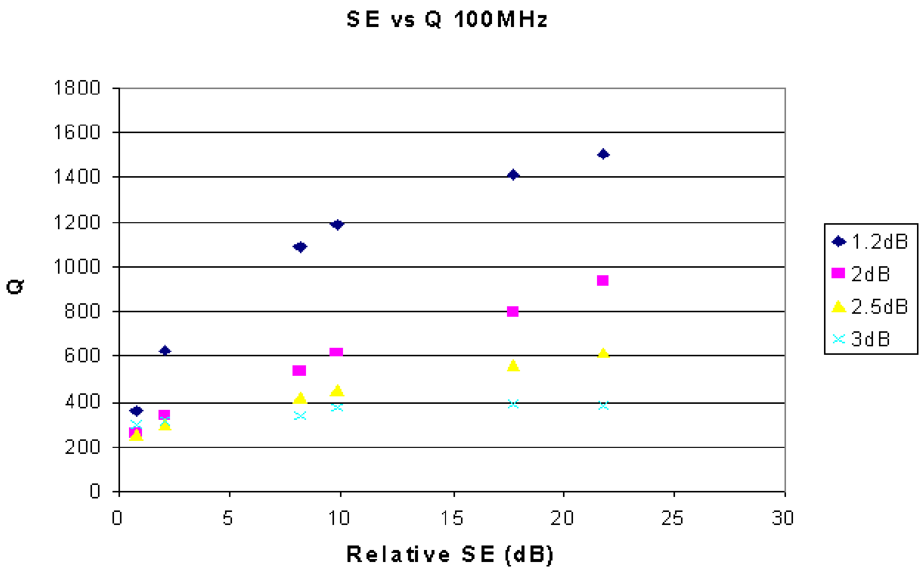

Figure 7.11: Measured $Q-$factor plotted against measured SE for 100MHz bandwidth

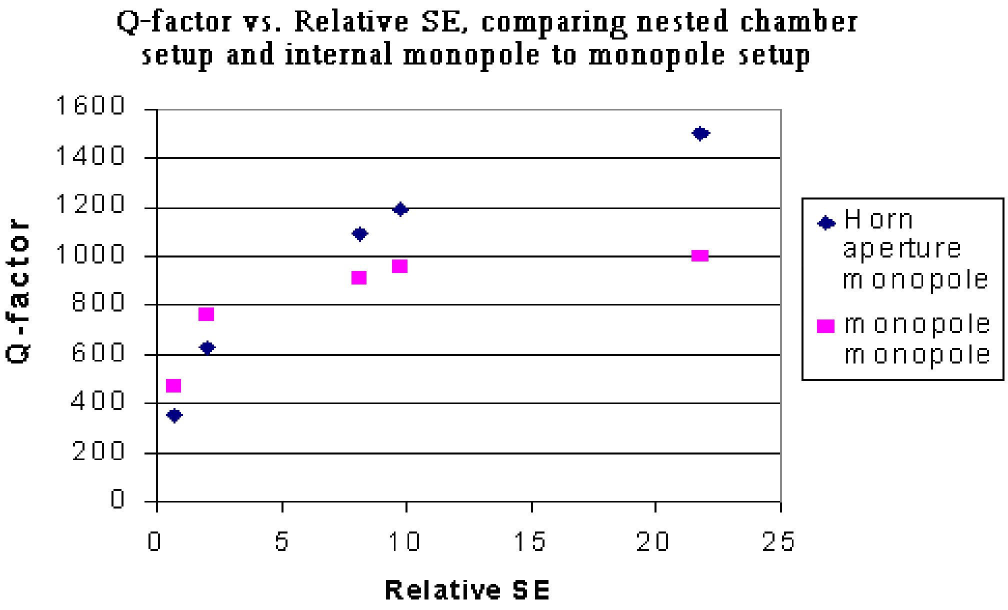

Figure 7.12: Q factor against realitve SE for different experiment environments

It can be seen from 7.12 that the monopole to monopole plot is also monotonic. The $Q-$factor would be expected to be different as there are now two (not ideally matched) monopole antennas affecting the value of Q_4, the antenna $Q-$factor. The two measurement techniques are comparable at lower values of relative SE but deviation is seen at higher levels where the extra losses introduced by the second monopole antenna may be apparent.

7.9 Chapter Summary

It can be seen from Figures 7.10, 7.11 and 7.12 that there is a relationship between measured $Q-$factor and relative Shielding Effectiveness. It has also become apparent that obtaining the $Q-$factor using the autocorrelation and WA method is dependent on the number of modes seen by the detecting instrument. Using the WA method for obtaining $Q-$factor, a high cut-off value of 1.2dB is the most useful. A comparison can also be made between two different methods of obtaining the average $Q-$factor, seen in 7.12, with the monopole to monopole method mirroring the external horn to monopole method for low values of relative SE. Such a technique would be of use in evaluating the SE of electrically large metallic equipment enclosures with modest levels of SE where the SE is dominated by the aperture losses. This will be explored in the next chapter.

Chapter 8

Electrical Scalability of Resonant Enclosures

8.1 Introduction

Current SE measurements using the nested reverberation chamber method require an electrically large enclosure to ensure predictable field statistics. This leads to a limitation on the size of the enclosure-under-test used for this type of measurement, in that the lowest usable frequency becomes higher as enclosure size decreases. Real world equipment enclosures are continuing to reduce in physical size, for example the downsizing trend in laptops, meaning that the standards for enclosures need to be updated for enclosures of size less than 10cm. This results in the need for an improved and/or different approach to the testing of enclosures outside the size restraints governed by the IEEE 299 standard, and present in the draft IEEE 299.1 standard, which is only applicable to enclosures of side dimension between 0.1m and 2m. In this section, the idea of electrical scalability is investigated, which involves using a larger enclosure to mimic a smaller one by testing them when they are the same electrical size, i.e. they are the same number of wavelengths across. Results from three electrically scaled, aperture dominated enclosures are presented and the relationship between them discussed. The use of $Q-$factor suggested in earlier work (detailed in chapter 7) is applied to the three enclosures-under-test and the relationship is examined.

8.2 Enclosure Setup

The measurement of SE in physically small but electrically large enclosures is limited by the requirement to place a measurement antenna within the enclosure without substantially affecting the performance of the enclosure, as well as the minimum frequency needed to obtain sufficient modes to enable satisfactory statistics and allow the nested reverberation chamber method to be viable. In this chapter the possibility of using a physically larger enclosure as a means of estimating the SE of a smaller enclosure is investigated. The larger enclosure will be referred to as the analogue enclosure and the small enclosure referred to as the subject enclosure. This larger enclosure is of sufficient size to facilitate the inclusion of a suitable measurement antenna without a substantial effect on the enclosure performance. The assumptions made here are that both the subject enclosure and the analogue enclosure are both made from metallic conductors, in this case, brass, and that the ingress of electromagnetic energy that determines the SE is principally through apertures in the enclosure. This is what is meant by reference to aperture dominated enclosures, and allows the measured $Q-$factor to be compared with the SE. All of the subject enclosure dimensions and subject enclosure aperture dimensions are scaled by the same factor to produce the analogue enclosure. The SE measurement technique is that described in [5] using a pair of reverberation chamber in which either the subject or analogue enclosure forms the internal nested chamber. The three enclosures used can be seen in figure 8.1; the large enclosure on the bottom acting as the analogue enclosure for the other two subject enclosures. In this chapter the three enclosures are referred to as the 'large', 'medium' and 'small' enclosures. Measurements are made using a Vector Network Analyser through a 19mm SMA monopole antenna mounted on the wall of the enclosure, situated opposite the aperture. The same antenna is used for all three enclosures and is connected to a bulkhead N-type connector that is mounted to the enclosure using the hole visible on the large enclosure in figure 8.1. All three enclosures have similar mounting holes. The full $S11$ corrected calculation for the SE is used, seen in equation 8.1.

$$SE_{dB} = 20\log_{10}\left(\frac{<|S12_R|^2>(1-|<S11>|^2)}{<|S12|^2>(1-|<S11_R>|^2)}\right) \tag{8.1}$$

Recalling from earlier sections, $S12_R$ is the transmission from port 2 into port 1 of the network analyser with the transmit horn antenna on port 2 and the reference monopole antenna on port 1, $S11$ is the reflection coefficient on the monopole antenna when it is present in the EUT, $S12$ is the transmission into the EUT (measured on the monopole antenna on port 1) from the horn antenna on port 2, and $S11_R$ is the reflection coefficient for the reference monopole antenna on port 1.

Figure 8.1: The three enclosures used in this chapter - designated ’large’, ’medium’ and ’small’

The three enclosures in figure 8.1 are all cubic and have side dimensions of 100mm, 200mm and 300mm. One of the sides is removable via a set of brass screws, with four interchangeable front panels, the dimensions of which can be seen in figure 8.2. The front panels are made of 0.5mm thick brass sheet. The enclosures all have inset shielding gaskets around the seal between the front panel and enclosure; this helps any reduce any leakage from the removable front panel. The gasket can be seen on the small enclosure in figure 8.1, as the grey surround around the large hole on the body of the enclosure. The apertures are cut into thin brass sheet and clamped between the top plate (visible to the left, on top of the medium enclosure) and the shielding gasket.

The SE measurements are taken as per the standard nested reverberation chamber technique, with the outer chamber measuring 4.70m × 3.00m × 2.37m, using 200 positions on the mechanical stirrer present in the chamber. The enclosure under test forming the inner chamber is frequency stirred using the post-processing stirring method with a 10MHz stirring bandwidth. The post-processing stirring is carried out within a 100MHz measurement bandwidth about the test frequency. The enclosure is supported within the working volume of the outer chamber on polystyrene blocks. Also present in the chamber is a 19mm monopole on a ground plane that acts as the receive antenna for the reference measurement required by the technique. Stirring in the large chamber is effective (a Rayleigh distribution of electric field is present) and as such the positioning of the EUT and reference antenna within the working volume of the chamber is irrelevant. The $Q-$factors of the various enclosures were obtained using the WA method detailed in chapter 7, using the frequency response of the twin chamber system over a 100MHz measurement bandwidth. The centre frequencies for the $Q-$factor are the same as those used for the nested chamber measurements with a 100MHz measurement span. The $Q-$factor measurement is also taken using the nested chamber setup, ensuring uniform illumination of the aperture on the EUT.

The four aperture configurations used are designated 'Slot' (1), shown in red, 'Small Hole' (2), in green, 'Medium hole' (3), in blue, and 'Large hole' (4) in orange. These are shown in figure 8.2. The labels on figure 8.2 indicate the number of wavelengths (λ) the apertures are, with respect to the test frequency.

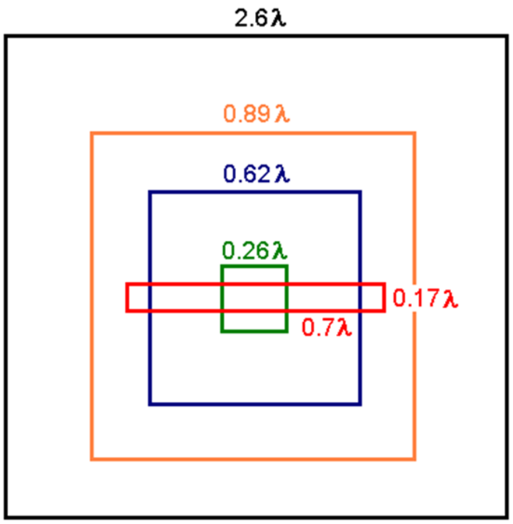

Figure 8.2: Aperture configuration applicable to all three enclosures. The black outer square is the dimesion of the inside of the test enclosure

The aperture configuration chosen is wavelength based to allow the three different enclosures to be compared. The three enclosures are tested at different frequencies to retain the wavelength relationship; so the small enclosure is examined at 8GHz, the medium enclosure at 4GHz and the large enclosure at 2.6GHz. The apertures in the three enclosures are designed to be the same number of wavelengths in size, i.e. the same electrical size, at each of these test frequencies. This means that the apertures and enclosures should be comparable at the three test frequencies.

The frequencies chosen are as high as possible (the VNA has a maximum frequency of 8.5GHz). The result of this setup is that the three enclosures are the same electrical size and as such should give the same internal field statistics, the same distribution of internal power and thus the same values for the SE. it can be seen in figure 8.1 that the medium enclosure has aperture (4) ('Large Hole') installed.

8.3 Mode density considerations

The use of the technique described in [7] requires that the number of resonances present at the operating frequency is above a minimum number typically estimated at 60 [14]. The minimum useable frequency f_{min} stems from Weyl's law [31], relating the number of modes N_m below a certain frequency f with the geometric properties of the enclosure, seen in equation 8.2.

$$N_m = \frac{8\pi V f^3}{3{c_0}^3} \tag{8.2}$$

In equation 8.2, V_e is the enclosure volume and c_0 is the velocity of light. It is not possible to use the more exact form of Weyl's law as the enclosures here are not rectangular cuboids but cubic. Cubic enclosures are less efficient as reverberation chambers because of mode degeneracy: due to the equal distances in the x,y,and z directions some modes overlap, creating gaps in a mode number vs. frequency plot. It is for this reason that a good reverberation chamber will be built with unequal lengths in the x,y,and z directions. Mode degeneracy becomes less of a problem at higher frequencies as the missing modes are lost in the large number of modes generated. It can be seen that for a smaller enclosure, the frequency f must increase to retain the same N_m, the number of modes below f. This can be seen in figure 8.3 for cubic enclosures of varying side measurements.

It is suggested [7],[14] a rule of thumb to ensure reasonable statistical uniformity is to have 60 modes excited below the test frequency f. Of course if this is increased to 100 or 150 then the field becomes closer to the uniform ideal once averaged. The more excited modes that are present below the test frequency the higher the mode density. The actual number of modes depends on the ratio between the mode density and the mode bandwidth [32][22] and can be calculated using models as in [22]. The important quantity for satisfactory field statistics is the ratio of the mode density to the bandwidth of a single

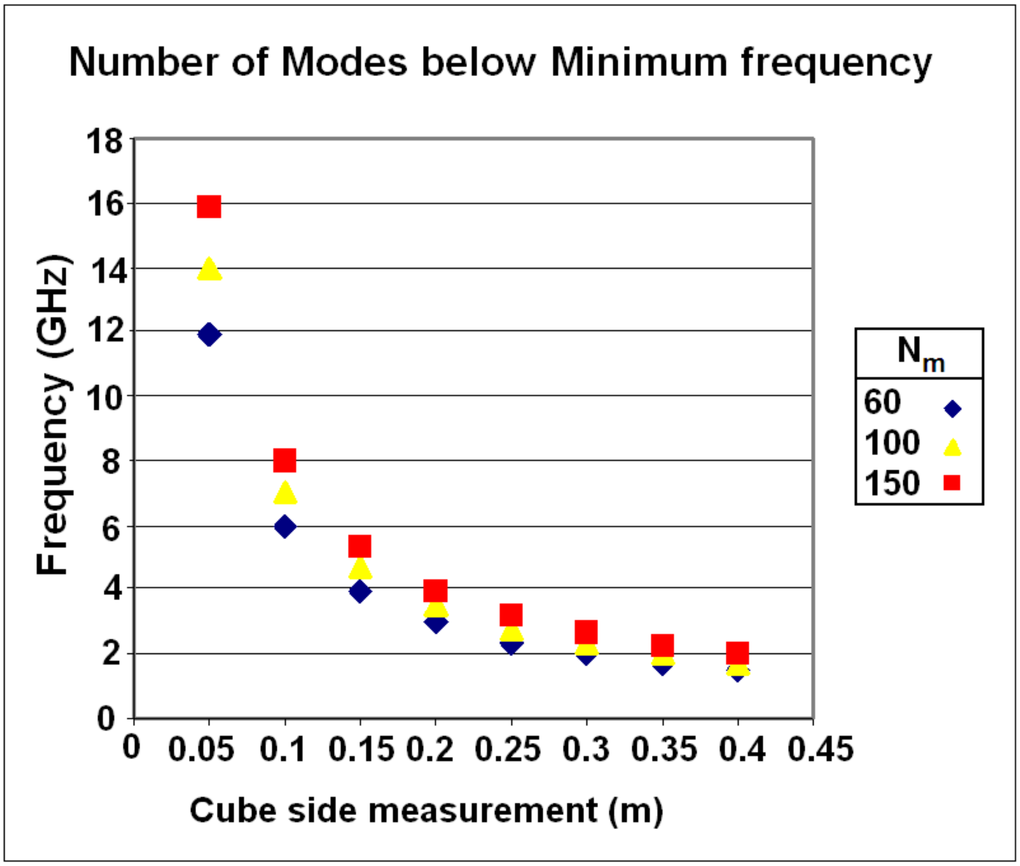

Figure 8.3: Number of modes below the minimum frequency for cubic enclosures with varying side dimension

mode. This ratio should be greater than 1. As the frequency increases, the modes become closer together and more are coupled to the excitation frequency, resulting in better field statistics [22]. The work presented in [32] suggests that purely using a rule of thumb to ensure satisfactory statistics may not be sufficient.

Using the same electrical size to test each of these three enclosures with electrically identical apertures should result in similar values of SE, provided that the SE is aperture dominated. This will allow testing of physically small enclosures without resorting to high frequency measurements. For reference, it is interesting to note that if using 60 modes below f as a limit for statistical uniformity, an equipment enclosure of side dimension 5cm (for example, a connector housing enclosure or small equipment enclosure) the test frequency is required to be around the 12GHz region, necessitating more expensive measuring equipment. When using the approach in [32] there is still a benefit in increasing frequency to retain statistical uniformity, however the line between acceptable statistics when using the number of modes superposed within a -3dB bandwidth is not as clear, as the precise estimate of modal density is difficult to obtain in an experimental environment.

8.4 Simulation of the $Q-$factor

Chapter 7's discussion on Q factor applicable to an aperture dominated EUT is also valid in this chapter. To avoid unnecessary repetition section 7.3 should be referenced.

Calculations of the values of the separate aspects of the $Q-$factor detailed in the previous chapters are shown in figure 8.4. Absorption loss within the chamber is not shown in figure 8.4, as these give a very large $Q-$factor that eclipses the other results. The calculations shown in figure 8.4 are for the large enclosure.

Wall losses are estimated using equation 7.3, with the skin depth δ and relative permeability μ_r of brass. The surface area S_a is modified as the size of the aperture changes. This small surface area effect can be seen in that the plot for the wall $Q-$factor is not quite flat.

The antenna $Q-$factor is estimated using experimental $S11$ reflection coefficient measurements to obtain a value for the antenna mismatch m_a (shown in equation 8.3), then using equation 7.6 to obtain a value for the antenna $Q-$factor

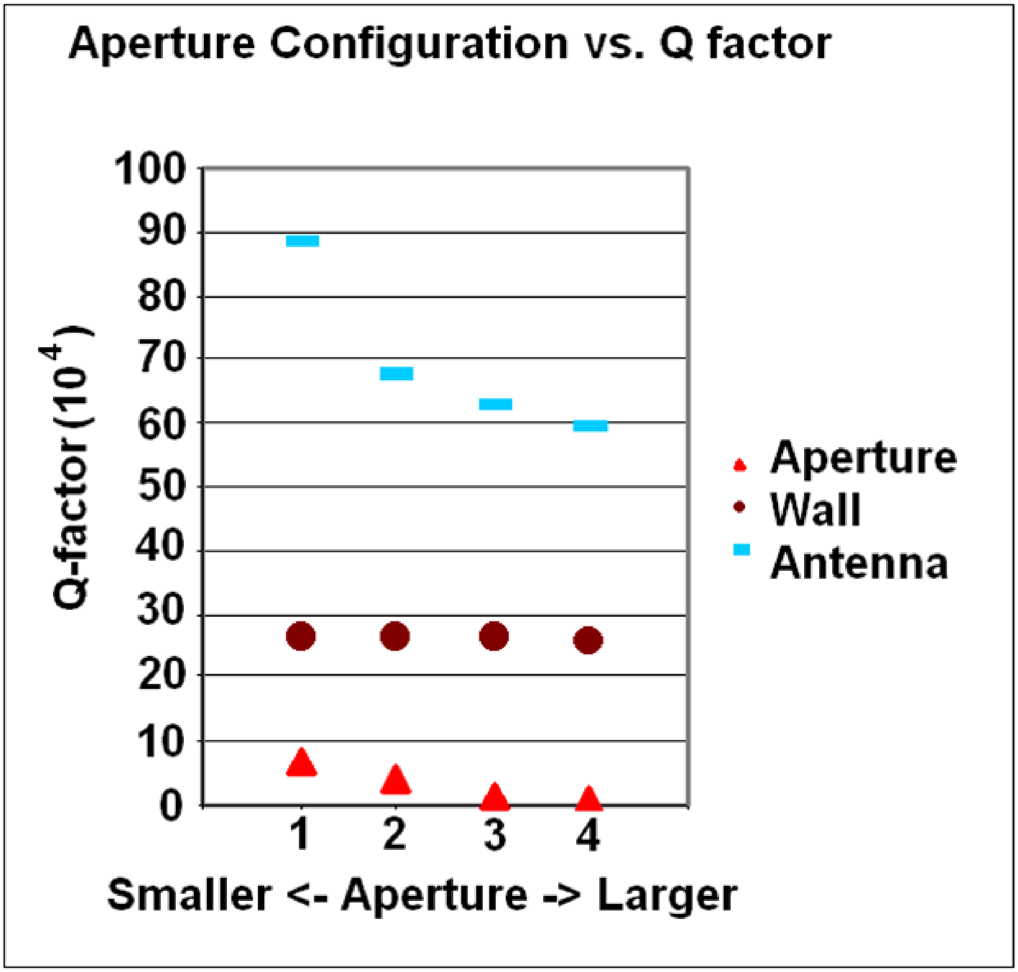

Figure 8.4: Calculated Q factor components for different aperture configurations using the large 300mm enclosure. The apertures vary in size (see figure 8.2) from the smallest (1) to the largest (4)

$$m_a = 1 - |S11|^2 \tag{8.3}$$

$$< \sigma_a >= \frac{A_a}{2} \tag{8.4}$$

The aperture component is simulated using equation 7.5 (remembering equation 8.4) for the apertures shown in figure 8.2. It can be seen from figure 8.4 that the red triangles representing the aperture component (Q_3) result in a lower $Q-$factor than the antenna and wall components. Recalling that equation 7.2 is obtained from reciprocal values of the $Q-$factor, the Q_3 component can be said to dominate the total $Q-$factor. This is due to the fact that the other, larger, $Q-$factors (Q_1,Q_2, and Q_4) become small when the reciprocal is taken. From this it can be deduced that if the SE is aperture dominated, then the SE can be linked to the $Q-$factor for such enclosures as the one tested here. With a better matched antenna then the antenna component would contribute less to the overall $Q-$factor.

Figure 8.5 shows the calculated values of Q_3 (the aperture $Q-$factor) for the three enclosures at the same electrical size. These are calculated from simulated autocorrelation widths, using the simulation program written for the analysis carried out in the previous chapter, which can be seen in the Appendix (Chapter 10). This takes into account the apertures but not the walls or antennas, simulating a truly aperture dominated enclosure.

It can be seen in figure 8.5 that the expected contributions from the aperture $Q-$factor are very similar for the three enclosures, suggesting that the aperture dominated SE will follow the same pattern, and that an aperture dominated analogue enclosure can be used to mimic a smaller subject enclosure. The small differences seen are artifacts of the statistical nature of the simulations, as in a perfect simulation with a very large number of simulation points these small differences would disappear. The wall and antenna $Q-$factors differ between the three enclosures due to the volume and surface area components present in their formulae; however the values are still high enough to be able to say that the contributions from them to total $Q-$factor are small and that these enclosures are aperture dominated.

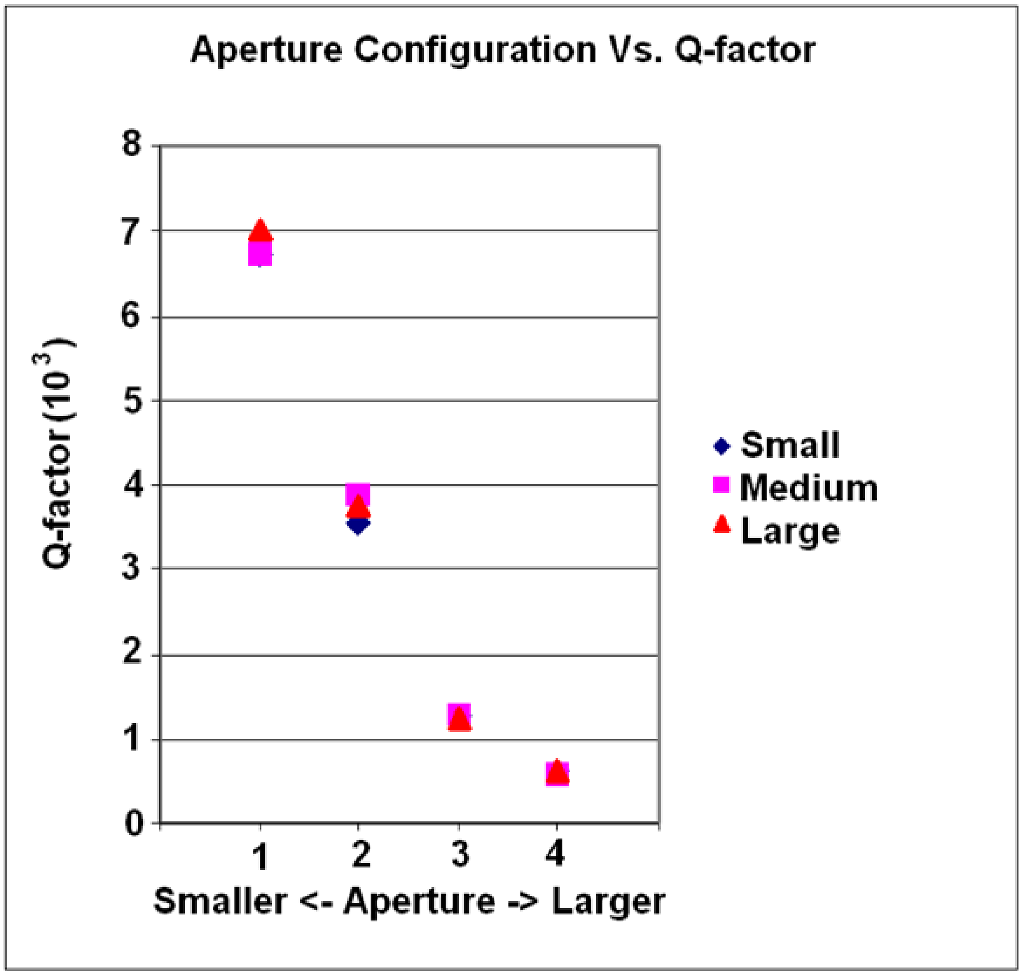

Figure 8.5: Aperture Q factor for the three enclosures under test.

8.5 Experimental Results

The concept of electrical scalability from experimental results is shown in figure 8.6. Here, the measured SE obtained by the nested chamber method is plotted against the aperture configurations shown in figure 8.2. As expected, the smaller apertures provide higher SE values. The three enclosures are plotted, and show very good agreement of SE across the aperture configurations. Better agreement between the three enclosures is to be found at the lower SE end of the scale, where the enclosures become more aperture dominated. The small (100mm) enclosure has higher SE values for all aperture configurations, but is never more than 5dB different from the lower values for the large enclosure. As demonstrated in previous sections, 5dB is within the accuracy limits obtainable with removing and replacing aperture panels.

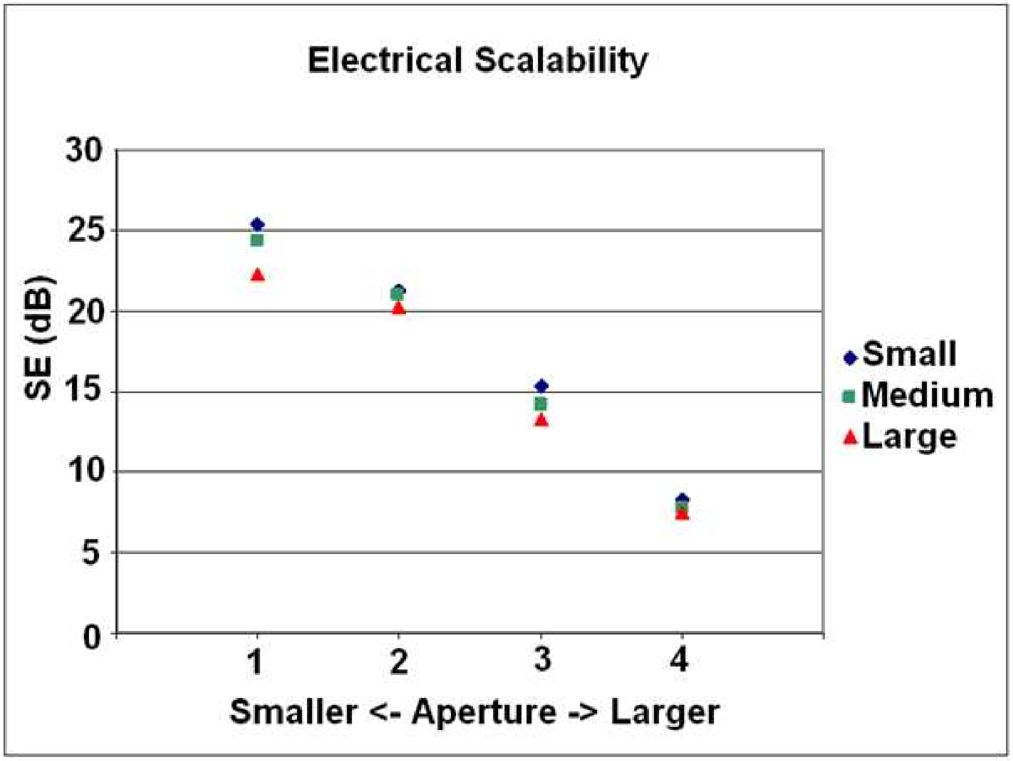

Figure 8.6: comparison for the three different enclosures.

Figure 8.7 shows the observed relationship between the measured total $Q-$factor of all three enclosures and the simulated aperture $Q-$factor for the large enclosure. The disparity between the measured small aperture results and the simulation is due to the presence of the antenna and wall losses reducing the aperture dominance. As mentioned, the simulation does not take into account the wall and antenna losses whereas the experimental results do. This effect becomes more pronounced as the apertures get smaller: the enclosure becomes less aperture dominated and the wall and antenna $Q-$factors start to have more of an effect. This manifests itself as a ‘flattening’ of the curve with regards to the experimental results.

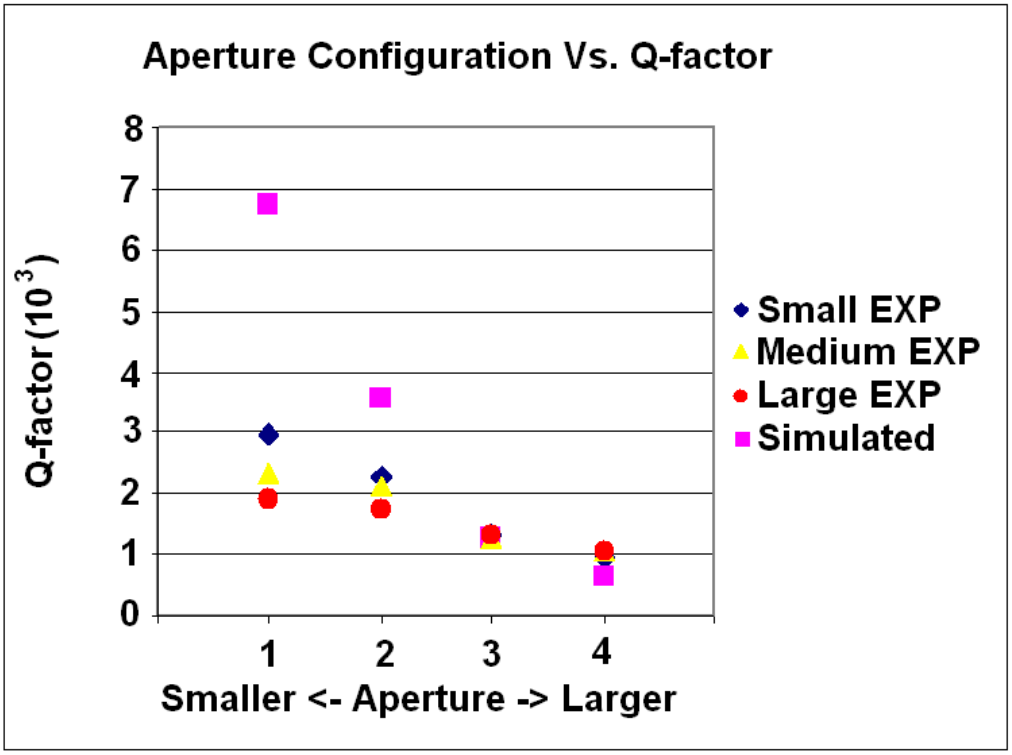

Figure 8.7: Aperture configuration against measured $Q-$factor. The pink squares are the simulated aperture $Q-$factor

The difference between the simulated aperture $Q-$factor and the measured $Q-$factor for the aperture configurations that provide higher values of SE, suggests that this method works best when the enclosure becomes more dominated by the aperture. It is worth noting that the measured $Q-$factor shown here is the total $Q-$factor, as it is not possible to identify the different $Q-$factor components from a measured result. One of these aspects not taken into account is the volume that the measurement antenna occupies within the volume of the enclosure. Another is that the simulation is only examining the enclosure separately, not the whole measurement setup, which in this case includes the larger outer reverberation chamber. All of these points result in the measured $Q-$factor being smaller than the simulated aperture only $Q-$factor, indicative of more losses present in the experiment than are accounted for in the simulation.

Figure 8.8 shows the relationship between the measured SE and the measured $Q-$factor. The monotonic relationship is similar for all three enclosures, and matches the results re-

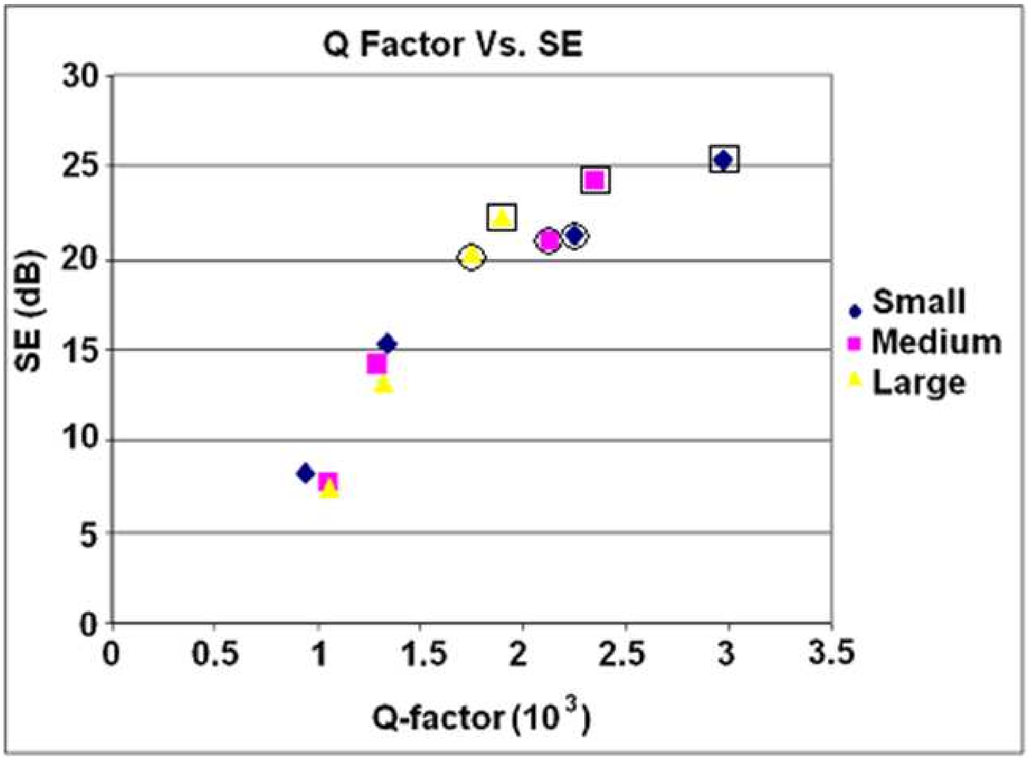

Figure 8.8: Measured Q factor vs. SE. Higher $Q-$factor groupings are within circles and squares for clarity.

ported in the previous chapters. This may result in an empirically defined relationship between the SE and the $Q-$factor that could allow the SE to be inferred from a measurement of the $Q-$factor of a real enclosure using this method. With real enclosures with no contents, the situation is likely to be that the enclosure is aperture dominated; such enclosures as PC or laptop cases and chassis are often full of very large apertures. This technique would allow these types of enclosure to be tested relatively easily, especially if the enclosures in question are small.

8.6 Chapter Summary

This chapter has shown the possibility of using an electrical scalability method to estimate the SE of enclosures that are physically too small to conveniently test using the conventional test method. It has been shown that the SE of a smaller enclosure could be estimated using a larger enclosure with electrically equivalent apertures using analysis of the $Q-$factor of the enclosure in question. The method is shown to work better as the enclosure becomes more aperture dominated. Using the $Q-$factor to obtain SE has been demonstrated in the previous chapter, so it can be said that the scaling of $Q-$factor can be used similarly to estimate the SE for an enclosure that cannot be tested by conventional means. The success of this method also means that the SE of a small enclosure could be estimated without penetrating the enclosure in question or changing it in any way by means of making an electrical scale model. This would be potentially useful for production testing of enclosures, where destructive testing of end products may be undesirable. This method could also be used the other way, in order to measure large low frequency problems (Substation EMC, or some rail applications) in a high frequency environment of more manageable size.

Chapter 9

Conclusions and Further Work

This thesis covered a variety of ways to measure the shielding effectiveness of enclosures. The first part of this work concerns the use of a separate source, a York EMC Services developed comb generator, designated CGE-02, to investigate shielding effectiveness measurements. This aspect was driven by the need to develop an instrument that is capable of creating statistically uniform fields in enclosures. It is shown that such an instrument is a possibility, however due to time and funding constraints the instrument could benefit from further development. This aspect of the work highlighed some issues with the existing draft IEEE 299.1 standard, used for testing the shielding of enclosures. The main issue identified involves the lack of rigour in testing the statistical distribution of the field present in both the testing chamber and the enclosure when using a nested reverberation chamber setup. This can have a marked effect on the measured value of the SE. It is hoped that the work presented in this thesis will add to the knowedge base that will be used in the creation of new standards for enclosure testing, or help with updates to the existing IEEE 299.1.

Another part of this work was to investigate how the shielding effectiveness measurement can be developed from a simple ratio of average received power outside the enclosure to the average received power inside the enclosure. The effect of a direct path on the measurement of SE is examined, and the use of the enclosure $Q-$factor is also considered as a potential measure of SE. Each chapter will be concluded here, followed by an overall conclusion of the thesis.

9.1 Separate Source Measurements - Uniformity, Shielding Effectiveness and Frequency Modulation

This chapter presented results obtained when a separate source and spectrum analyser was used to measure the shielding effectiveness of enclosures. The CGE-02 comb generator has been shown to be effective at establishing statistically uniform fields inside enclosures when used in conjunction with a small, stepped stirrer, however it does need to be powered by a separate power supply from the motor used to operate the stirrer. It has also been shown that the SE is measurable in a number of different ways using the CGE-02 as the source. If the simple SE equation is examined then the methods at first seem to be equivalent, as the same enclosure with the same aperture separates the source and receive antennas. These methods prove not to be experimentally equivalent due to the effect of the antenna changing the $Q-$ factors in the enclosure and the chamber and therefore affecting the measured received power. This highlights the need to involve the $Q-$ factor in the calculation of SE, or at the very least consider it in order to have representative measurements. It is also shown in this chapter how it is possible to use frequency modulation to stir an enclosure and chamber setup using a frequency stirring method. It appears that the frequency stirring method is more sensitive to the number of modes in the enclosure. This is as far as this investigation using the CGE-02 goes, however there is scope for further experimentation to create a ready-to-market instrument that could be used to create statistically uniform electric fields inside enclosures.

9.2 Comparing Reverberation Chambers Using a Shielded Enclosure

This chapter has provided a useful insight into the repeatability of shielding effectiveness measurements of enclosures. Using an enclosure that employs a small internal mechanical stirrer, and finger strip to electrically seal the lid, it is possible to get good agreement between repeated measurements of the SE. The repeatability of the SE measurement of 7dB between runs obtained at the University of York has been replicated at Ancona in Italy, showing that this sort of enclosure could be used to check different chambers in different labs are capable of producing the same results. Comparing results between the UK and Italy, however, the measured SE is not the same between the two labs. Unfortunately reasons for this are not deducible from these results. It may be that human error plays a part in these discrepncies, or it is possible that there are differences in the reverberation chambers in the two countries that can influence a measurement such as this. A comparison between stirring the enclosure using the post processing frequency stirring method and using a stepped small internal mechanical stirrer is also shown, this shows good agreement (within 5dB difference in measured SE for the majority of the frequency range) between the two methods.

9.3 Rician Statistics and the $K-$factor

Here, an investigation into the effect that a direct path component has on the measured shielding effectiveness is carried out. As a Rician distribution in the chamber is indicative of a direct path component, a simulation program was written in order to model the nested chamber setup, allowing different magnitude Rician distributions and their effect on the measured SE to be examined. Experimental results were also taken and these show that the presence of a direct path can cause a large disparity in the measured SE. Due to this potential for measuring a value of the SE that misrepresents the actual SE of the enclosure, it would seem important to check that the distribution within a chamber or enclosure being used for shielding effectiveness measurements was indeed as assumed. There is no mention of a check in the IEEE 299, meaning that it is possible that SE measurements can be unreliable if the chamber or enclosure is not working as expected. This chapter proves the importance of making sure the field is uniformly distributed before making a measurement of the shielding effectiveness. The Rician $K-$factor can be used to measure the stirring effectiveness and therefore the chamber performance, leading to knowledge about the statistical uniformity of the electric field and hence the distributions. Both simulated and experimentally taken results show that if the offset of the mean of the Gaussian distributions, termed ϕ, is less than 1.4 when the distributions have a variance of 1 then the chamber or enclosure is achieving satisfactory field uniformity. In order to be sure of shielding effectiveness measurements in a reverberation chamber this check has to be performed every time the experiment setup is changed.

9.4 Estimating Shielding Effectiveness using Absorber Cross Sections

This chapter demonstrates that using the absorption cross section of the reverberation chamber with a loaded, aperture dominated EUT present in order to estimate the SE of the enclosure is not a viable method. The aim was to measure the differences in the received power across the chamber that occur due to a loaded enclosure with varying aperture sizes. This method works best for enclosures with large apertures, i.e. enclosures with very low SE. It has been found that for an enclosure of similar size to a standard 19 inch rack unit there is an available measurement window of around 10dB, the narrowness of which results in a method that is extremely sensitive. The high sensitivity of the method results in poor resolution, as the differences between expected high SE and low SE enclosure setups is very small, of the order of 1dB. This is too small to be of any practicable use, as this level change can easily be masked by chamber uncertainty. The SE of the enclosure would have to be so low, i.e. the apertures so large, for this method to provide a large enough effect to be robust, that the enclosure would not be able to be classified as an ’enclosure’ any more. Further investigation into the relationship between the loss ratio and the SE of the enclosure was not carried out, as it was thought that the measurement technique was just too sensitive, and not applicable to the moderate or higher shielding levels of shielding enclosures generally encountered.

9.5 Using $Q-$factor to Estimate Shielding Effectiveness

This chapter examines the use of the measured $Q-$ factor to estimate the shielding effectiveness of an enclosure. It is shown that there is a relationship between measured $Q-$ factor and relative Shielding Effectiveness. The relationship stems from the fact that the enclosure is aperture dominated with no absorbing contents, making the aperture the dominant loss mechanism within the enclosure. As the $Q-$factor is a measure of the loss in the enclosure, it is, in this case where the enclosure is aperture dominated, dependent on the SE of the enclosure. It has also become apparent that obtaining the $Q-$factor using a method involving autocorrelation of the frequency response of the enclosure and calculation of the width of the autocorrelation (WA) is dependent on the number of modes seen by the detecting instrument. When using the WA method for obtaining $Q-$factor, a high cut-off value of 1.2dB below the autocorrelation peak when measuring the WA is the most useful. A comparison can also be made between two different methods of obtaining the average $Q-$ factor, with the monopole to monopole method with the enclosure on the desk in the lab mirroring the external horn to monopole method for low values of relative SE. Such a technique would be of use in evaluating the SE of electrically large metallic equipment enclosures with modest levels of SE, provided that the SE is dominated by the aperture losses.

9.6 Electrical Scalability of Resonant Enclosures

This chapter has shown the possibility of using enclosures of equivalent electrical size to estimate the SE of enclosures that are physically too small to conveniently test using conventional test methods such as IEEE299. It has been shown that the SE of a smaller enclosure can be estimated using a larger enclosure with electrically equivalent apertures using analysis of the $Q-$factor of the enclosure in question. The method is shown to work better as the enclosure becomes more aperture dominated. Using the $Q-$factor to obtain SE has been demonstrated in the previous chapter, so it can be said that the scaling of $Q-$factor can be used similarly to estimate the SE for an enclosure that cannot be tested by conventional means. The success of this method also means that the SE of a small enclosure could be estimated without penetrating the enclosure in question or changing it in any way by means of making an electrical scale model. This would be potentially useful for production testing of enclosures, where destructive testing of end products may be undesirable. This method could also be used the other way around, in order to measure large low frequency problems (Substation EMC, or some rail applications) in a high frequency environment of more manageable size.

9.7 Overall Conclusions

This thesis set out aiming to help inform future testing standards for physically small electrically large enclosures, be it further iterations of IEEE 299.1 or otherwise. The IEEE 299.1 standard has a number of failings in its current guise, most notable for reference in this work being the lack of definition of the internal stirring mechanism and the associated issues discovered with non-uniform field distribution, and the limitations on enclosure size.

The importance of obtaining a uniform distribution of electric field within a reverberant volume (be it the test chamber or the enclosure being tested) has been illustrated, and it is hoped that the application of some of the methodology outlined in this work can help improve the confidence level of shielding levels when taking measurements in a reverberation chamber. As shown, the Rician $K-$factor can be used as a measure of the stirring effectiveness of an enclosure or chamber. Due to the large influence a direct path has on the measured SE, an easy check on the distribution of electric field has been demonstrated as a useful addition to a reverberation chamber measurement.

As well as demonstrating the importance of a distribution check, a number of methods of measuring the SE have been investigated, with varying degrees of success. Investigations beyond the current measurement procedure outlined in IEEE 299 has resulted in some new ways of obtaining the SE of equipment enclosures, with the intent of making the measurement quicker and easier to obtain, while bearing in mind the lessons learned from analysing the field statistics.

It has been shown that incorporating $Q-$factor considerations into a shielding effectiveness measurement is of benefit to testing without a reverberant external environment, and that the idea can be extended to use an equivalent enclosure to estimate the SE of an enclosure that is too small to practicably test. As the importance of a uniform electric field becomes more apparent, thus the ability to test smaller enclosures is reduced, as there now has to be space for a mechanical stirrer if that method is to be used. Therefore a representative enclosure of larger side dimensions is more use as there is more internal volume for stirrers and antennas.

If testing enclosures to standards is to be more representative of the real world then the enclosures have to be tested with contents, either representative or otherwise, and the use of a scaled test enclosure would be beneficial in this scenario. The separate source measurements also provide insight into how shielding measurements could be made with an internal source representative of emitting contents, and as the losses due to the contents increase and the scattered component potentially reduces in relation to the direct component of the measured electric field, such tests on the distribution of the electric field as outlined in this work become more important.

9.8 Further Work

The ideas and experiments presented in this thesis could be examined and developed further in order to fully understand measurements of shielding effectiveness in enclosures. Future research based on this work could take one of two directions. The first is to carry on the investigation into an instrument for creating statistical uniform electric fields inside enclosures. The CGE-02 and small mechanical stirrer have been proven to be functional in this capacity, however there is scope to carry on with the mechanical stirrer to obtain a ready to market instrument, as well as a possibility to develop the CGE-02 itself using a frequency stirring method.

The other direction future work could take is to continue to inform future versions of testing standards for measuring the SE of enclosures. Aspects of this work that were not possible in this research due to time constraints include continuing the investigation into the effect that the $Q-$ factor has on the measured SE in a reverberation chamber. This would include further investigations into the reduction and elimination of direct paths in reverberant environments, particularly in enclosures that are loaded with contents. Further research into the field distribution obtained when using frequency stirring would also be beneficial. It would also be useful and interesting to send the test enclosure used in Chapter 4 to more EMC laboratories, and to further investigate differences (if any) that might be found, including the unknows around the aspect of the repeatability of the SE measurement. The measurement of real-world shielding enclosures with multiple apertures and contents is still an interesting and rich seam of research, along with the continuing study of reverberant enclosures, and future work into this would have real world applicability.

Chapter 10

Appendix 1: MatLab Code

Section 10.1 details the code used when using mechanical stirring

Section 10.2 details the code used when using frequency stirring

Section 10.3 details the code used when finding peaks for use with the CGE-02

Section 10.4 details the code used to simulate direct and indirect paths in a nested chamber environment

10.1 Mechanical Stirring Code

Spectrum analyser data in three sections

```
% DATA FROM ENCLOSURE
figure (1)
clear ('f1L','f1M','f1R','step1','s1L1','s1M1','s1R1','fT1','dB1','i','j','mW1','mV1','data1','A','N',
'sigma','v_mon1','Hr1','Pr1','Hm1','Pm1');
clf(1,'reset');
[f1L,step1,s1L1] = readSAN(FILEL,START,END,STEP); %read in data
[f1M,step1,s1M1] = readSAN(FILEM,START,END,STEP);
[f1R,step1,s1R1] = readSAN(FILER,START,END,STEP);
s1M1(1,:) = [ ];
f1M(1,:) = [ ];
s1R1(1,:) = [ ];
f1R(1,:) = [ ];
fT1 = [f1L;f1M;f1R];
dB1 = [s1L1;s1M1;s1R1];  % combine into big matrix (still in dBm)


for i=1:1501,
for j=1:80,
mW1(i,j) = (10^((dB1(i,j))/10))/1000;  %convert to mW
end
end


for i=1:1501,
for j=1:80,
mV1(i,j) = ((mW1(i,j)));  %convert to mV
```

```
end
end

for i = 1:80,
C = mV1(:,i);
data1(1,i) = mean(C);  % average over frequency bandwidth
clear('C');
end

for i=1:80,
A(1,i) = (data1(1,i))ˆ2;
end
N = 80;
duck = sqrt((1/(2*N))*sum(A));  % create Rayleigh Parameter


v_mon1 = raylrnd (duck,1,1000000);
[Hr1,Pr1] = hist(v_mon1,50);
Hr1 = ((Hr1/sum(Hr1))/(max(Pr1)-min(Pr1)))*50;  %Siimulate Rayleigh Curve

[Hm1,Pm1] = hist(data1,20);
Hm1 = ((Hm1/sum(Hm1))/(max(Pm1)-min(Pm1)))*20;  % Histogram of data

figure (1)
bar(Pm1,Hm1,'w')
hold on
plot(Pr1,Hr1,'r')  %plot both
title(sprintf('Normalised P.D.F. plot for mechanical stirring at %d GHz, Small Enclosure',(f/1000000000)));

%REFERENCE DATA
figure (2)
clear ('f1L','f1M','f1R','step1','s1L1','s1M1','s1R1','fT1','dB1','i','j','mW1','mV1','data1','A','N',
'sigma','v_mon1','Hr1','Pr1','Hm1','Pm1');
clf(2,'reset');
[f1L,step1,s1L1] = readSAN(FILERL,START,END,STEP);
```

```
[f1M,step1,s1M1] = readSAN(FILERM,START,END,STEP);
[f1R,step1,s1R1] = readSAN(FILERR,START,END,STEP);
s1M1(1,:) = [ ];
f1M(1,:) = [ ];
s1R1(1,:) = [ ];
f1R(1,:) = [ ];
fT1 = [f1L;f1M;f1R];
dB1 = [s1L1;s1M1;s1R1];


for i=1:1501,
for j=1:80,
mW1(i,j) = (10^((dB1(i,j))/10))/1000;
end
end


for i=1:1501,
for j=1:80,
mV1(i,j) = ((mW1(i,j)));
end
end

for i = 1:80,
C = mV1(:,i);
data1(1,i) = mean(C);
clear('C');
end

for i=1:80,
A(1,i) = (data1(1,i))^2;
end
N = 80;
sigma = sqrt((1/(2*N))*sum(A));
```

```
v_mon1 = raylrnd (sigma,1,1000000);
[Hr1,Pr1] = hist(v_mon1,50);
Hr1 = ((Hr1/sum(Hr1))/(max(Pr1)-min(Pr1)))*50;

[Hm1,Pm1] = hist(data1,20);
Hm1 = ((Hm1/sum(Hm1))/(max(Pm1)-min(Pm1)))*20;

figure (2)
bar(Pm1,Hm1,'w')
hold on
plot(Pr1,Hr1,'r')
title(sprintf('Normalised P.D.F. plot for mechanical stirring at %d GHz, Big Chamber',(f/1000000000)));
```

10.2 Frequency Stirring Code

Post Processing frequency stirring code

```
% FStir_NA

num=320; %Stirrer steps
freq_num=1601;% frequency points
step = 20;%file name post fix need this



for file_num=1:num
filename1=sprintf('D:\\Documents\\PhD\\Work\\Results\\10_01 January\\18Jan\\data%04d.dat',(file_num-1)*step);
```

```
temp1 = importdata(filename1);
temp2 = temp1.data;
x_axis = temp2(:,1);
s21_real(:,file_num) = temp2(:,4);
s21_imag(:,file_num) = temp2(:,5);
end

for filter_envelope = 1:50;
    A(1,filter_envelope) = 1/50;
    end;

s21_avg_real = filter(A,1,s21_real);
s21_avg_imag = filter(A,1,s21_imag);

s21_mag = sqrt(s21_avg_imag.ˆ2+s21_avg_real.ˆ2);

s21_mag_2 = filter(A,1,(sqrt((s21_real.ˆ2)+(s21_imag.ˆ2))));

figure(101)
PlotAxisAtOrigin2(s21_avg_real,s21_avg_imag)



draylparam = draylfit(s21_mag);

drayl_sim = draylrnd (draylparam,1,1000000);

[Hr_1,Pr_1] = hist(drayl_sim,100);
               Hr_1_n = ((Hr_1/sum(Hr_1))/(max(Pr_1)-min(Pr_1)))*100;


[H_1,P_1] = hist(s21_mag,30);
               H_1_n = ((H_1/sum(H_1))/(max(P_1)-min(P_1)))*30;
```

```
 figure(1)
        bar(P_1,H_1_n,'w')
        hold on
        plot(Pr_1,Hr_1_n,'r','Linewidth',2)
```

10.3 Peak finding Code

Code used to isolate the peaks obtained with the CGE-02

```
%¬¬¬ ROB ARMSTRONG March 2009 ¬¬¬%

%FILEX = filename without extension, X = L,M,R data sets
%START = start value (0)
%END = end value (step* no.of measurements)
%STEP = stirrer steps between measurements
%Fcent = central frequency of data set
%DEV = distance either side of Fcent that the peak should be found in [5 works well]
%CUTOFF = peak height ¬-60dB for reference data, ¬-70 for Shielded measurements

%if more than one trace appears on the final plot,  reduce DEV

clear ('B','data','data2','f','centrepos','peak','loc','F','s','s1','step')  %Clears previous data
 %-if not done then Plot does not work
[fL,step,s1L] = readSAN(FILEL,START,END,STEP);  % Reads files using readSAN m-file
 % - makes a big matrix of frequency vs stirrer position
[fM,step,s1M] = readSAN(FILEM,START,END,STEP);
[fR,step,s1R] = readSAN(FILER,START,END,STEP);
fM(1,:) = [ ];
```

```
fR(1,:) = [ ];
s1M(1,:) = [ ];
s1R(1,:) = [ ];
fT = [fL;fM;fR];
s1T = [s1L;s1M;s1R];%joins 3 seperate matrices together
S = size(s1T);
Sr = S(1,1);
Sc = S(1,2);
for j=1:Sr,
   for i=1:Sc,
s1TmV(j,i) = [(sqrt((10ˆ(s1T(j,i)/10))/10))*1000]; %delog and convert into mV
end
end
data = s1TmV(:,1); % frequency spectrum stripped from big matrix
centrepos = find(fT == Fcent);  %finds where in the matrix the centre frequency is
B = DEV; % set deviation from center frequency
A = data(centrepos-B:centrepos+B); %isolate data around centre frequency
[peak,loc] = findpeaks(A,'minpeakheight',CUTOFF); %find peak in isolated data
peak
F = centrepos - (B-loc); % actual position of centre frequency
mechanicalstirring = s1TmV(F,:); %strip the centre frequency data from the big matrix
figure(1)
plot(step,mechanicalstirring)   % and plot
ylabel('mV')
xlabel('Stirrer Position')
%title('mV for full stirrer rotation')
title(sprintf('Mechanical Stirring at %d GHz',(Fcent/1000000000)));

sigma = mode(mechanicalstirring);  % Rayleigh parameter
sigma
v_mon = raylrnd (sigma,1,10000000); % random Rayleigh distribution with the correct parameter,
 %1*10ˆ7 is the max number of points computer can cope with

[Hm,Pm] = hist(mechanicalstirring,20); % histogram of data forom chamber, 20 = bin number
Hm = ((Hm/sum(Hm))/(max(Pm)-min(Pm)))*20; % normalising
```

```
[Hr,Pr] = hist(v_mon,50);  %histogram of simulated Rayleigh, bin number = 50
Hr = ((Hr/sum(Hr))/(max(Pr)-min(Pr)))*50; %normalising Rayleigh

figure(2) % new figure!

bar(Pm,Hm,'w') %plot the histogram fomr data, with no shading ('w')
hold on
plot(Pr,Hr,'r') %plot the Rayleigh distribution in RED
ylabel('Normalised mV')
title(sprintf('Normalised P.D.F. plot for mechanical stirring at %d GHz',(Fcent/1000000000)));
```

10.4 Distribution Combination code

Code used to combine distributions when examining direct paths

```
%%% Rob Armstrong December 2009 %%%

function [P,Q,R,S,T,U] = W_I_P(choice,A,B,C,a,b,c,A_E,B_E,C_E,a_E,b_E,c_E,Cf_1,Cf_2,Cf_3,path_no)

%[P,Q,R,S,T,U] = W_I_P(choice,A,B,C,a,b,c,A_E,B_E,C_E,a_E,b_E,c_E,Cf_1,Cf_2,Cf_3,path_no)

%&&&  inputs  &&&

% % choice [0 or 1]
    % 0 calculates from simulated normal data
    % 1 calculates from experimental data

% %path offsets [integer between 0 and 500]
```

```
    % A = imaginary component, distrubution 1
    % a = real component, distrubution 1
    % B = imaginary component, distrubution 2
    % b = real component, distrubution 2
    % C = imaginary component, distrubution 3
    % c = real component, distrubution 3
    % A_E = imaginary component, distrubution 1 in enclosure
    % a_E = real component, distrubution 1 in enclosure
    % B_E = imaginary component, distrubution 2 in enclosure
    % b_E = real component, distrubution 2 in enclosure
    % C_E = imaginary component, distrubution 3 in enclosure
    % c_E = real component, distrubution 3 in enclosure

% %coupling factors [integer between 0 and 100]

    % CF_1
    % CF_2
    % CF_3

% % number of paths [1,2,or 3]

    % path_no

%&&& outputs &&&

% P, Q, R, for one path, P = path_1, Q = path_2, R = path_3
%          for two paths, P = path_1_2, Q = path_1_3, R = path_2_3
%          for three paths, P = path_1_2_3, Q = 0, R = 0



if choice == 0 %choose between experimental or simulated

    %N_i = normrnd(0,1,1,100000); % generate random normal data, imaginary
    %N_r = normrnd(0,1,1,100000); % generate random normal data, real
```

```
    % split into 3 different paths


            path_1_i = normrnd(0,1,1,100000)+(A);

            path_1_r = normrnd(0,1,1,100000)+(a);

            path_2_i = normrnd(0,1,1,100000)+(B);

            path_2_r = normrnd(0,1,1,100000)+(b);

            path_3_i = normrnd(0,1,1,100000)+(C);

            path_3_r = normrnd(0,1,1,100000)+(c);

    %multiply by coupling factor

            path_1_i_C = path_1_i.*Cf_1;
            path_1_r_C = path_1_r.*Cf_1;

            path_2_i_C = path_2_i.*Cf_2;
            path_2_r_C = path_2_r.*Cf_2;

            path_3_i_C = path_3_i.*Cf_3;
            path_3_r_C = path_3_r.*Cf_3;


%     enclosure distributions

            path_1_i_E = normrnd(0,1,1,100000)+(A_E);


            path_1_r_E = normrnd(0,1,1,100000)+(a_E);
```

```
        path_2_i_E = normrnd(0,1,1,100000)+(B_E);

        path_2_r_E = normrnd(0,1,1,100000)+(b_E);

        path_3_i_E = normrnd(0,1,1,100000)+(C_E);

        path_3_r_E = normrnd(0,1,1,100000)+(c_E);

%combine

if path_no == 1
    %E = sqrt((a.*c - b.*d).^2 + (a.*d + b.*c).^2);
    o1_path_1 = sqrt((path_1_r_C.*path_1_r_E - path_1_i_C.*path_1_i_E).^2 +
     (path_1_r_C.*path_1_i_E + path_1_i_C.*path_1_r_E).^2);
    o1_path_2 = sqrt((path_2_r_C.*path_2_r_E - path_2_i_C.*path_2_i_E).^2 +
     (path_2_r_C.*path_2_i_E + path_2_i_C.*path_2_r_E).^2);
    o1_path_3 = sqrt((path_3_r_C.*path_3_r_E - path_3_i_C.*path_3_i_E).^2 +
     (path_3_r_C.*path_3_i_E + path_3_i_C.*path_3_r_E).^2);

    P = o1_path_1;
    Q = o1_path_2;
    R = o1_path_3;

    %raylegh plot
        rayl_param_1 = raylfit(o1_path_1);
        rayl_param_2 = raylfit(o1_path_2);
        rayl_param_3 = raylfit(o1_path_3);

        rayl_sim_1 = raylrnd (rayl_param_1,1,1000000);
        rayl_sim_2 = raylrnd (rayl_param_2,1,1000000);
```

```
rayl_sim_3 = raylrnd (rayl_param_3,1,1000000);

[Hr_1,Pr_1] = hist(rayl_sim_1,80);
   Hr_1_n = ((Hr_1/sum(Hr_1))/(max(Pr_1)-min(Pr_1)))*80;

[Hr_2,Pr_2] = hist(rayl_sim_2,80);
   Hr_2_n = ((Hr_2/sum(Hr_2))/(max(Pr_2)-min(Pr_2)))*80;

[Hr_3,Pr_3] = hist(rayl_sim_3,80);
   Hr_3_n = ((Hr_3/sum(Hr_3))/(max(Pr_3)-min(Pr_3)))*80;

   %double rayleigh plot

         drayl_param_1 = draylfit(o1_path_1);
         drayl_param_2 = draylfit(o1_path_2);
         drayl_param_3 = draylfit(o1_path_3);

         drayl_sim_1 = draylrnd (drayl_param_1,1,10000000);
         drayl_sim_2 = draylrnd (drayl_param_2,1,10000000);
         drayl_sim_3 = draylrnd (drayl_param_3,1,10000000);

        [Hdr_1,Pdr_1] = hist(drayl_sim_1,80);
           Hdr_1_n = ((Hdr_1/sum(Hdr_1))/(max(Pdr_1)-min(Pdr_1)))*80;

        [Hdr_2,Pdr_2] = hist(drayl_sim_2,80);
           Hdr_2_n = ((Hdr_2/sum(Hdr_2))/(max(Pdr_2)-min(Pdr_2)))*80;

        [Hdr_3,Pdr_3] = hist(drayl_sim_3,80);
           Hdr_3_n = ((Hdr_3/sum(Hdr_3))/(max(Pdr_3)-min(Pdr_3)))*80;

                % rician plot

                [rice_param_1_1,rice_param_1_2] = normfit(o1_path_1);
                [rice_param_2_1,rice_param_2_2] = normfit(o1_path_2);
                [rice_param_3_1,rice_param_3_2] = normfit(o1_path_3);
```

```
                     rice_sim_1 = normrnd (rice_param_1_1,rice_param_1_2,1,1000000);
                     rice_sim_2 = normrnd (rice_param_2_1,rice_param_2_2,1,1000000);
                     rice_sim_3 = normrnd (rice_param_3_1,rice_param_3_2,1,1000000);

                    [Hri_1,Pri_1] = hist(rice_sim_1,80);
                       Hri_1_n = ((Hri_1/sum(Hri_1))/(max(Pri_1)-min(Pri_1)))*80;

                    [Hri_2,Pri_2] = hist(rice_sim_2,80);
                       Hri_2_n = ((Hri_2/sum(Hri_2))/(max(Pri_2)-min(Pri_2)))*80;

                    [Hri_3,Pri_3] = hist(rice_sim_3,80);
                       Hri_3_n = ((Hri_3/sum(Hri_3))/(max(Pri_3)-min(Pri_3)))*80;


[H_1,P_1] = hist(o1_path_1,40); %histogram
H_1_n = ((H_1/sum(H_1))/(max(P_1)-min(P_1)))*40;

[H_2,P_2] = hist(o1_path_2,40); %histogram
H_2_n = ((H_2/sum(H_2))/(max(P_2)-min(P_2)))*40;

[H_3,P_3] = hist(o1_path_3,40); %histogram
H_3_n = ((H_3/sum(H_3))/(max(P_3)-min(P_3)))*40;

figure(1)
figure(2)
figure(3)
clf(1)
clf(2)
clf(3)

figure(1)
bar(P_1,H_1_n,'w')
hold on
plot(Pr_1,Hr_1_n,'r','Linewidth',2)
```

```
    plot(Pdr_1,Hdr_1_n,'b','Linewidth',2)
    %plot(Pri_1,Hri_1_n,'g','Linewidth',2)
    title(sprintf('Single Rician, Normal offset = 1.4'));

    figure(2)
    bar(P_2,H_2_n,'w')
    hold on
    plot(Pr_2,Hr_2_n,'r','Linewidth',2)
    plot(Pdr_2,Hdr_2_n,'b','Linewidth',2)
    %plot(Pri_2,Hri_2_n,'g','Linewidth',2)
    title(sprintf('Single Rician, Normal offset = 5'));

    figure(3)
    bar(P_3,H_3_n,'w')
    hold on
    plot(Pr_3,Hr_3_n,'r','Linewidth',2)
    plot(Pdr_3,Hdr_3_n,'b','Linewidth',2)
    %plot(Pri_3,Hri_3_n,'g','Linewidth',2)
    title(sprintf('Single Rician, Normal offset = 10'));

    S = rayl_sim_1;
    T = drayl_sim_2;
    U = rice_sim_3;

else
end %if for combining 3 seperate single paths

if path_no == 2
    o2_path_1_2 = sqrt(((path_1_r_C.*path_1_r_E - path_1_i_C.*path_1_i_E) +
    (path_2_r_C.*path_2_r_E - path_2_i_C.*path_2_i_E)).^2 + ((path_1_r_C.*path_1_i_E +
    path_1_i_C.*path_1_r_E) + (path_2_r_C.*path_2_i_E + path_2_i_C.*path_2_r_E)).^2);

    o2_path_1_3 = sqrt(((path_1_r_C.*path_1_r_E - path_1_i_C.*path_1_i_E) +
    (path_3_r_C.*path_3_r_E - path_3_i_C.*path_3_i_E)).^2 + ((path_1_r_C.*path_1_i_E +
    path_1_i_C.*path_1_r_E) + (path_3_r_C.*path_3_i_E + path_3_i_C.*path_3_r_E)).^2);
```

```
o2_path_2_3 = sqrt(((path_2_r_C.*path_2_r_E - path_2_i_C.*path_2_i_E) +
(path_3_r_C.*path_3_r_E - path_3_i_C.*path_3_i_E)).^2 + ((path_2_r_C.*path_2_i_E +
path_2_i_C.*path_2_r_E) + (path_3_r_C.*path_3_i_E + path_3_i_C.*path_3_r_E)).^2);

P = o2_path_1_2;
Q = o2_path_1_3;
R = o2_path_2_3;

%raylegh plot
    rayl_param_1 = raylfit(o2_path_1_2);
    rayl_param_2 = raylfit(o2_path_1_3);
    rayl_param_3 = raylfit(o2_path_2_3);

    rayl_sim_1 = raylrnd (rayl_param_1,1,1000000);
    rayl_sim_2 = raylrnd (rayl_param_2,1,1000000);
    rayl_sim_3 = raylrnd (rayl_param_3,1,1000000);

    [Hr_1,Pr_1] = hist(rayl_sim_1,80);
       Hr_1_n = ((Hr_1/sum(Hr_1))/(max(Pr_1)-min(Pr_1)))*80;

    [Hr_2,Pr_2] = hist(rayl_sim_2,80);
       Hr_2_n = ((Hr_2/sum(Hr_2))/(max(Pr_2)-min(Pr_2)))*80;

    [Hr_3,Pr_3] = hist(rayl_sim_3,80);
       Hr_3_n = ((Hr_3/sum(Hr_3))/(max(Pr_3)-min(Pr_3)))*80;

       %double rayleigh plot

             drayl_param_1 = draylfit(o2_path_1_2);
             drayl_param_2 = draylfit(o2_path_1_3);
             drayl_param_3 = draylfit(o2_path_2_3);

             drayl_sim_1 = draylrnd (drayl_param_1,1,1000000);
             drayl_sim_2 = draylrnd (drayl_param_2,1,1000000);
```

```
             drayl_sim_3 = draylrnd (drayl_param_3,1,1000000);

            [Hdr_1,Pdr_1] = hist(drayl_sim_1,80);
               Hdr_1_n = ((Hdr_1/sum(Hdr_1))/(max(Pdr_1)-min(Pdr_1)))*80;

            [Hdr_2,Pdr_2] = hist(drayl_sim_2,80);
               Hdr_2_n = ((Hdr_2/sum(Hdr_2))/(max(Pdr_2)-min(Pdr_2)))*80;

            [Hdr_3,Pdr_3] = hist(drayl_sim_3,80);
               Hdr_3_n = ((Hdr_3/sum(Hdr_3))/(max(Pdr_3)-min(Pdr_3)))*80;

                    % rician plot

                    [rice_param_1_1,rice_param_1_2] = normfit(o2_path_1_2);
                    [rice_param_2_1,rice_param_2_2] = normfit(o2_path_1_3);
                    [rice_param_3_1,rice_param_3_2] = normfit(o2_path_2_3);

                     rice_sim_1 = normrnd (rice_param_1_1,rice_param_1_2,1,1000000);
                     rice_sim_2 = normrnd (rice_param_2_1,rice_param_2_2,1,1000000);
                     rice_sim_3 = normrnd (rice_param_3_1,rice_param_3_2,1,1000000);

                    [Hri_1,Pri_1] = hist(rice_sim_1,80);
                       Hri_1_n = ((Hri_1/sum(Hri_1))/(max(Pri_1)-min(Pri_1)))*80;

                    [Hri_2,Pri_2] = hist(rice_sim_2,80);
                       Hri_2_n = ((Hri_2/sum(Hri_2))/(max(Pri_2)-min(Pri_2)))*80;

                    [Hri_3,Pri_3] = hist(rice_sim_3,80);
                       Hri_3_n = ((Hri_3/sum(Hri_3))/(max(Pri_3)-min(Pri_3)))*80;


[H_1,P_1] = hist(o2_path_1_2,40); %histogram
H_1_n = ((H_1/sum(H_1))/(max(P_1)-min(P_1)))*40;

[H_2,P_2] = hist(o2_path_1_3,40); %histogram
```

```
H_2_n = ((H_2/sum(H_2))/(max(P_2)-min(P_2)))*40;

[H_3,P_3] = hist(o2_path_2_3,40); %histogram
H_3_n = ((H_3/sum(H_3))/(max(P_3)-min(P_3)))*40;

figure(4)
figure(5)
figure(6)
clf(4)
clf(5)
clf(6)

figure(4)
bar(P_1,H_1_n,'w')
hold on
plot(Pr_1,Hr_1_n,'r','Linewidth',2)
plot(Pdr_1,Hdr_1_n,'b','Linewidth',2)
plot(Pri_1,Hri_1_n,'g','Linewidth',2)
title(sprintf('Path through pinch points 1 and 2, simulated'));

figure(5)
bar(P_2,H_2_n,'w')
hold on
plot(Pr_2,Hr_2_n,'r','Linewidth',2)
plot(Pdr_2,Hdr_2_n,'b','Linewidth',2)
plot(Pri_2,Hri_2_n,'g','Linewidth',2)
title(sprintf('Path through pinch points 1 and 3, simulated'));

figure(6)
bar(P_3,H_3_n,'w')
hold on
plot(Pr_3,Hr_3_n,'r','Linewidth',2)
plot(Pdr_3,Hdr_3_n,'b','Linewidth',2)
plot(Pri_3,Hri_3_n,'g','Linewidth',2)
title(sprintf('Path through pinch points 2 and 3, simulated'));
```

```
else
end %if for combining 2 paths

if path_no == 3
    o3_path_1_2_3 = sqrt(((path_1_r_C.*path_1_r_E - path_1_i_C.*path_1_i_E) +
    (path_2_r_C.*path_2_r_E - path_2_i_C.*path_2_i_E) + (path_3_r_C.*path_3_r_E -
    path_3_i_C.*path_3_i_E)).^2 + ((path_1_r_C.*path_1_i_E + path_1_i_C.*path_1_r_E) +
    (path_2_r_C.*path_2_i_E + path_2_i_C.*path_2_r_E) + (path_3_r_C.*path_3_i_E +
    path_3_i_C.*path_3_r_E)).^2);

    P = o3_path_1_2_3;
    Q = 0;
    R = 0;

    %raylegh plot
        rayl_param_1 = raylfit(o3_path_1_2_3);


        rayl_sim_1 = raylrnd (rayl_param_1,1,1000000);

        [Hr_1,Pr_1] = hist(rayl_sim_1,80);
           Hr_1_n = ((Hr_1/sum(Hr_1))/(max(Pr_1)-min(Pr_1)))*80;



           %double rayleigh plot

                 drayl_param_1 = draylfit(o3_path_1_2_3);


                 drayl_sim_1 = draylrnd (drayl_param_1,1,1000000);

                [Hdr_1,Pdr_1] = hist(drayl_sim_1,80);
                   Hdr_1_n = ((Hdr_1/sum(Hdr_1))/(max(Pdr_1)-min(Pdr_1)))*80;
```

```
                            % rician plot

                            [rice_param_1_1,rice_param_1_2] = normfit(o3_path_1_2_3);

                             rice_sim_1 = normrnd (rice_param_1_1,rice_param_1_2,1,1000000);


                            [Hri_1,Pri_1] = hist(rice_sim_1,80);
                               Hri_1_n = ((Hri_1/sum(Hri_1))/(max(Pri_1)-min(Pri_1)))*80;



        [H_1,P_1] = hist(o3_path_1_2_3,40); %histogram
        H_1_n = ((H_1/sum(H_1))/(max(P_1)-min(P_1)))*40;

        figure(7)
        clf(7)

        figure(7)
        bar(P_1,H_1_n,'w')
        hold on
        plot(Pr_1,Hr_1_n,'r','Linewidth',2)
        plot(Pdr_1,Hdr_1_n,'b','Linewidth',2)
        %plot(Pri_1,Hri_1_n,'g','Linewidth',2)
        title(sprintf('Path through pinch points 1,2 and 3, simulated'));

    else
    end %if for combining all 3 paths


else %choice between experimental and simulation - experimental below

% read in experimental normal data
```

```
num=200;

step = 2;

s12_real = zeros(1600,200);
s12_imag = zeros(1600,200);
for file_num=1:num

    filename1=sprintf('D:\\Documents\\PhD\\Work\\Results\\10_09 October\\30 Oct\\more pos\\port 2
    to port 3\\data%04d.dat',(file_num-1)*step); % Rayleigh data)
    temp1 = importdata(filename1);
    temp2 = temp1.data;

    s12_real(:,file_num) = temp2(:,4);
    s12_imag(:,file_num) = temp2(:,5);
end

freq = temp2(:,1);


f = 5;

F = f*10^9;
freq_pos = find(freq == F);


MS_imag = s12_imag(freq_pos,:); % taking the specified frequency out of the big matrix
MS_real = s12_real(freq_pos,:);

mu_i = mean(MS_imag);  % means of data
mu_r = mean(MS_real);

sigma_i = std(MS_imag,1); % Standard deviations of data
sigma_r = std(MS_real,1);
```

```
N_i = normrnd(mu_i,sigma_i,1,100000); %generate data from mu and sigma from experiment
N_r = normrnd(mu_r,sigma_r,1,100000);

% split into 3 different paths
for i = 0:500;
    if A == i
        path_1_i = N_i+(A/1000);
        path_1_r = N_r+(A/1000);
    else
    end
    if B == i
        path_2_i = N_i+(B/1000);
        path_2_r = N_i+(B/1000);
    else
    end
    if C == i
        path_3_i = N_i+(C/1000);
        path_3_r = N_r+(C/1000);
    else
    end
end

%multiply by coupling factor
for j = 0:100
    if Cf_1 == j
        path_1_i_E = path_1_i.*Cf_1;
        path_1_r_E = path_1_r.*Cf_1;
    else
    end

    if Cf_2 == j
        path_2_i_E = path_2_i.*Cf_2;
        path_2_r_E = path_2_r.*Cf_2;
    else
    end
```

```
    if Cf_3 == j
        path_3_i_E = path_3_i.*Cf_3;
        path_3_r_E = path_3_r.*Cf_3;
    else
    end
end

%combine

if path_no == 1
    o1_path_1 = sqrt(path_1_i_E.^2 + path_1_r_E.^2);
    o1_path_2 = sqrt(path_2_i_E.^2 + path_2_r_E.^2);
    o1_path_3 = sqrt(path_3_i_E.^2 + path_3_r_E.^2);

    P = o1_path_1;
    Q = o1_path_2;
    R = o1_path_3;

     [H_1,P_1] = hist(o1_path_1,40); %histogram
    H_1_n = ((H_1/sum(H_1))/(max(P_1)-min(P_1)))*40;

    [H_2,P_2] = hist(o1_path_2,40); %histogram
    H_2_n = ((H_2/sum(H_2))/(max(P_2)-min(P_2)))*40;

    [H_3,P_3] = hist(o1_path_3,40); %histogram
    H_3_n = ((H_3/sum(H_3))/(max(P_3)-min(P_3)))*40;

    figure(11)
    bar(P_1,H_1_n,'w')
    title(sprintf('Path through pinch point 1, experimental'));

    figure(12)
    bar(P_2,H_2_n,'w')
    title(sprintf('Path through pinch point 2, experimental'));
```

```
    figure(13)
    bar(P_3,H_3_n,'w')
    title(sprintf('Path through pinch point 3, experimental'));

else
end

if path_no == 2
    o2_path_1_2 = sqrt((path_1_i_E + path_2_i_E).^2 + (path_1_r_E + path_2_r_E).^2);
    o2_path_1_3 = sqrt((path_1_i_E + path_3_i_E).^2 + (path_1_r_E + path_3_r_E).^2);
    o2_path_2_3 = sqrt((path_2_i_E + path_3_i_E).^2 + (path_2_r_E + path_3_r_E).^2);

    P = o2_path_1_2;
    Q = o2_path_1_3;
    R = o2_path_2_3;

    [H_1,P_1] = hist(o2_path_1_2,40); %histogram
    H_1_n = ((H_1/sum(H_1))/(max(P_1)-min(P_1)))*40;

    [H_2,P_2] = hist(o2_path_1_3,40); %histogram
    H_2_n = ((H_2/sum(H_2))/(max(P_2)-min(P_2)))*40;

    [H_3,P_3] = hist(o2_path_2_3,40); %histogram
    H_3_n = ((H_3/sum(H_3))/(max(P_3)-min(P_3)))*40;

    figure(14)
    bar(P_1,H_1_n,'w')
    title(sprintf('Path through pinch points 1 and 2, experimental'));

    figure(15)
    bar(P_2,H_2_n,'w')
    title(sprintf('Path through pinch points 1 and 3, experimental'));

    figure(16)
```

```
        bar(P_3,H_3_n,'w')
        title(sprintf('Path through pinch points 2 and 3, experimental'));

    else
    end

    if path_no == 3
        o3_path_1_2_3 = sqrt((path_1_i_E + path_2_i_E + path_3_i_E).^2 + (path_1_r_E + path_2_r_E +
        path_3_i_E).^2);

        P = o3_path_1_2_3;
        Q = 0;
        R = 0;

        [H_1,P_1] = hist(o3_path_1_2_3,40); %histogram
        H_1_n = ((H_1/sum(H_1))/(max(P_1)-min(P_1)))*40;

        figure(17)
        bar(P_1,H_1_n,'w')
        title(sprintf('Path through pinch points 1,2 and 3, experimental'));

    else
    end

end
clear ('choice','A','B','C','a','b','c','A_E','B_E','C_E','a_E','b_E','c_E','Cf_1','Cf_2','Cf_3','path_no')
end
```

List of Acronyms

These acronyms are all used within this thesis

ACF	Autocorrelation Function
AN79	Radio frequency absorber designation
BNC	Bayonet NeillConcelman (connector type, coaxial 50Ω)
BP	Battery Pack
BW	Bandwidth
CDF	Cumulative Density Function
CGE	Comb Generator Emitter
CISPR	Comité International Spécial des Perturbations Radioélectriques
dB	Decibels
DC	Direct Current
EM	Electromagnetic
EMC	Electromagnetic Compatibility
EMI	Electromagnetic Interference
EU	European Union
EUT	Enclosure Under Test
FS	Frequency Stirring
FM	Frequency Modulation
IEC	International Electro-technical Committee
IEEE	Institute of Electrical and Electronic Engineers
IF	Inter Frequency
IFBW	Inter Freqency Bandwidth
KS	Kolmogorov-Smirnov
LUF	Lowest Usable Frequency

MIL	Shorthand for Military
MS	Mechanical Stirring
NA	Network Analyser
N-type	Type N connector (connector type, coaxial 50Ω)
OATS	Open Area Test Site
PC	Personal Computer
PCB	Printed Circit Board
PDF	Probability Density Function
RAM	Radio Absorbing Material
RF	Radio Frequency
R & S	Rohde and Schwarz
SA	Spectrum Analyser
SE	Shielding Effectiveness
SMA	Sub Miniature revision A (connector type, coaxial 50Ω)
UoA	University of Ancona, Italy
UoY	University of York, UK
VNA	Vector Network Analyser
WA	Width of Autocorrelation
YES	York EMC Services

List of Symbols

These symbols are all used within this thesis

δ	Skin depth
η_0	Impedance of free space
λ	Wavelength
ν	Peak offset from reference (used when defining Rician distributions)
μ	Magnetic permeability
μ_m	Mean
μ_r	Relative permeability
ϕ	Gaussian distribution offset from a zero mean
ϕ_{min}	Minimum offset from zero for a Gaussian distribution with a variance of 1
σ	Electrical conductivity
σ_v	Variance
$< \sigma_a >$	Absorption cross section
$< \sigma_t >$	Transmission cross section
A	Path A through aperture A used in direct path measurements
a	Reverberation chamber dimension in the x direction (length)
A_E	Axis of histogram representative of electric field strength
a_o	Offset of Gaussian mean from zero on the ‘imaginary’ axis
A_a	Area of an aperture
A_o	Offset of distribution centre from zero in the ‘imaginary’ direction
A_s	‘No slot’ configuration in comparative enclosure
B	Path B through aperture B used in direct path measurements
b	Reverberation chamber dimension in the y direction (width)
b_o	Offset of Gaussian mean from zero on the ‘real’ axis
B_o	Offset of distribution centre from zero in the ‘real’ direction

B_s	‘Short slot’ configuration in comparative enclosure
C	Path C through aperture C used in direct path measurements
c	Reverberation chamber dimension in the z direction (height)
c_0	Speed of light in a vacuum
$C[i]$	Autocorrelation of i samples
C_s	‘Medium slot’ configuration in comparative enclosure
d	Thickness of shielding material
D	Size of an antenna
d_a	Deviation of $F_0(x)$ from $F(x)$
D_m	Density of modes (per Hertz)
D_s	‘Long slot’ configuration in comparative enclosure
E	Electric Field Strength
$E_{d\theta}$	Unstirred component of measured electric field
E_{xj}	Imaginary (phase quadrature) component of the electric field in the x direction
E_{xr}	Real (in phase) component of the electric field in the x direction
E_{yj}	Imaginary (phase quadrature) component of the electric field in the y direction
E_{yr}	Real (in phase) component of the electric field in the y direction
E_{zj}	Imaginary (phase quadrature) component of the electric field in the z direction
E_{zr}	Real (in phase) component of the electric field in the z direction
E_i	Incident (Reference or unshielded) electromagnetic wave
E_0	Electric field
E_r	Reflected (shielded) electromagnetic wave
E_t	Transmitted electromagnetic wave
E_x	Electric field component in the x direction
E_y	Electric field component in the y direction
E_z	Electric field component in the z direction
e	exponential
f	frequency
f_{110}	frequency at first mode 110
f_{min}	minimum useable frequency
f_{mnp}	Frequency at particular modes (m,n,p)
$F_0(x)$	Simulated function CDF (for use with KS test)
f_r	frequency range
$F(x)$	Stepped function (for use with KS test)
H	Magnetic Field Strength

H_i	Incident (Reference or Unshielded) magnetic field strength
H_t	Transmitted (shielded) magnetic field strength
H_x	Magnetic field component in the x direction
H_y	Magnetic field component in the y direction
H_z	Magnetic field component in the z direction
I	Number of samples in a sequence x_i
i	integer number
j	square root of minus 1
K	K-factor
k	integer number
$K_{\sigma_v=1}$	K-factor with specified variance of 1
K_0	Zeroth order Bessel function
L_R	Loss ratio
m	Mode number in the x direction
m_a	Antenna mismatch factor
n	Mode number in the y direction
N_{avgBW}	Number of frequency points needed for average
N_f	Number of frequency points in frequency range
N_m	Number of resonant modes below particular f
N_s	Number of samples when calculating error
p	Mode number in the z direction
$P_{CGE_{S1}}$	Average power received from the CGE, shielded, Method 1
$P_{CGE_{S2}}$	Average power received from the CGE, shielded, Method 2
$P_{CGE_{S3}}$	Average power received from the CGE, shielded, Method 3
P_{CGE_u}	Average power received from the CGE, unshielded
$P_{CGE_{u3}}$	Average power received from the CGE, unshielded, Method 3
P_{in}	Average received power inside an enclosure
P_{out}	Average received power outside an enclosure
P_r	Received power on an antenna
$P(x)$	Distributed data set
Q	Quality (as in Quality-factor)
Q_{AN}	Q-factor contribution from absorber in an EUT
Q_{AP}	Q-factor contribution from aperture in an EUT
Q_{EUT}	Q-factor of an EUT
Q_{tot}	Total composite Q-factor

Q_{wall}	Wall Q-factor
Q_1	Q-factor of an empty chamber
Q_2	Q-factor contribution from absorber
Q_3	Q-factor contribution from aperture
Q_4	Q-factor contribution from antenna
R	Distance from antenna
r	Autocorrelation of mechanical stirrer positions
S	Electromagnetic field power density
S_a	Surface area
S_i	Incident (Reference or Unshielded) electromagnetic field power density
S_t	Transmitted (Shielded) electromagnetic field power density
$S11$	Reflection coefficient (Port 1)
$S1_h1_h$	Reflection coefficient (Port 1 connected to a horn)
$S1_m1_m$	Reflection coefficient (Port 1 connected to a monopole)
$S11_R$	Reflection coefficient (Port 1), reference (unshielded) measurement
$S12$	Transmission into Port 1 from Port 2
$S1_h2$	Transmission into Port 1 from Port 2 when Port 1 is connected to a horn
$S1_m2$	Transmission into Port 1 from Port 2 when Port 1 is connected to a monopole
$S12_R$	Transmission into Port 1 from Port 2, reference (unshielded) measurement
$S21$	Transmission into Port 2 from Port 1
$S21_h$	Transmission into Port 2 from Port 1 when Port 1 is connected to a horn
$S21_m$	Transmission into Port 2 from Port 1 when Port 1 is connected to a monopole
$S22$	Reflection coefficient (Port 2)
S_p	Scale Parameter
SE_{dB}	Shielding Effectiveness in dB
$SE1_{dB}$	Shielding Effectiveness in dB resulting from Method 1
$SE2_{dB}$	Shielding Effectiveness in dB resulting from Method 2
$SE3_{dB}$	Shielding Effectiveness in dB resulting from Method 3
V	Volume of a reverberant cavity
V_e	Volume of an enclosure
x_i	Sequence of values
x	data set
y	data set x +1
Z	Wave impedance

Bibliography

[1] P.A. Johnson and K.R. Goldsmith. An Experimental Study of the Placement an Aircraft Inside a Lange Welded Zinc-Plated Steel Electromagnetic Reverberation Chamber. In *Proceedings of Digital Avionics Systems Conference*, 1998.

[2] L Klinkenbusch. On the Shielding Effectiveness of Enclosures. *IEEE TRANSACTIONS ON ELECTROMAGNETIC COMPATIBILITY*, 47(3):589–601, 2005.

[3] M.Z.M Jenu and F.A. Po'ad. Electric and Magnetic Shielding Effectiveness of Metallic Enclosures with Apertures. In *Proceedings of Asia Pacific Microwave conference 2006*, volume 2, pages 3–6, 2006.

[4] International Electrotechnical Commission. IEC 61000-4-21, Electromagnetic Compatibility (EMC), part 4: Testing and Measurement Techniques, Section 21: Reverberation Chamber Test Methods., 2011.

[5] M.S. Sarto, A.C. Marvin, J Catrysse, and Et Al. Draft Standard for P299 . 1 / D2 Draft Full-Use Std . Method for Measuring the Shielding Effectiveness of Enclosures and Boxes Having All Dimensions between 0 . 1 m and 2 m. Technical report, 2009.

[6] C.L Holloway, D.A Hill, J. Ladbury, G. Koepke, and R. Garzia. Shielding Effectiveness Measurements of Materials Using Nested Reverberation Chambers. *IEEE TRANSACTIONS ON ELECTROMAGNETIC COMPATIBILITY*, 45(2):350–356, 2003.

[7] C.L. Holloway, D.A. Hill, M. Sandroni, J.M. Ladbury, J. Coder, G. Koepke, A.C. Marvin, and Y. He. Use of Reverberation Chambers to Determine the Shielding Effectiveness of Physically Small , Electrically Large Enclosures and Cavities. *IEEE TRANSACTIONS ON ELECTROMAGNETIC COMPATIBILITY*, 50(4):770–782, 2008.

[8] D. Heirman and M. Stecher. A History of the Evolution of EMC Regulatory Bodies and Standards. In *International Symposium on EMC, Zurich*, 2005.

[9] MIL Standard 285. Method of Attenuation Measurement for Enclosures, Electromagnetic Shielding for Electronic Test Purposes, 1956.

[10] ASTM D4935. ASTM - Standard Test Method for Measuring the Electromagnetic Shielding Effeciveness of Planar Materials. 1989.

[11] International Electrotechnical Commission. CISPR 25: Vehicles, boats and internal combustion engines - Radio disturbance characteristics - Limits and methods of measurement for the protection of on-board receivers. 2008.

[12] International Electrotechnical Commission. CISPR 12: Vehicles, boats and internal combustion engines Radio disturbance characteristics Limits and methods of measurement for the protection of off-board receivers. 2007.

[13] S. A. Schelkunoff. The Impedance Concept and Its Application to Problems of Reflection, Shielding and Power Absorption. *Bell System Technical Journal*, 17:17–31, 1938.

[14] A.C. Marvin and Y. He. A Study of Enclosure Shielding Effectiveness Measurement using Frequency Stirring in a Mode-Stirred Chamber. In *IEEE International Symposium on Electromagnetic Compatibility, 2008*, pages 1–6, 2008.

[15] A.C. Marvin, J.F. Dawson, S. Ward, L. Dawson, and J. Clegg. A Proposed New Definition and Measurement of the Shielding Effect of Equipment Enclosures. *IEEE TRANSACTIONS ON ELECTROMAGNETIC COMPATIBILITY*, 46(3):459–468, 2004.

[16] C.A. Balanis. *Antenna Theory Analysis and Design (second edition)*. J Wiley and Sons, 2 edition, 1997.

[17] York EMC Services, J.F. Dawson, and A.C. Marvin. *Advanced EMC Measurements Course Notes*. 2011.

[18] Yong Cui. *A New Measure for Evaluating Shielding Performance of an Equipment Enclosure at Frequencies above 1GHz*. PhD thesis, University of York, 2007.

[19] G. Breed. Basic Principles of Electrically Small Antennas. *In High Frequency Electronics, February*, 2007.

[20] D.A. Hill. Electronic Mode Stirring for Reverberation Chambers. *IEEE TRANSACTIONS ON ELECTROMAGNETIC COMPATIBILITY*, 36(4):2–7, 1994.

[21] D.A. Hill. Boundary Fields in Reverberation Chambers. *IEEE Transactions on Electromagnetic Compatibility*, 47(2):281–290, May 2005.

[22] J.F. Dawson, T. Konefal, M.P. Robinson, A.C. Marvin, S.J. Porter, and L.C. Chirwa. Field Statistics in an Enclosure with an Aperture - Effect of Q-factor and Number of Modes. *2005 International Symposium on Electromagnetic Compatibility, 2005*, 1:141–146, 2005.

[23] W.H. Emerson. Electromagnetic Wave Absorbers and Anechoic Chambers Through the Years. *IEEE Transactions on Antennas and Propagation*, 24(4), 1973.

[24] M.L. Crawford and G. Koepke. NBS TECHNICAL NOTE 1092 Design , Evaluation , and Use of a Reverberation Chamber for Performing Electromagnetic Susceptibility / Vulnerability Measurements. 1986.

[25] G Wilson, P, Koepke, J Ladbury, and C L Holloway. Emission and Immunity Standards : Replacing Field-at- a-Distance Measurements with Total-Radiated-Power Measurements. In *International Symposium on Electromagnetic Compatibility, 2001*, pages 964–969, 2001.

[26] J.F. Dawson, M Hatfield, L.R. Arnaut, and N Eulig. *Introduction to Reverberation (Stirred Mode) Chambers*. Compliance Club: Introduction to Reverberation Chambers, http://www.compliance-club.com/archive/old_archive/030530.htm (last accessed Jan 2013), 2003.

[27] C. L. Holloway, J. Ladbury, J. Coder, G. Koepke, and D.A. Hill. Measuring the Shielding Effectiveness of Small Enclosures/Cavities with a Reverberation Chamber. *2007 IEEE International Symposium on Electromagnetic Compatibility*, pages 1–5, July 2007.

[28] Daming Zhang and Erping Li. Loading Effect of EUT on Maximal Electric Field Level in a Reverberation Chamber for Immunity Test. In *IEEE International Symposium on Electromagnetic Compatibility, 2002*, pages 972–975, 2002.

[29] F. Olyslager, E. Laermans, and D. Zutter. Numerical and Experimental Study of the Shielding Effectiveness of a Metallic Enclosure. *IEEE TRANSACTIONS ON ELECTROMAGNETIC COMPATIBILITY*, 41(3):202–213, 1999.

[30] J Ladbury, G Koepke, and D Camell. NIST Technical Note 1508: Evaluation of the NASA Langley Research Center Mode-Stirred Chamber Facility. *NIST*, 1999.

[31] D.A. Hill. Electromagnetic Theory of Reverberation Chambers: NIST Techical Note 1506. *NIST*, 1998.

[32] A. Cozza. The Role of Losses in the Definition of the Overmoded Condition for Reverberation Chambers and Their Statistics. *IEEE Transactions on Electromagnetic Compatibility*, 53(2):296–307, May 2011.

[33] J.F. Dawson. *Reverberation Chambers for EMC, Part 1: Principles of Reverberation Chambers*. York EMC Services Advanced Measurements Course, 2006.

[34] L.R. Arnaut. Operation of Electromagnetic Reverberation Chambers With Wave Diffractors at Relatively Low Frequencies. *IEEE TRANSACTIONS ON ELECTROMAGNETIC COMPATIBILITY*, 43(4):637–653, 2003.

[35] T.A. Loughry. Frequency Stirring - An Alternate Approach to Mechanical Mode-Stirring for the Conduct of Electromagnetic Susceptibility Testing. Technical report, 1991.

[36] P. Corona, J. Ladbury, and G. Latmiral. Reverberation Chamber Research - Then and Now: A Review of Early Work and Comparison with Current Understanding. *IEEE Transactions on Electromagnetic Compatibility*, 44(1):87–94, 2002.

[37] L.R. Arnaut. Effect of Local Stir and Spatial Averaging on Measurement and Testing in Mode-Tuned and Mode-Stirred Reverberation Chambers. *IEEE TRANSACTIONS ON ELECTROMAGNETIC COMPATIBILITY*, 43(3):305–325, 2001.

[38] G. Cerri, V.M. Primiani, C. Monteverde, and P. Russo. A Theoretical Feasibility Study of a Source Stirring Reverberation Chamber. *IEEE Transactions on Electromagnetic Compatibility*, 51(1):3–11, February 2009.

[39] F Leferink, J Boudenot, and W VanEtten. Experimental results obtained in the vibrating intrinsic reverberation chamber. *Proc. IEEE Int. Symp. Electromagnetic Compatibility*, 2000.

[40] S. Greco and M.S. Sarto. Hybrid Mode-Stirring Technique for Shielding Effectiveness Measurement of Enclosures Using Reverberation Chambers. *IEEE International Symposium on Electromagnetic Compatibility, 2007*, 2007.

[41] Yuhui He. *Application of the Reverberation Chamber to the Shielding Effectiveness measurement of Physically Small Enclosures*. PhD thesis, University of York, 2009.

[42] Lizhou Bai, Lin Wang, and W Baikuan. Effects of Paddle Configurations on the Uniformity of the Reverberation Chamber. *IEEE International Symposium on Electromagnetic Compatibility, 1999*, pages 12–16, 1999.

[43] J.G Kostas and B. Boverie. Statistical model for a mode-stirred chamber. *IEEE TRANSACTIONS ON ELECTROMAGNETIC COMPATIBILITY*, 33(4), 1991.

[44] Charles F Bunting, Shih-Pin Yu, and Zulfiqar A. Khan. Statistical shielding effectiveness - a modal/moment method approach to characterize the average shielding effectiveness over a wide frequency range including resonances. In *IEEE International Symposium on Electromagnetic Compatibility, 2003*, pages 2–6, 2003.

[45] U. Carlberg, P. Kildal, and J. Carlsson. Numerical Study of Position Stirring and Frequency Stirring in a Loaded Reverberation Chamber. *IEEE TRANSACTIONS ON ELECTROMAGNETIC COMPATIBILITY*, 51(1):12–17, 2009.

[46] C. Lemoine, P. Besnier, and M. Drissi. Estimating the Effective Sample Size to Select Independent Measurements in a Reverberation Chamber. 50(2):227–236, 2008.

[47] M.T. Ma, M. Kanda, M.L Crawford, and E.B Larsen. A Review of Electromagnetic Compatibility / Interference Measurement Methodologies. *Proceedings of the IEEE*, 73(3), 1985.

[48] B.H. Liu, D.C. Chang, and M.T. Ma. Eigenmodes and the Composite Quality Factor of a Reverberating Chamber: NBS Technical Note 1066. Technical report, NBS, 1983.

[49] D.A. Hill, M.T. Ma, A.R. Ondrejka, B.F. Riddle, M.L. Crawford, and R.T. Johnk. Aperture Excitation of Electrically Large, Lossy Cavities. *IEEE TRANSACTIONS ON ELECTROMAGNETIC COMPATIBILITY*, 36(3):169–178, 1994.

[50] B Esen. *QUALITY FACTOR OF MICROWAVE REVERBERATION CHAMBERS*. MSc Thesis, Texas Tech University, 1996.

[51] L.R. Arnaut. Statistics of the Quality Factor of a Rectangular Reverberation Chamber. *IEEE TRANSACTIONS ON ELECTROMAGNETIC COMPATIBILITY*, 45(1):61–76, 2003.

[52] Chalmers M Butler, Yahya Rahmat-Samii, and Raj Mittra. Electromagnetic Penetration Through Apertures in Conducting Surfaces. *IEEE TRANSACTIONS ON ELECTROMAGNETIC COMPATIBILITY*, 20(1):82–93, 1978.

[53] R.H . Price, H.T. Davis, and E.P. Wenaas. Determination of the statistical distribution of electromagnetic-field amplitudes in complex cavities. *Physical Review E*, 48(6), 1993.

[54] T.H Lehman. A Statistical Theory of Electromagnetic Fields in Complex Cavities. *Interaction Notes, Note 494*, 1993.

[55] L.R. Arnaut. NPL REPORT TQE 2 Measurement Uncertainty in Reverberation Chambers I . Sample Statistics. *National Physical Library*, (December), 2008.

[56] Y He and A.C Marvin. Aspects of Field Statistics inside Nested Frequency- Stirred Reverberation Chambers. In *IEEE International Symposium on Electromagnetic Compatibility, 2009*, pages 171–176, 2009.

[57] F.B.J Leferink. Using reverberation chambers for EM measurements. In *International Conference on Software, Telecommunications and Computer Networks*, 2010.

[58] D.A. Hill and J.M. Ladbury. Spatial-correlation functions of fields and energy density in a reverberation chamber. *IEEE Transactions on Electromagnetic Compatibility*, 44(1):95–101, 2002.

[59] C.L. Holloway, D.A Hill, J.M. Ladbury, P.F. Wilson, G. Koepke, and J. Coder. On the Use of Reverberation Chambers to Simulate a Rician Radio Environment for the Testing of Wireless Devices. *IEEE Transactions on Antennas and Propagation*, 54(11):3167–3177, November 2006.

[60] R Armstrong and A.C. Marvin. The Effect of Rician Statistics on the Shielding Effectiveness of Enclosures in Reverberation Chambers. In *EMC Europe, Wroclaw, 13th to 17th September*, 2010.

[61] C Jiaqi. *A Study of the Statistical Characteristics of the Re-radiated Spectrum Measured in a Reverberation Chamber*. PhD thesis, University of York, 2011.

[62] F.J. Massey. The Kolmogorov-Smirnov Test for Goodness of Fit. *American Statistical Association*, 46(253):68– 78, 1951.

[63] York EMC Services. York EMC Services Instrument Brochure, 2002.

[64] M. Hatfield. Shielding effectiveness measurements using mode-stirred chambers: a comparison of two approaches. *IEEE TRANSACTIONS ON ELECTROMAGNETIC COMPATIBILITY*, 30(3), 1988.

[65] K. Hardin, R.A. Oglesbee, and F. Fisher. Investigation Into the Interference Potential of Spread-Spectrum Clock Generation to Broadband Digital Communications. *IEEE TRANSACTIONS ON ELECTROMAGNETIC COMPATIBILITY*, 45(1):10–21, 2003.

[66] M Stecher. Possible Effects of Spread-Spectrum-Clock Interference on Wideband Radiocommunication Services. In *International Symposium on Electromagnetic Compatibility, 2005*, pages 60–63, 2005.

[67] C.D Hoekstra. Frequency Modulation of System Clocks for EMI Reduction. *Hewlett-Packard Journal*, (August):1–7, 1997.

[68] Yongsam Moon, Deog-kyoon Jeong, and Gyudong Kim. Clock Dithering for Electromagnetic Compliance using Spread Spectrum Phase Modulation. *1999 IEEE International Solid-state Circuits Conference*, pages 186–188, 1999.

[69] C.L. Holloway, D.A. Hill, J.M. Ladbury, and G. Koepke. Requirements for an Effective Reverberation Chamber : Unloaded or Loaded. *IEEE TRANSACTIONS ON ELECTROMAGNETIC COMPATIBILITY*, 48(1):187–194, 2006.

[70] P Corona, G Ferrara, and M Migliaccio. Reverberating chamber electromagnetic field in presence of an unstirred component. *IEEE TRANSACTIONS ON ELECTROMAGNETIC COMPATIBILITY*, 42(2):111–115, 2000.

[71] Batool Talha and Matthias Patzold. On the Statistical Properties of Double Rice Channels. *10th International Symposium on Wireless Personal Multimedia, Jaipur, India*, pages 517–522.

[72] C Orlenius, M. Franzén, P. Kildal, and U. Carlberg. Investigation of Heavily Loaded Reverberation Chamber for Testing of Wideband Wireless Units. In *IEEE Antennas and Propagation Society International Symposium, Singapore*, number 1, pages 3569–3572, 2006.

[73] U. Carlberg, P. Kildal, A. Wolfgang, and O. Sotoudeh. Calculated and Measured Absorption Cross Sections of Lossy Objects in Reverberation Chamber. *IEEE TRANSACTIONS ON ELECTROMAGNETIC COMPATIBILITY*, 46(2):146–154, 2004.

[74] M.P. Robinson, J. Clegg, and A.C. Marvin. Radio Frequency Electromagnetic Fields in Large Conducting Enclosures : Effects of Apertures and Human Bodies on Propagation and Field-Statistics. *IEEE TRANSACTIONS ON ELECTROMAGNETIC COMPATIBILITY*, 48(2):304–310, 2006.